Potassium channel β-subunits as voltage-controlled biochemical memories



Hans Olof Rorsman

Trinity College

University of Oxford

A thesis submitted for the degree of

Doctor of Philosophy

Hilary 2022

Acknowledgements

I often describe this DPhil project as being the toughest yet best years of my life and as I approach the end of it, this still rings true. I would like to acknowledge in-vivo *Drosophila* voltage clamp experiments and miniSOG experiments as a truly Sisyphus-like experience that has been incredibly "character building". On the other hand, I've been fortunate enough to be able to befriend some of the brightest individuals I have ever met at the CNCB who have made the experience truly enjoyable and something I will forever cherish.

I would like to individually acknowledge the support and friendship of R. Sarnataro, K. Christodoulou, P. Vargas-Gutierrez, A. Krebbers, T. Wong, L. Ballenberger, all of whom I could not have endured the trials of this DPhil without. I also want to thank A. Kempf, J. Kropf, P. Hasenhütl and E. Vrontou for their invaluable advice and helpful discussions (not to mention the often unscientific yet hilarious additional discussions). Finally, I wish to acknowledge the excellent supervision of Professor G. Miesenböck and my secondary supervisor Professor S. Waddell.

I would also like to thank the Wellcome Trust for generously funding this DPhil project and the Centre for Neural Circuits and Behaviour (CNCB) for hosting me for the past few years.

Abstract

Recent work has demonstrated a role for Reactive Oxygen Species (ROS) in promoting sleep. In the Drosophila melanogaster brain, two dozen sleep-inducing neurons with projections to the dorsal fan-shaped body (dFB) integrate cumulative ROS burden over the duration of the day. The neurons' exposure to ROS is thought to be integrated by the K_v channel Shaker's β-subunit Hyperkinetic, whose oxidoreductase domain metabolises ROS-derived aldehydes with the help of a nicotinamide adenine dinucleotide phosphate (NADPH) co-factor. ROS exposure oxidises this co-factor to $NADP^+$ and slows the inactivation of the Shaker-mediated A-type current, which is permissive of higher frequency neuronal activity and thereby aids sleep promotion. Typical models of homeostatic sleep posit that gradual integration of sleep promoting signals (e.g. ROS) must rapidly dissipate following sleep induction. However, the specific identity of ROS signalling molecules and how these signals are dissipated remains unclear.

Using whole cell in-vivo patch clamp recordings from dFB neurons, I demonstrate that lipid peroxidation products, such as 4-oxo-2-nonenal (4-ONE), readily interact with Hyperkinetic. 4-ONE significantly slows the A-type current inactivation and thus can act as potential physiological ROS derived messenger. Further, I show that integration of ROS molecules by Hyperkinetic can be dissipated by simulating high frequency activity within the dFB neurons. While producing a marked effect on A-type inactivation, the effects of intracellular 4-ONE in dFB neurons did not translate into an overall increased activity. Finally, assessing the sleep behaviour of a broad selection of Hyperkinetic mutants, possible amino acid residues of interest were identified as having a potential role in the long-term ROS signal integration capabilities of Hyperkinetic.

Contents

List of Abbreviations **1**

1 Introduction **5**

1.1 A Brief History of Sleep Research 5

1.1.1 Early sleep research 5

1.1.2 *Drosophila melanogaster* as a sleep model 8

1.2 Sleep Regulation 9

1.2.1 The two-process model of sleep 9

1.2.2 Homeostatic sleep circuitry of *Drosophila* 9

1.2.3 Sleep and Reactive Oxygen Species (ROS) 14

1.2.4 ROS and *Drosophila* sleep model 17

1.3 Shaker, a K_v Channel 18

1.3.1 How are the inactivation kinetics of K_v modulated? 19

1.3.2 The $K_v\beta$ subunit 21

1.4 ROS, Sleep and Hyperkinetic 24

1.5 Hypothesis and aims 30

2 Oxidative By-products and Hyperkinetic **31**

2.1 Introduction 31

2.2 miniSOG photostimulation significantly slows Shaker inactivation . 33

2.3 Intracellular 4-ONE slows Shaker inactivation 34

2.4 The effects of 4-ONE are Hyperkinetic dependent 40

2.5 Summary 43

3 Effects of oxidative by-products are reversible by simulated spiking 47

3.1 Introduction 47

3.2 Simulated spiking facilitates NADP(H) cofactor exchange of Hyperkinetic 48

3.3 Reversal of Shaker inactivation kinetics by simulated spiking require Hyperkinetic 52

3.4 Summary 55

4 Do 4-ONE related changes influence spiking in dFB neurons? 59

4.1 I_A current and neuronal activity 59

4.2 Investigating baseline excitability 60

4.3 Investigating spontaneous spiking rate and pattern 66

4.4 Summary 71

5 Is it possible to generate a "forgetful" Hyperkinetic? 75

5.1 Introduction 75

5.1.1 Hyperkinetic residues of interest 76

5.2 Sleep characteristics of new constructs 77

5.3 Summary 81

6 Reflections & further directions 93

6.1 Main Findings 93

6.2 Discussion 95

6.3 Potential Future Directions 99

7 Materials and Methods 103

7.1 Fly Strains 103

7.2 Sleep measurements 104

7.3 Electrophysiology 104

7.4 Statistical analysis 107

7.4.1 Statistical tests 107

7.4.2 Equations 107

7.5 Miscellaneous contributions 109

References **111**

List of Abbreviations

4-CY 4-Cyanobenzaldehyde

4-HNE 4-Hydroxynonenal

4-ONE 4-Oxo-2-Nonenal

α-DTX . . . . α-Dendrotoxin

AA . . . . . Arachidonic Acid

ADP . . . . . Adenosine Diphosphate

AHP . . . . . Afterhyperpolarisation

AIS . . . . . Axon-Initial Segment

AKR . . . . . Aldo-keto Reductase

ANOVA . . . . Analysis of Variance

AOX . . . . . Alternative Oxidase

AstA . . . . . Allatostatin-A

ATP . . . . . Adenosine Triphosphate

BI . . . . . Burstiness Index

CS . . . . . Canton Special

CoQ . . . . . Coenzyme Q

C_v . . . . . Coefficient of Variation

cv-c . . . . . Crossveinless-c

DAG . . . . . Diacylglycerol

DAM . . . . . Drosophila Activity Monitors

dFB . . . . . Dorsal Fan-shaped Body

EEG . . . . . Electroencephalogram

EMS . . . . . Ethyl-Methyl Sulfonate

EPSC . . . . . Excitatory Postsynaptic Current

ETC . . . . . Electron Transport Chain

GAL4 . . . . . Galactosidase-4

GSH . . . . . Glutathione

HVA . . . . . High Voltage Active

H_2O_2 . . . . . Hydrogen Peroxide

I_A . . . . . A-type Current

I_{Non-A} . . . . . Non A-type Current

I_{Tot} . . . . . Total Current

IF . . . . . Current-Frequency

ISI . . . . . Interspike Interval

IV . . . . . Current-Voltage

KC . . . . . Kenyon Cell

K_{Ca} . . . . . Calcium-activated Potassium Channels

K_{cat} . . . . . Turnover Number

K_m . . . . . Michaelis Constant

K_v . . . . . Voltage-gated K^+-channel

LDE . . . . . Lipid Derived Electrophile

LFP . . . . . Local Field Potential

LNv . . . . . Ventral Lateral Neurons

LPP . . . . . Lipid Peroxidation Product

LTD . . . . . Long-term Depression

MAO . . . . . Monoamino Oxidase

MeAc . . . . . Methyl Acetate

miniSOG . . . mini Singlet Oxygen Generator

MnPn . . . . . Medial Preoptic Nuclei

NADP(H) . . Nicotinamide Adenine Dinucleotide Phosphate

$\mathbf{Na}_v$ . . . . . Voltage gated Na^+channel

NMJ . . . . . Neuromuscular Junction

NREM . . . . Non-Rapid Eye Movement

$\mathbf{O}_2^-$ . . . . . Superoxide

$^1\mathbf{O}_2$ . . . . . Singlet Oxygen

PDH . . . . . Pigment Dispersing hormone

$\mathbf{PIP}_2$ . . . . . Phosphatidylinositol 4,5-bisphosphate

PLA . . . . . Phospholipase A

PLC . . . . . Phospholipase C

$\mathbf{P}_o$ . . . . . Open Probability

PUFA . . . . . Polyunsaturated Fatty Acid

$\mathbf{R}_a$ . . . . . Access Resistance

REM . . . . . Rapid Eye movement

RES . . . . . Reactive Electrophilic Species

Rho-GAP . . . Rho-GTPase activating protein

$\mathbf{R}_m$ . . . . . Membrane Resistance

RM-ANOVA . Repeated Measures Analysis of Variance

RNAi . . . . . RNA Interference

ROS . . . . . Reactive Oxygen Species

RRS . . . . . Redox Regulation Sequence

SCAMP . . . . Sleep and Circadian Analysis MATLAB Program

SEM . . . . . Standard Error of the Mean

SHY . . . . . Synaptic Homeostasis Hypothesis

SI . . . . . Sparseness Index

SK . . . . . Small Conductance Calcium-activated Potassium Channels

SOD . . . . . Superoxide Dismutase

SWA . . . . . Slow Wave Activity

τ_1 . . . . . First Inactivation Time Constant

τ_2 . . . . . Second Inactivation Time Constant

τ_m . . . . . Membrane Time Constant

TEA . . . . . Tetraethylammonium

TTX . . . . . Tetrodotoxin

TUNEL . . . . Terminal deoxynucleotidyl transferase (TdT) dUTP Nick-End Labeling

UAS . . . . . Upstream Activation Sequence

UV . . . . . Ultraviolet

VLPO . . . . . Ventral Lateral Preoptic

Je n'ai fait celle-ci plus longue que parce que je n'ai pas eu le loisir de la faire plus courte.

I have made this longer than usual because I have not had time to make it shorter.

— Blaise Pascal's *Lettres Provinciales*

1 Introduction

Contents

1.1 A Brief History of Sleep Research 5
1.1.1 Early sleep research 5
1.1.2 *Drosophila melanogaster* as a sleep model 8
1.2 Sleep Regulation 9
1.2.1 The two-process model of sleep 9
1.2.2 Homeostatic sleep circuitry of *Drosophila* 9
1.2.3 Sleep and Reactive Oxygen Species (ROS) 14
1.2.4 ROS and *Drosophila* sleep model 17
1.3 Shaker, a K_v Channel 18
1.3.1 How are the inactivation kinetics of K_v modulated? . . 19
1.3.2 The $K_v\beta$ subunit 21
1.4 ROS, Sleep and Hyperkinetic 24
1.5 Hypothesis and aims 30

1.1 A Brief History of Sleep Research

1.1.1 Early sleep research

Sleep pervades human history as an enigmatic yet necessary behaviour of natural life. This forms an ever present curiosity as to what necessitates such a behaviour and what possible purpose it would be fulfilling. Sleep inherently forces an organism to undertake a large risk by entering a state of inactivity with reduced awareness

to external stimuli, rendering an animal vulnerable. It also significantly reduces periods spent performing useful tasks such as foraging. Considering the risks that sleep brings, it must logically serve a critical purpose to offset this in order for it to have evolved as a conserved process. The majority of research show that impaired sleep leads to reduced lifespan [1] and learning deficits [2] and plays a regulatory role in synaptic plasticity and pruning [3–5].

Early biomedical researchers considered sleep a mere response to a lack of sensory inputs brought on by the darkness and silence of night and considered it as a simple and homogeneous off state of the brain, then termed as the "passive process theory" [6]. Early theories also did little to suggest the actual reason for its occurrence beyond its obvious restorative properties. While there have been notable contributions throughout history to the field of sleep science, it is perhaps surprising that most of our understanding comes only from the last few decades. Exceptions include d'Ortous de Mairan who in 1729 showed that the *Mimosa pudica* plant maintained a cyclical behaviour of opening and closing its leaves in the complete absence of external stimuli, such as sunlight, laying the foundation for the concept of a sensory-independent endogenous clock which prompts a behavioural change [7]. In 1875, Richard Caton's demonstration of electrical waves in animal brains inspired Hans Berger's later work, culminating in the first electroencephalogram (EEG) recordings in humans and subsequent discovery of differences in brain waves during wakefulness and sleep. Alfred Loomis later demonstrated, via EEG recordings, that sleep consisted of several distinct states and established the early characteristics of the distinct states of what would be later known as non-rapid eye movement (NREM) sleep [8]. The latter is frequently termed as slow wave activity (SWA) and presents with high power δ-band (0.5-4Hz) oscillations and often indicates deep sleep [9]. Almost two decades later, Aserinsky & Kleitman demonstrated that eye motility (i.e. rapid eye movement (REM) sleep) coincided with the occurrence of dream states [10]. This led to Dement & Kleitman's collaborative description of the human sleep cycle, demonstrating stages of increasing depths of NREM sleep interrupted by short intervals of REM sleep [11].

Another significant advance came in 1971 from a mutation screen of *Drosophila melanogaster* (henceforth simply *Drosophila* or Fly). Using ethyl-methyl sulfonate (EMS) to induce random mutation in the Drosophila genome, the identified gene was termed "period" (*per*). This gene, when mutated, produced a variety of effects on the circadian rhythm of a fly: instead of a normal 24-hour rhythm, a fly would present a rhythmic cycle period of 19- 28-hours or be completely arrhythmic depending on the specific mutation within the gene [12]. This set the foundation for several follow-up studies that aimed to unearth the exact mechanism of the circadian clock. These early observations were soon followed by the discovery that *per* mRNA levels were cyclical in nature and would oscillate over a 24-hour period in synchrony with the circadian cycle. This hinted that *per* regulated its own expression via a feedback loop. Another clock gene, timeless (*tim*), was soon identified as a gene whose mRNA oscillated in synchrony with per [13]. Further *Drosophila* mutagenesis assays soon unearthed two further clock genes to complete the core feedback cycle: CLOCK (*clk*) and CYCLE (*cyc*) [14, 15]. In a simplified model, the gene products of *clk* and *cyc*, CLK and CYC, dimerise in the nucleus to promote *per* and *tim* expression peaking in the mid-afternoon. The resulting gene products TIM and PER accumulate and dimerise in the cytoplasm and in the early night translocate to the nucleus to inhibit CYC and CLK function, thus stopping further gene expression. Meanwhile, the PER protein will also become ubiquitinated by local ubiquitin ligases and subsequently degraded, thus alleviating the *per* and *tim* repression and resetting the cycle in the early morning [16]. While these genes have complex interactions with several downstream genes, one notable clock gene output is the pigment-dispersing hormone (PDH), a hormone belonging to the pigment-dispersing factor (PDF) family [17]. In *Drosophila*, a set of principal pacemaker neurons were identified as the numerically sparse ventral Lateral Neurons (LNv) where PDF was determined to be one of the core circadian neurotransmitters [18, 19]. A critical concept in sleep regulation is that electrical activity from small subsets of neurons such as these LNv neurons are known to be capable of exerting a general circadian effect on the rest of the body [20].

These relatively recent studies represent significant leaps in delineating the circuitry underlying circadian sleep regulation and paved the way for *Drosophila melanogaster* to become a dependable animal model for sleep studies. While this early research in *Drosophila* yielded a plethora of detail surrounding the regulation of the circadian rhythm, the governing factors of the homeostatic sleep pressure that account for time spent awake rather than time of day, remain relatively obscure.

1.1.2 *Drosophila melanogaster* as a sleep model

Drosophila share many characteristics with vertebrates regarding sleep e.g. sleep tends to decrease with age in flies and humans and both experience rebound sleep following sleep deprivation and exhibit distinct sleep phases [21–24]. Owing to their relative simplicity compared to mammalian models and their genetic malleability, *Drosophila* have allowed detailed descriptions of sleep regulatory mechanisms.

While both vertebrates and invertebrates display periods of inactivity and activity usually linked to a circadian rhythm, identifying sleep in *Drosophila* can be difficult [21]. This can be comparatively simple in larger animals like mammals where a combined approach of behavioural and electrophysiological monitoring is used, the latter of which is not easily achieved in a long-term, high throughput manner using *Drosophila* [21, 25]. Therefore, behavioural observations are typically used instead when describing sleep in *Drosophila*. Nevertheless, local field potential (LFP) measurements in the *Drosophila* brain demonstrated the presence of sleep-like activity with oscillations that resemble SWA [26, 27]. Behaviourally, sleep is typically defined as periods of immobility paired with a reversibly raised arousal threshold and a further demand for rest following any periods of sleep deprivation [21, 28]. High resolution activity observation of *Drosophila* using either video tracking or ultrasound showed a strong correlation between sustained periods of quiescence (approximately 5 minutes or longer) and elevated arousal threshold [21, 25]. Given this, it is commonly assumed that after 5 minutes of quiescence, a fly is asleep [21, 25, 29]. This assumption is strengthened as overall periods of quiescence become not only longer following 12 hours of sleep deprivation but also require

greater stimuli to arouse from, demonstrating a homeostatic rebound as both the length and resilience of the quiescence (and thereby sleep) increases after sleep deprivation [25].

1.2 Sleep Regulation

1.2.1 The two-process model of sleep

A core concept of sleep regulation emerged in 1982: the two process model [30]. This model refers to two independent processes which regulate sleep pressure: the well-known circadian process, process C, and the more obscure, sleep dependent homeostatic process, process S (Fig. 1.1). In this model, homeostatic sleep pressure gradually builds during wakefulness and rapidly dissipate upon sleep initiation [30]. In the original proposal of the model, sleep deprivation did not result in a linear increase in compensatory sleep, and famous examples e.g. 90 hours of sleep deprivation only required 10 hours of subsequent sleep suggested that, as homeostatic pressure increases, compensation occurs not only in the duration of sleep but also its intensity [30]. This intensity was proposed to be mimicked by alterations in electrical activity of the brain, reflected in mammals in EEG recordings, particularly in the power of the 0.5 - 4 Hz band seen during SWA. Following sleep deprivation, both power and overall SWA as a proportion of sleep would increase in correlation to the degree of sleep deprivation [30].

1.2.2 Homeostatic sleep circuitry of *Drosophila*

The relative simplicity of the fly brain makes delineating the sleep regulating circuitry more manageable compared to other model animals [29]. Genetic engineering has played a significant role in the study of circadian rhythm in *Drosophila*. A common genetic expression system used in *Drosophila* is the galactosidase-4 (GAL4) - upstream activation sequence (UAS) system [31]. This allows for expression in highly specific anatomical pattern. During a high throughput screen of several GAL4 drivers, the activating bacterial sodium channel NaChBac was expressed in a small subset of neurons in the central complex of the *Drosophila* brain [32].

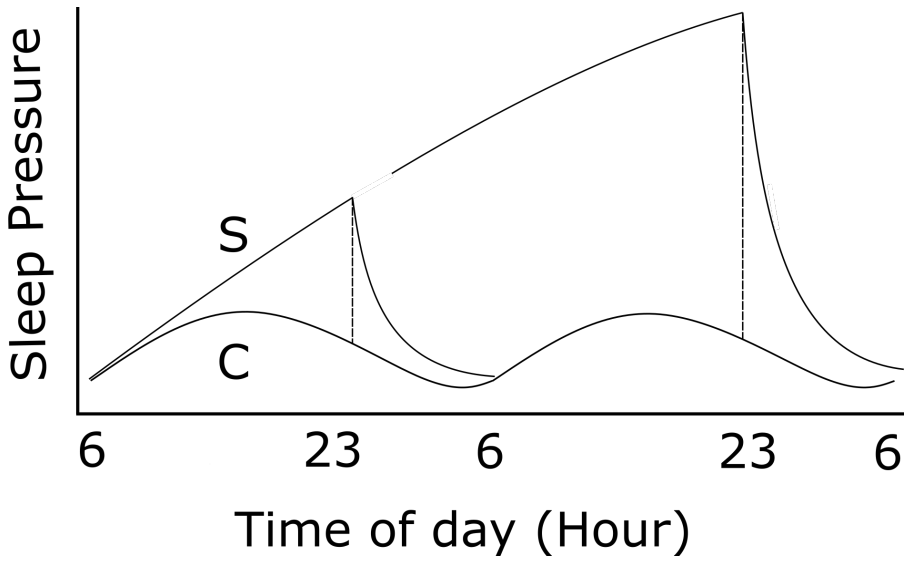


Figure 1.1: Adapted figure from [30] outlining the two-process model with a consistent cycling circadian process (C) and the homeostatic process (S). The latter is characterised by a gradual build-up during wakefulness and rapid dissipation during sleep. Should sleep be disrupted, this homeostatic pressure will continue to build.

Activity derived from these neurons appeared to strongly drive sleep induction [32]. The expression pattern of these neurons showed axonal projections to the dorsal fan-shaped body of the central complex, these neurons were thus termed the dorsal fan-shaped body (dFB) neurons. In a separate study, recognising that dopamine is a common potent wake promoter [33, 34], expressing the heat sensitive, activating, dTrpA1 within a small subset of dopaminergic neurons reinforced this notion as activation led to diminished sleep [35]. These neurons were shown to project to the sleep promoting dFB neurons [35]. This highlighted the dFB neurons as a significant component of the sleep regulating network and paved the way for investigating the internal molecular machinery that confers the dFB neuron's sleep promoting activity. One example is the *crossveinless-c* (*cv-c*) gene which encodes a Rho-GTPase activating protein (Rho-GAP) and was found to significantly reduce sleep when mutated [36, 37]. Furthermore, *cv-c* was implicated in homeostatic sleep control. Mutations in *cv-c* manifested as a reduced capacity for rebound sleep following sleep deprivation in addition to overall reduced sleep. In addition, the circadian rhythm was unperturbed by *cv-c* mutations [37]. In the same study, a reintroduction of *cv-c* expression specifically into dFB neurons on a *cv-c* null background rescued the defects

[37]. Given that activation of dFB neurons led to sleep promotion, it was speculated that *cv-c* mutations may impact the electrical properties of the dFB neuron [37, 38]. Whole cell patch clamp experiments revealed some diversity within the dFB population, where different neurons exhibited widely varying degrees of excitability in response to depolarising current injections [37]. The majority of wildtype dFB neurons were excitable, whereas *cv-c* mutant neurons were mostly electrically silent [37]. Further characterisation of the underlying electrophysiological properties revealed a decreased input resistance and reduced membrane time constant in *cv-c* mutant dFB neurons. These were seen as contributing factors to the altered excitability, as decreased input resistance led to smaller voltage deflection in response to depolarising currents or excitatory postsynaptic currents (ESPCs) and the reduced time constant allowed for impaired temporal summation of excitatory neuronal input [37].

Flies were kept sleep-deprived overnight and subsequently used for whole cell patch clamp experiments. In contrast to normal sleeping flies, sleep-deprived flies showed increased dFB neuron excitability. This showed a direct correlation of dFB activity with sleep history [37]. Furthermore, *cv-c* mutations nullified these increases, suggesting that *cv-c* is required for electrophysiological alterations. This study of the dFB properties ultimately demonstrated that the excitability of dFB neurons was linked to homeostatic sleep pressure.

By artificially delivering dopamine to the dendritic tufts of the dFB neurons by either local injection of dopamine or optogenetic activation of dopaminergic neurons, the conditions seen in *cv-c* mutants were replicated, although now in a reversible manner [38]. The relatively rapid speed at which dopamine induced changes hinted at post-translational modification or trafficking of ion channels as the responsible mechanism [38]. Two main ion channels were demonstrated to govern the electrophysiological properties of dFB neurons: Shaker and Sandman. Shaker mediates the repolarising A-type current (I_A) while Sandman gives rise to an inhibitory non A-type (I_{Non-A}) current. I_A constitutes a repolarising force following

an action potential and its presence permits for rapid and repetitive action potential firing [39]. In the excitable state, I_A is the dominant current. However, in response to dopamine I_{Non-A} amplitude almost quadruples and the resulting K^+ leak renders the neuron silent due to neuronal hyperpolarisation [38]. This was suggested to be due to a large reservoir of Sandman channels in intracellular storage vesicles, which translocate to the plasma membrane in response to dopamine [38]. Given that *cv-c* mutants exhibited persistently silent dFB neurons, it was proposed that the activity of the encoded Rho-GAP is involved in recycling Sandman channels presented on the plasma membrane [38].

Immunostaining of likely candidate messengers showed that the inhibitory neuropeptide allatostatin-A (AstA), the *Drosophila* homologue of galanin, overlapped with the dFB axons [40]. The role of AstA in homeostatic sleep regulation was demonstrated via the homozygous expression of a defective AstA gene which resulted in both a decrease of baseline sleep and a complete loss of compensatory sleep following sleep deprivation while having no effect on the circadian rhythm, similar to the *cv-c* mutants [38, 40]. It is noteworthy that AstA mutants did not completely recapitulate the *cv-c* mutant phenotype, suggesting that AstA is not the sole mediator of dFB signalling [40]. However, having a known effector of dFB signalling allowed for the search of downstream targets. Tagging AstA receptors with GFP led to four interneurons being described as postsynaptic targets of dFB neurons, termed helicon cells [40]. Reflecting the earlier AstA experiments, depleting functional AstA receptors in these helicon cells also had a diminishing effect on homeostatic sleep regulation [40]. Patch clamp experiments revealed that helicon cells were strongly responsive to visual input and existed in either an "up" or "down" state where depending on the state, visual input would elicit a varying response with the "up" state being the much more responsive state [40]. Furthermore, when the "up" state was observed in helicon cells, the fly was much more likely to initiate spontaneous movement in response to visual stimulation. This indicated that "helicon cells played a permissive role in visually guided movement" and that dFB neurons were inhibitory to such actions to promote rest [40]. This was demonstrated by recording

spontaneous activity of helicon cells while artificially activating dFB neurons; the dFB activity resulted in rapid hyperpolarisation of the helicon cells [40].

Helicon cells have a strong synaptic connection to another subset of neurons within the ellipsoid body of the central complex known as the R5 neurons [40]. These neurons have been previously implicated in homeostatic sleep control but crucially their activity does not acutely enforce sleep [41]. Inhibition of R5 neurons' neurotransmission using tetanus toxin (TNT) results in a significant loss of homeostatic rebound sleep following sleep deprivation [41]. Furthermore, R5 neurons' electrical activity is directly correlated with sleep history. Immediately prior to sleep or following sleep deprivation, R5 neurons have a significantly higher spontaneous firing rate than that observed in flies in the wake of undisturbed sleep [41]. Further investigation showed calcium dependent synaptic plasticity was the underlying factor of the increased activity and was thus proposed as a potential conduit for conveying homeostatic sleep pressure [41]. Expressing the genetically encoded calcium indicator GCaMP6s in dFB neurons while simultaneously activating the R5 neurons showed that R5 neurons acted upstream of the dFB neurons, most likely indirectly [41]. Considering the interconnectivity of the discussed groups of neurons, it is perhaps not surprising that continuously optogenetically activating helicon cells for 24 hours triggers rebound sleep in the subsequent day, sleeping almost 8 hours on average more than control flies [40]. The emerging link between key groups of neurons gave rise to a proposed model of the homeostatic sleep circuit. In this model, the R5 and dFB neurons both store and signal homeostatic pressure: presumably different forms of pressure originating from separate sources accumulate in either set. However, the source of this pressure and in what form it is stored remains unknown. The dual nature (i.e. electrically quiescent versus highly active) of the dFB neuron however is believed to represent the terminal sleep switch, whose activity inhibits the helicon cells and their associated visually stimulated locomotion to induce sleep. Furthermore, the inhibition of the helicon cells also reduce stimulating inputs to the downstream R5 neuron. This reduces overall activity of the R5 neurons and reduces the activity dependent synaptic

plasticity. This results in reduced transmission to the dFB neuron and diminishes subsequent dFB activity and alleviates helicon cell inhibition [40], illustrated in Fig. 1.2. Importantly, this model is still susceptible to input from outside circuits, notably dopamine's overriding effect on dFB activity [38]. While it remains to be determined whether a comparable circuitry exists in a mammalian context there are certain sleep promoting neurons, such as the ventrolateral preoptical (VLPO) nucleus, which share similarities with the dFB neurons [42]. dFB neurons are targets of the anaesthetic isoflurane, similarly, the VLPO whose activity is a target of isoflurane in mammals [43]. Furthermore, VLPO neurons are galanin positive, the mammalian AstA homologue of dFB neuron [40, 44]. While of course this does not demonstrate the same circuitry in mammals, it does show potential for the existence of at least a similar type of circuit.

1.2.3 Sleep and Reactive Oxygen Species (ROS)

While publications in recent years have begun to delineate the homeostatic sleep circuitry in *Drosophila* [32, 37, 38, 40, 41] and mammals [46–48], there remains a great deal of uncertainty on the exact ancestral purpose of sleep and in terms of the two-process model, exactly what signals the gradually building homeostatic sleep pressure.

One hypothesis of a unifying function of sleep was made in 1994. It was suggested that the central function for sleep was the clearance of reactive oxygen species (ROS) [49]. In this case, the rising sleep pressure would be imposed via a gradual increase in ROS stress. This was based on the fact that the brain is a high energy demanding organ and would therefore produce a correlative high amount of ROS as a by product of oxidative phosphorylation [49]. The metabolic rate would be correlated with the apparent brain activity, where during the day the brain would be highly active and relatively quiescent during sleep. ROS presence can produce further reactive products such as hydrogen peroxides through local oxidation of catecholamines or via the action of local monoamine oxidase (MAO) activity; hydrogen peroxide can then further react to produce hydroxyl radicals and lipid peroxidation products

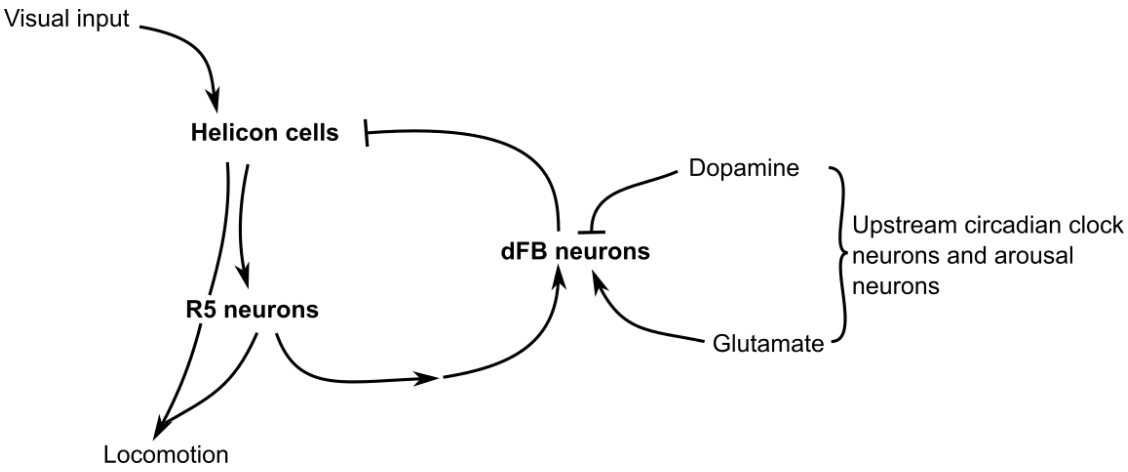


Figure 1.2: Adapted figure from [40] showing a simplified model of the homeostatic sleep circuit. In this model, dFB neurons switch between an electrically excitable and quiescent state and thus are able to act as a 'on-off' sleep switch. In the active sleep promoting state, dFB neurons act to inhibit helicon cell. Helicon cells respond to visual inputs to and are permissive for locomotion and their inhibition allows for entry into a sleep state. Helicon cells are pre-synaptic to R5 neurons which are themselves indirectly excitatory of dFB neurons. The circuitry thus forms a 'charge and dissipate' circuitry where once a dFB neuron enters the active state (or a 'charged' state where it has accrued a degree of sleep pressure to promote activity) it begins to inhibit helicon cells to promote sleep. This also has the consequence of reducing excitatory inputs to the R5 neurons and thus also reducing excitatory inputs to the dFB neuron, over time this will lead to reduced activity of the dFB neuron and a relaxation of the circuitry. This system however also obviously needs overriding inputs to prevent continuous drifting between twilight states of waking and sleep such as the electrical quiescence imposed on dFB neuron via the action of dopamine derived from arousal neurons [38, 41, 45]. There is also potential for fine-tuning of this circuitry via further excitatory and inhibitory action on the dFB neurons from circadian clock neurons [45]. Importantly, the above is not an exhaustive schematic of all interactions of the circuitry with outside inputs but is purposed to illustrate the basic circuit and the potential for modulation.

(LPPs) [49–51]. It was thus suggested that during the day, during high overall brain activity, the brain's inherent ROS clearance mechanisms are unable to keep up with the high ROS production and a gradual build-up of ROS will occur. The fact that neurons are highly sensitive to ROS implies that there must be a concerted effort to regularly clear this ROS accumulation before any lasting damage can be incurred [49]. In this model, this effort is sleep where a decreased ROS generation combined with perhaps an increased efficiency of antioxidant capabilities allows for effective ROS clearance. When the ROS load is sufficiently reduced, wakefulness is restored. Considering this, the encompassing model assumed a linear rise of free

radicals, which at a certain threshold would either induce sleep or impart a strong sleep pressure on the animal. At the point of sleep initiation, these radicals would be rapidly cleared and wakefulness would resume (illustrated in Fig. 1.3).

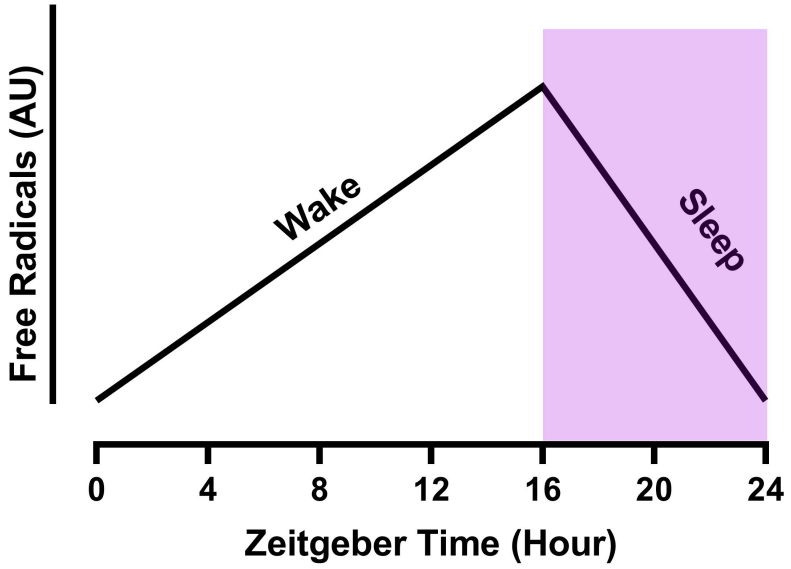


Figure 1.3: Adapted figure from 1994 study [49] showing proposed model of radical build-up (arbitrary units, AU) during wakefulness and then rapid clearance at sleep initiation at the 16 hours time point. Time is in Zeitgeber hours when 0 hours would be the waking time-point (typically 8 am)

While this theory proposed an attractive, simple unifying function of sleep, subsequent studies produced an array of conflicting data [1]. For instance, data to support the model came from studies that showed reduced brain antioxidant capacity such as reduced activity in the antioxidant enzyme, superoxide dismutase (SOD) following chronic sleep deprivation in mice [52]. Additionally, sleep deprivation was characterised by a decrease in the antioxidant scavenger reduced glutathione (GSH), in the brain [53].

The fact that extensive sleep deprivation (approximately between two and three weeks) leads to death in rats would suggest that some damage should occur prior to death, which would agree with the 1994 model. However, quantifying markers of cell death via changes in apoptotic genes expression and terminal deoxynucleotidyl transferase dUTP nick-end labeling (TUNEL) assays following varied lengths of sleep

deprivation (up to two weeks) showed no increase in cell degeneration compared to control [54]. Another study aimed to see if there was a link between ROS accumulation and the motor weakness, organ lesions and fatality following prolonged sleep deprivation. By measuring a myriad of oxidative stress-related proteins, it was concluded that 96 hours of sleep deprivation produced no oxidative stress response [55]. To add further to the uncertainty, there is recent evidence to suggest that ROS accumulation in gut occurs as a result of sleep deprivation and by artificially preventing this ROS accumulation animal lethality can be prevented [56]. However, recent work in *Drosophila* showed that short-sleeping mutants suffered significantly increased lethality during oxidative stress. This effect was consistent across mutations in several distinct genes. This suggested that a common consequence of sleep loss caused by the different mutations was deficient ROS clearance as opposed to effects specific to the individual mutated proteins [1]. Furthermore, driving excess sleep via artificial activation of dFB neurons in these mutants conferred a robust resistance to oxidative stress [1]. This study, in line with the above model, suggests that ROS promotes sleep, and sleep clears ROS [1, 49].

1.2.4 ROS and *Drosophila* sleep model

Considering the dFB's demonstrated role in regulating homeostatic sleep pressure [37, 38], and the potential role of ROS in generating sleep pressure, dFB neurons could gradually integrate cumulative oxidative pressure during wakefulness and convert it to increased electrical activity, which in turn would rapidly dissipate the accumulated sleep pressure. A potentially elegant and efficient method to achieve this would be to link the resulting activity within the dFB neurons to the clearing of the sleep promoting signal.

To explain how the dFB neuron is in fact equipped to fulfil both the integration of sleep pressure in the form of ROS and its dissipation through the resulting activity, the remainder of this chapter will give a brief general introduction to potassium

channels and further explain how their role becomes crucial to sleep promotion within the dFB neuron.

1.3 Shaker, a K_v Channel

Shaker was one of the first potassium channels to be characterised. The gene locus was discovered in the X-chromosome in the *Drosophila* genome by random EMS mutations. These mutations resulted in a vigorous shaking phenotype in response to ether, the behaviour from which the name is derived [57, 58]. While attempting to recapitulate the Shaker mutation, similar phenotypes were produced when alternate loci were mutated, these were dubbed "ether-a-go-go (*eag*)" and "Hyperkinetic (*Hk*)" [58]. It was suspected that Shaker encoded an ion channel component based on structural similarities of its suspected protein product to other known ion channels. Namely, the Shaker sequence encoded multiple hydrophobic sequences characteristic of a transmembrane protein and also contains sequences comparable to the voltage sensitive domain of voltage gated Na^+ channels (Na_v) [59]. Expressing the Shaker gene in Xenopus oocytes produces transient, outward currents in response to depolarising steps and confirms that Shaker is indeed a voltage-gated potassium channel subunit [60]. Inactivation is a prominent feature of K_v channels; depending on the specific channel, the inactivation time constant can range from single figure milliseconds to several seconds. The *Drosophila* Shaker channel has one of the fastest inactivation time constants of approximately 3-8 ms [61, 62].

While Shaker's initial inactivation is exceedingly quick and produces a very rapid decay in current flow, the multiexponential decay profile of Shaker currents implied the presence of more than one mode of inactivation acting in parallel [63]. Tetraethylammonium (TEA), a potent K_v blocker, when applied on the intracellular face of the channel competes with fast inactivation but applied on the extracellular side interferes instead with a slower, more enduring form of inactivation [64]. The fast component of Shaker inactivation was determined to be reliant on an N-terminal

peptide chain (thereby termed N-type inactivation) [63, 65]. This peptide forms a "ball and chain" component which upon prolonged channel activation enters the pore from the intracellular side and blocks ion passage [65]. Notably, while reliant on voltage dependent opening of the channel pore to take place, the entry of the peptide to the pore is itself voltage independent [66].

The second, slower inactivation involves primarily the outwards facing C-terminal of the Shaker protein (hence termed C-type inactivation) [65]. Despite typically identified as a wholly autonomous process from N-type inactivation, C-type inactivation does in fact occur more readily when the channel is in the N-type inactivated state, suggesting that there is at least a partial coupling between the two types of inactivation. [65]. Interestingly, while N-type inactivation is vulnerable to most N-terminal deletions and excessive deletions can even abolish N-type inactivation completely, C-type inactivation is more resistant to C-terminal alterations. Most mutations are innocuous in terms of C-type inactivation time constants and often specific single amino acids alterations in K_v e.g. K463V are required to significantly affect entry into the C-type inactivated state, in this case increasing entry rate while also stabilising it, making recovery substantially slower. It is unlikely that C-type inactivation utilises a ball-and-chain method as N-type does, and may instead utilise a form of pore constriction to block the channel [65, 67].

1.3.1 How are the inactivation kinetics of K_v modulated?

Most K_v channels operate in an almost identical way: depolarisation promotes a state-switch from a closed state to an open state and extended depolarisation leads to the channel entering a third, non-conductive inactivated state [61]. Modelling suggests N-type inactivation can only be entered through transitioning via the open state, while C-type can be entered already through a partially opened state [68]. In the case of A-type K_v channels (such as Shaker), the inactivation gives rise to a typical macro-current shape seen in whole cell patch clamp where large transients form upon membrane depolarisations that rapidly decay as a swiftly increasing proportion of K_v channels enter the inactivated state (Fig. 1.4).

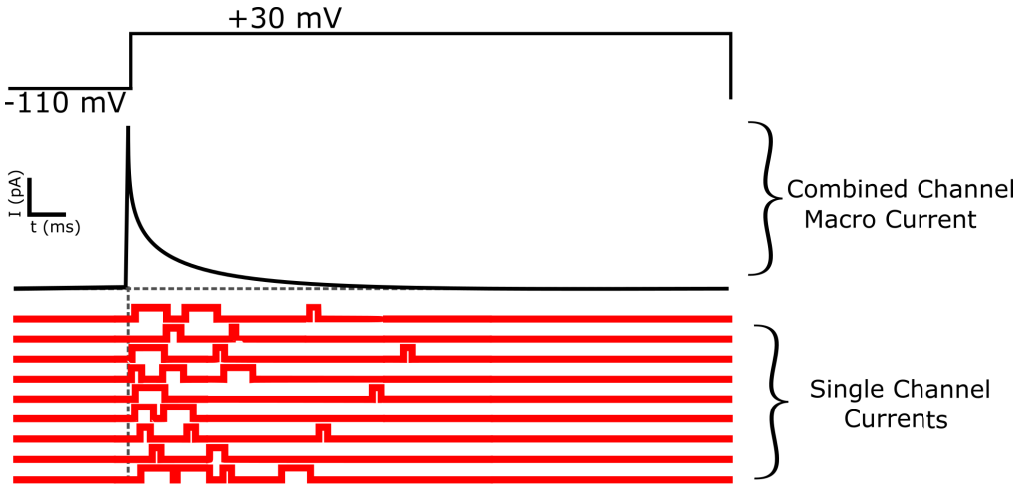


Figure 1.4: Illustration demonstrating the underlying single channel states which produce the typical A-type current shape. In response to a strong depolarising pulse (+30 mV) from a hyperpolarised state (-110 mV), most K_v channels open briefly. Some of these will quickly inactivate via N-type inactivation. These channels can quickly recover from this inactivation and reopen. However, extended periods of depolarisation initiate a second, slower but more permanent inactivation which leads to sustained inactivation of the channels resulting in a lasting decay in the macro current. Recovery from this state is improbable until a hyperpolarised membrane potential is restored.

The rate of current decay is determined by how rapidly individual channels enter the inactivated state, from which they recover on a timescale of approximately 100 ms [69]. This allows for an opportunity of fine-tuning the K_v channel activity by either slowing down or speeding up the rate of the channel's state switching. Fatty acids are common intracellular messenger molecules of ion channel modulation. For example, the polyunsaturated fatty acid (PUFA) arachidonic acid (AA) is a signalling molecule produced via the activity of phospholipase A (PLA) or C (PLC) metabolising diacylglycerol (DAG) or membrane phospholipids respectively [70]. Applying AA to the intracellular face of a K_v ion channel complex enforces a rapid, reversible inactivation, effectively turning delayed rectifiers into A-type channels [71, 72]. Interestingly, this inactivation is unaffected by the K_v blocker TEA, thus ruling out a physical channel block and instead hinting at a "lipid-induced gating process" by inducing conformational changes to the selectivity filter [73]. In contrast to N- and C-type inactivation, AA mediated block is highly voltage dependent [73]. Conversely, phosphatidylinositol-4,5-bisphosphate (PIP_2) had the opposite

action with intracellular application abolishing N-type inactivation of the channel consequently turning an A-type channel into a delayed rectifier by immobilising the N-terminal ball domain to the membrane and preventing it from entering the pore [73]. Follow-up studies to these initial experiments revealed a large variation in sensitivity to different membrane lipids [74].

Early studies of K_v channels used simplified systems, e.g. cell lines or Xenopus oocytes, to investigate their properties. These experiments showed noticeable differences in inactivation compared to native Shaker channels expressed in native tissue [75, 76]. While some variation was likely due to differences in local environments, it soon became clear that the main difference between native and reconstituted K_v channels was the presence of a $K_v\beta$ subunit. The existence of a $K_v\beta$ subunit was subsequently confirmed from purified α-dendroxtoxin (α-DTX) receptors [77, 78]. These studies predicted a likely potassium ion channel complex consisting of 4 larger ($\sim$78 KDa) α-subunits and 4 smaller ($\sim$39 KDa) β-subunits (Fig. 1.5). $K_v\beta$ subunits were shown to endow fast N-type inactivation on the previously only slow-inactivating potassium channels [79, 80]. Later, 3 isoforms of the $K_v\beta$ gene were cloned from the mouse genome ($K_v\beta$1-3). cDNA analysis determined that the protein encoded by Hyperkinetic showed a strong homology to mammalian $K_v\beta$ subunits [62]. Interestingly, the sole $K_v\beta$ member of *Drosophila*, Hyperkinetic, and the mammalian $K_v\beta$2 isoform both lack the typical ball-and-chain N-terminus required to confer N-type inactivation, raising some mystery as to the exact purpose of the $K_v\beta$ subunit that implied the existence of perhaps an additional function as opposed to solely conferring N-type inactivation [62, 79].

1.3.2 The $K_v\beta$ subunit

When the sequence and subsequent structure of $K_v\beta$ was delineated, an early striking similarity was observed of $K_v\beta$ to aldo-keto reductase (AKR) enzymes in both overall structure and sequence homology complete with an active site [62, 82]. Typically, AKRs reduce aldehydes into alcohols using a NADPH cofactor as an electron donor. This cofactor is consequently oxidised to $NADP^+$ [83]. Interestingly

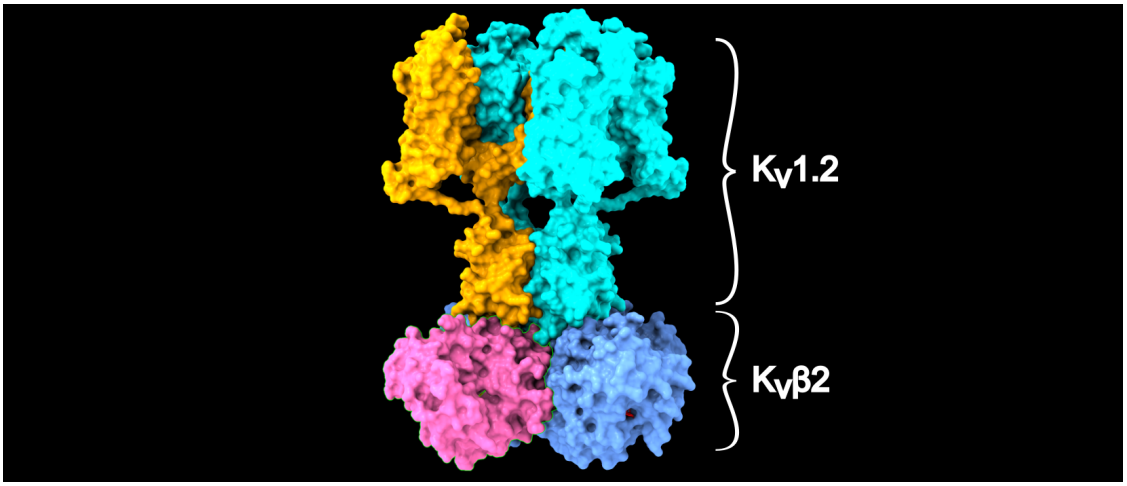


Figure 1.5: Structure of a $K_v1.2/2.1$ chimaera-$K_v\beta2$ ion channel complex showing the hetero tetrameric structure composed of 4 α-subunits and 4 coupled β-subunits (1 individual subunit coloured orange and pink respectively) [81].

and of high importance for this thesis, the redox state of the bound NADPH cofactor can influence the mean open time and open probability (P_o) of the ion channel complex. In the oxidised form, these values increased due to the bound $NADP^+$ delaying $K_v\beta$ mediated inactivation [84–86]. Furthermore, to strengthen this conclusion, exposure to reducing environments led to the opposite effect i.e. reduced open time and probability [84]. For AKR substrate conversion to continue, the exchange of oxidised $NADP^+$ for NADPH is required [83]. The rate of cofactor exchange can therefore become the rate-limiting step of the AKR reaction cycle [83]. However, the NADPH cofactor is almost completely enveloped within the structure of $K_v\beta$, with only the reactive nicotinamide ring exposed. This results in a very strong binding affinity with the $K_v\beta$ protein and prevents straightforward exchange [82]. Despite having some hallmarks of a non-functional enzyme, the rest of the catalytic system, which would be expected in an AKR, is present in $K_v\beta$ and constituted what appeared to be a fully operational enzyme, albeit one with a very low potential turnover rate [82]. A typical AKR has an approximate K_{cat} value ranging from 0.8 to 10 min^{-1} and a K_m in the micromolar range depending on specific subtype and substrate [83]. In contrast, $K_v\beta$ has a 10-100 times lower K_{cat} and a K_m in the millimolar range to sample carbonyls [87].

This raised the question as to why an effectively subpar enzyme would be shackled to a voltage-gated potassium channel. One suggestion is a potential bidirectional relationship between the α- and β-subunits, where altered inactivation of the channel subunit and resultant membrane potential change would, via voltage induced conformational change, expose the NADP(H) cofactor and mediate increased cofactor exchange and thus potentially impact the catalytic activity of the β-subunit. Due to its sensitivity to voltage, the degree of change in $K_v\beta$ would scale according to action potential firing rate [82]. The second possibility proposed that the $K_v\beta$ subunit acts as a sensor of oxidative strain of the host cell and that the oxidation of the NADPH cofactor into $NADP^+$ leads to a conformational change causing a significant effect on the gating of the channel complex [82]. Strikingly, in this scenario, due to the poor baseline exchange rate of the cofactor, a single hydride transfer as a result of even a transient exposure to the enzymatic substrate would result in a long-lasting effect on channel gating. These ideas suggested a link between the redox state of the cell environment and the Shaker potassium current via the channel's β-subunit.

Due to their close association with Shaker channel function, mutations in the *Drosophila* $K_v\beta$ Hyperkinetic gene are known to affect neuronal activity similarly to impaired Shaker activity. Studies detail spike broadening and a reduced degree of rhythmicity in Hyperkinetic null mutants [88–90].

The effectiveness of $K_v\beta$ as a fully fledged AKR enzyme at this point was however still undetermined although, notably key mutations in the putative active site of $K_v\beta$ exhibited a reduced or abolished capability of $K_v\beta$ to impact channel inactivation [85, 91]. Using rat $K_v\beta$ expressed in *E.coli* bacterium and monitoring NADP(H) redox state via spectrophotometry, the enzymatic capabilities of $K_v\beta$ were properly established [87]. This study showed that exposure to a wide variety of known AKR substrates (including both ketones and aldehydes) effectively drove the NADP(H) into the oxidised state, accompanied by the formation of the related reduced product

[87]. Furthermore, revisiting the previous putative active site mutations showed a reduced or nigh abolished AKR activity [87].

Interestingly, the earlier described *Drosophila* shaking while anaesthetised using ether turned out to not be the only behavioural effect of respective deficient mutants. Flies expressing a point mutation in the Shaker gene exhibited drastically reduced total sleep (reduced from 8-14 hours to 3-4 hours per night) [92]. This implicated a role of Shaker and I_A in sleep regulation. Later studies showed specific knockdown of Shaker specifically in dFB neurons also resulted in dramatic sleep loss. This knockdown also resulted in reduced dFB neuron excitability, suggesting Shaker played a role in dFB neuron's sleep promotion [38]. Crucially, the reduced sleep resulted in hallmarks of sleep deprivation, such as reduced lifespan [92]. This showed that the problem lay in converting actual sleep need into actual sleep promotion. Considering Shaker's role in sleep regulation, it was thus conceivable that Hyperkinetic mutants would also have similar effects on sleep. Indeed, Hyperkinetic mutants were later shown to have a similar effect on sleep and further also showed that this sleep deprivation resulted in a memory deficit [93].

1.4 ROS, Sleep and Hyperkinetic

In the vein of ROS clearance model where sleep is both promoted by and used to clear ROS build-up [49], the combination of Hyperkinetic's function as a redox sensor and its role in sleep promotion created an appealing hypothesis that Hyperkinetic could detect and measure cellular ROS and translate ROS load into sleep promotion via increased activity of sleep promoting dFB neurons. The resulting sleep would clear ROS and reset the cycle. When expressing the catalytic null mutant of Hyperkinetic Hk^{K289M} exclusively in dFB neurons on a Hyperkinetic deficient background, a sleep deficient phenotype was produced akin to Hyperkinetic null mutants [93, 94] The catalytic null mutant still confers the same amount of inactivation as a functional form, the only difference relating to sensitivity to ROS and the resulting altered inactivation [85]. Hyperkinetic mediates Shaker trafficking to the membrane

[95], but the catalytic function is not required for this [85, 86]. The phenotype observed with Hk^{K289M} could be rescued via the specific expression of a functional Hyperkinetic on the same background into dFB neurons, this restored normal sleep [94]. This showed that the catalytic activity (and thereby ROS sensitivity) of Hyperkinetic is the key component of promoting sleep. This likely occurs via the altered inactivation kinetics of the Shaker:Hyperkinetic channel complex increasing the neuronal activity and thus sleep promotion of the dFB neurons [38]. Curiously, the redox sensitivity of Hyperkinetic also has a demonstrated role in the regulation of light-entrained circadian rhythm in LNv neurons. Selective expression of functional Hyperkinetic in these neurons rescued the otherwise significantly diminished firing rate in response to light stimulation [96].

Sleep history is a strong determinant of ROS presence within the dFB neurons. Expressing MitoTimer, a fluorescent mitochondrial targetted green fluorescent protein which irreversibly shifts towards red emission after ROS exposure [97], within the dFB neurons showed a stark increase in red fluorescence when flies are sleep-deprived [94]. dFB neurons are typically less excitable during daytime and more active during nighttime. MitoTimer was then expressed in third order olfactory neurons, namely the Kenyon cells (KC) of the mushroom body. These KCs were presumed to have more consistent activity over time compared to dFB neurons and accordingly showed little increase in ROS. This suggested two things: first, in contrast to the traditional perspective, exceedingly low levels of activity will also lead to excess ROS production. Second, dFB neurons accumulate a larger degree of ROS pressure than the surrounding brain. An apt analogy perhaps is that they act as canaries in a mine, where an increased exposure and sensitivity to ROS pressure would signal for sleep in order to alleviate the overall ROS load of the rest of the brain before it reached harmful levels.

The proposed operating model for ROS production within the dFB neuron's considers that the principal source of ROS derives from the mitochondria, specifically in the electron transport chain (ETC) [98]. During sleep, neuronal activity is high

and thereby confers a high-energy demand. This results in a high ADP:ATP ratio, as most ATP is quickly used up by the neuronal machinery to sustain firing. However, during wake and reduced activity this ratio reverses as the neuron becomes less active and the energy demand plummets. In these circumstances, the Krebs cycle is still operating at the same rate and feeding excess electrons into the ETC [98, 99]. This leads to a highly reduced population of coenzyme Q (CoQ) as electrons accumulate and causes the electron transport chain to stall [99, 100]. These electrons can then directly interact with local oxygen molecules to produce superoxide, which is then subsequently dismuted to the membrane-permeable hydrogen peroxide [100]. These electrophiles can interact locally with lipids to produce lipid-derived electrophiles (LDEs) such as LPPs (Fig. 1.6). This proposed mode of ROS generation gains strength considering that a variety of mitochondrial uncoupling proteins become elevated in mice following prolonged sleep deprivation, presumably as a protective measure against excess ROS production [101].

While superoxide (O_2^-) and hydrogen peroxide (H_2O_2) are theoretically able to directly interact with and oxidise NADPH, I propose that it is in fact more likely that further peroxidation with local membrane lipids takes place to produce LPPs such as 4-Hydroxynonenal (4-HNE) and the established $K_v\beta$ substrate 4-oxo-2-nonenal (4-ONE) [87], illustrated in Fig. 1.7. These possess a relatively longer half life and are thus more likely to reach Hyperkinetic at the plasma membrane [51]. Further, the substrate binding pockets of $K_v\beta$s are highly hydrophobic, favouring a lipid-based substrate [82]. Upon interaction with Hyperkinetic, they are metabolised using the NADPH cofactor as the electron donor, resulting in its oxidation to $NADP^+$. This in turn leads to slowed Shaker inactivation, presumably by delaying the entrance of the N-terminal inactivation peptide into the channel pore. This allows for more sustained I_A, which permits for an elevated rate of neuronal firing (Fig. 1.8)

Considering ROS load as a marker and a potential source of sleep pressure whose main source of ROS is mitochondrial electron slippage, by circumventing or counteracting this ROS production pathway, one should be able to reduce sleep

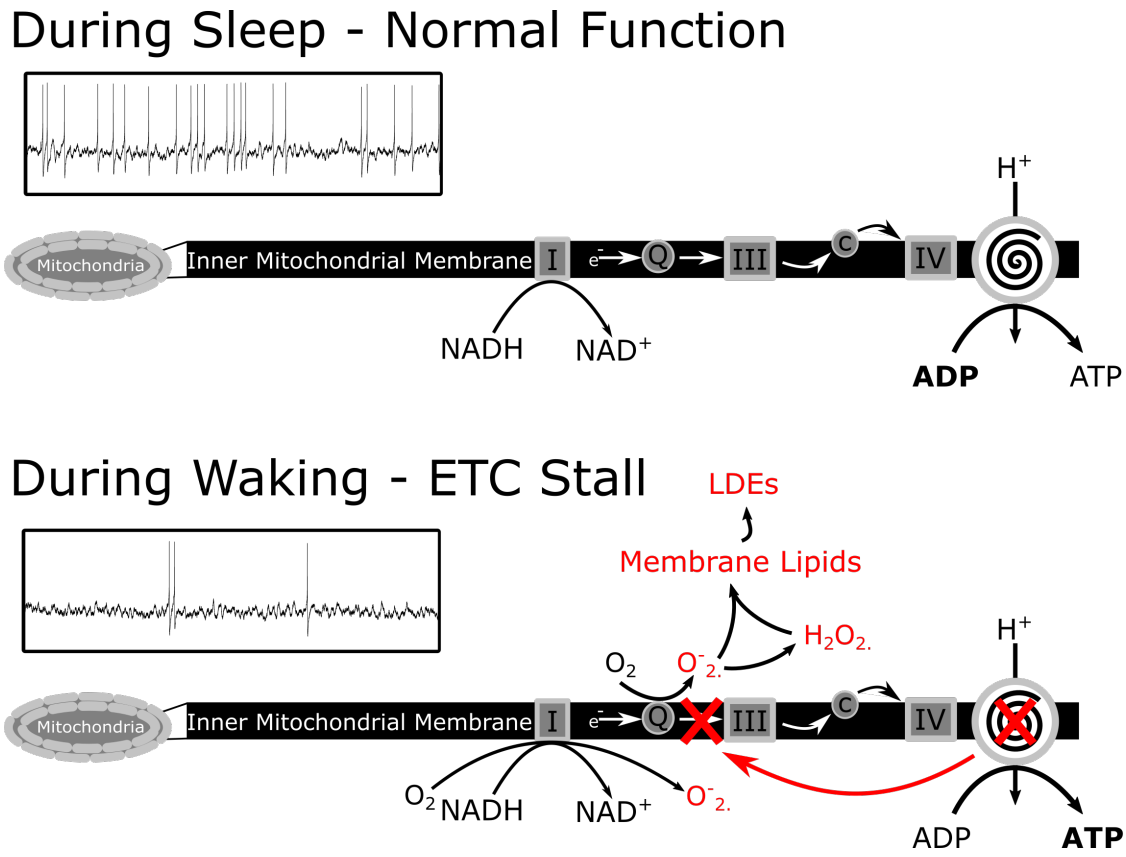


Figure 1.6: Model of ROS generation within the mitochondria of dFB neuron. During periods of sustained activity, where there is a high ADP:ATP ratio, little to no ROS is generated. However, during wake, the presence of a strong Sandman mediated K^+ leak, enforces electrical quiescence upon the dFB neuron. The resultant inactivity and low ATP demand leads to a reversal of the ADP:ATP ratio, where ATP is now the abundant form as little is used. Further, there remains a constant dropping-off of electrons to the ETC but inadequate supply of ADP to dissipate the protonmotive force built-up across the inner mitochondrial membrane. This causes the ETC to stall. The resulting over-reduced CoQ will then use alternate pathways to offload its electrons, mainly by interactions with local oxygens to produce superoxide [98, 99]. These interact locally with water to produce hydrogen peroxides. Either of these can further interact with local membrane lipids to produce LDEs, another form of ROS molecules [51].

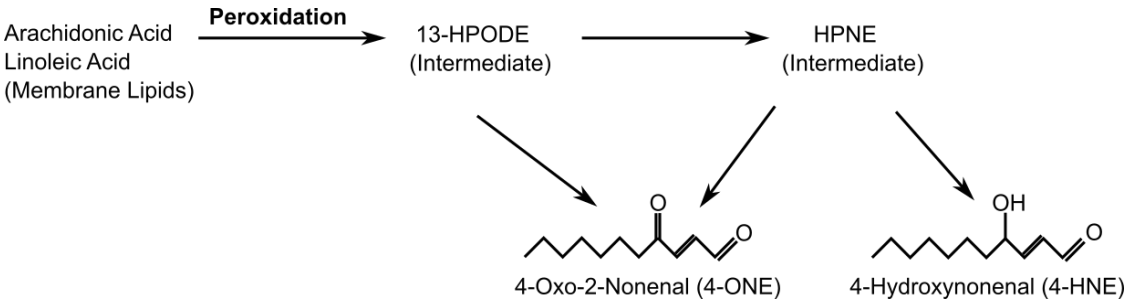


Figure 1.7: Adapted figure from [102] to show structure of 4-Hydroxynonenal (4-HNE) and 4-oxo-2-nonenal (4-ONE), derivates of lipid peroxidation of membrane lipids such as linolenic and arachidonic acid.

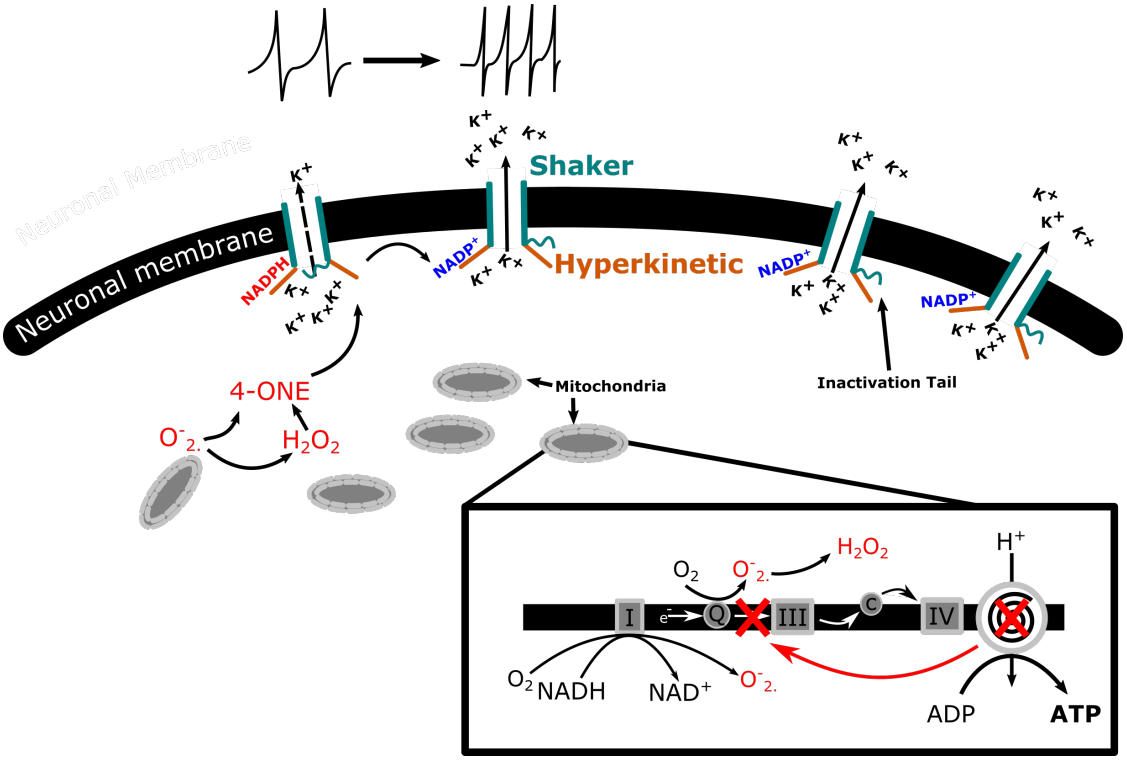


Figure 1.8: Model of ROS' interaction with Hyperkinetic. During wakefulness, sleep pressure is integrated in the form of ROS molecules. These likely take the form of LDEs such as 4-ONE due to their relative longevity and increased abundance during oxidative stress [51]. These molecules are metabolised by Hyperkinetic leading to the overall population of Hyperkinetic shifting to one bound to $NADP^+$. This slows the inactivation of the channel complex and permits for higher frequency firing and thereby sleep promotion.

pressure. Alternative oxidase (AOX) removes excess electrons from CoQ in the ETC and prevents superoxide formations [103]. Expression of AOX within the dFB neurons significantly reduces total sleep by up to 7 hours, strengthening the supposition that ROS pressure within the dFB neuron translates into sleep pressure [94]. Conversely, expressing the pro-oxidant SOD1(A4V) within dFB neurons had the opposite effect. Crucially, paired with the removal of Hyperkinetic, this pro-oxidant had no additional effect on sleep loss, showing that the likely route of effect of SOD1(A4V) is via Hyperkinetic [94].

Electrophysiological characterisation of the effects of these anti- and pro-oxidants showed a noticeable gap between inactivation time constants, where anti-oxidants had approximately half the Shaker inactivation time constants compared to pro-

oxidants [94]. Further, this correlated with dFB neurons expressing pro-oxidant exhibiting a significantly elevated action potential firing rate. Again, the opposite trend occurred with anti-oxidants [94]. A more direct application of ROS pressure utilised the genetically encoded flavoprotein mini singlet oxygen generator (miniSOG); miniSOG generates ROS in the form of singlet oxygen molecules ($^1O_2$) in response to blue light [104, 105]. Echoing the results of the pro-oxidant SOD1(A4V), miniSOG produced a strong, on-demand sleep promoting effect in flies when expressed exclusively in the dFB neurons. This effect was lost in the absence of functional Hyperkinetic and rescued when functional Hyperkinetic was expressed solely in the dFB neurons [94]. Furthermore, the biophysical characteristics of Shaker inactivation following miniSOG stimulation also showed sluggish inactivation. This was also paired with an increased firing rate [94]. Due to the relatively ubiquitous expression of Hyperkinetic it is likely that there is some degree of ROS sensitivity in other areas of the *Drosophila* brain. However, due to the demonstrated role of ROS and Hyperkinetic specifically in dFB neurons in a sleep context [94], it is likely that dFB neurons represent, if not the only, one of the major ROS sensors to promote sleep.

These experiments conclusively linked ROS and the Shaker:Hyperkinetic channel complex to dFB neuronal activity and subsequent sleep promotion. A few interesting considerations are drawn from this study [94]. First, considering the exceedingly slow co-factor exchange rate, it is likely that even transient exposure to ROS forms a long-lasting biochemical memory in the form of stably bound $NADP^+$ and altered Shaker kinetics. This allows the Hyperkinetic population within the dFB neuron to integrate daily ROS strain to promote sleep to different degrees, the intensity of sleep promotion determined by the overall proportion of $NADP^+$ bound Hyperkinetic as the resulting neuronal firing rate would be set by the altered Shaker inactivation. If ROS therefore is the main drive of sleep pressure, in the two-process model this gradual integration of cumulative ROS strain represents the rising phase in homeostatic pressure (Fig. 1.1). The degree of pressure would produce a corresponding degree of channel modulation, resulting in a compensatory

change in the intensity and duration of sleep. This homeostatic pressure must return to baseline during sleep, however. I hypothesise that this is achieved by bidirectional coupling of the enzymatic activity of Hyperkinetic and the electrical activity of the dFB neurons. In this model, during electrical quiescence (that is, during waking), the co-factor's release is impeded. During sleep, when dFB neurons are assumed to be more electrically active, action potential driven rearrangements of the channel would open an escape path for $NADP^+$ and allow for its exchange.

1.5 Hypothesis and aims

In this thesis I therefore propose that Hyperkinetic monitors the oxidative state of the cell via oxidative signalling conveyed by LPPs. The breakdown of these products by Hyperkinetic oxidises its NADPH co-factor leading to slower Shaker inactivation which is more permissive for persistent neuronal activity. The baseline activity is restored via action potential driven rearrangement of the $NADP^+$ binding site during sleep. This allows for the expulsion of $NADP^+$, rebinding of the >20-fold more abundant NADPH and a return to baseline Shaker inactivation.

In this project, I therefore aimed to answer 4 central questions:

1. Can I use potential physiological substrates (such as 4-ONE) of Hyperkinetic to influence the inactivation of the Shaker channel complex?
2. Can these effects (if any) be constrained to the action of the catalytic site of Hyperkinetic?
3. Is it possible to reverse the effects of oxidative substrates via intermittent, brief depolarisations that mimic an action potential train?
4. Do Hyperkinetic substrates influence the overall spiking dynamics of the cell?

2

Oxidative By-products and Hyperkinetic

Contents

2.1 Introduction 31
2.2 miniSOG photostimulation significantly slows Shaker inactivation 33
2.3 Intracellular 4-ONE slows Shaker inactivation 34
2.4 The effects of 4-ONE are Hyperkinetic dependent . . 40
2.5 Summary 43

2.1 Introduction

That Hyperkinetic constitutes a functional enzyme has been known for over a decade [85, 86, 106]. However, these studies were constrained to in-vitro systems and did not pursue the actual purpose as to why this catalytic activity existed beyond the suggestion that it may have a role as a sensor of oxidative products. As outlined in the introduction, the ROS sensitivity was recently verified in dFB neurons [94]. However, as one would expect, artificial genetically introduced constructs are an unlikely source of physiological ROS; LPPs are more stable and relevant as ROS-derived signalling molecules than the short-lived ROS themselves. These therefore make a suitable candidate for potential physiological messengers of ROS pressure

[51]. 4-ONE is one member of this class of molecules. It forms as a further oxidation product of another LPP, 4-Hydroxynonenal (4-HNE), which in turn arises through radical oxidation of local polyunsaturated membrane lipids. While structurally similar, 4-ONE is up to ten times more reactive [51]. These molecules are estimated to be present in the low to sub-micromolar range in basal physiological conditions, but significantly increase in prevalence during periods of oxidative stress [107]. 4-HNE produces generally cytotoxic effects in concentrations above approximately 200 μM but can achieve more specific effects e.g. DNA damage at lower concentrations [107]. 4-ONE is estimated to be present at lower physiological concentrations than 4-HNE, presumably due to its higher reactivity [51]. However, it is important to note that a high degree of variability in both stability and relative abundance exists between different tissue types so 4-ONE's prevalence and role as a messenger may vary depending on physiological context [51]. A distinction between 4-ONE and 4-HNE pertinent to this project is that only 4-ONE has any demonstrated affinity for $K_v\beta$. 4-HNE, at the same concentrations, has no detectable activity in the presence of $K_v\beta$ [87]. Therefore, we expect little interaction with Hyperkinetic as well.

In this chapter I therefore set out to confirm previously published electrophysiological results using miniSOG [94] and corroborate the ROS integrating capabilities of the Shaker:Hyperkinetic complex. Whether these results could be replicated using a potential physiological substrate, namely 4-ONE was then explored. Additionally, if any effects were observed, could these be constrained specifically to the catalytic action of Hyperkinetic?

While 4-ONE is a potential substrate that this project focuses on, it remains just that, a *potential* substrate. The actual substrate may be a related molecule to 4-ONE or more likely, envelops a larger family of several ROS molecules of which 4-ONE is a member.

2.2 miniSOG photostimulation significantly slows Shaker inactivation

Expressing and stimulating miniSOG within dFB neurons had a marked effect on the neuronal activity and channel kinetics [94]. Blue light photostimulation of miniSOG creates a sizeable ROS strain within the neuron and causes oxidation of the NADPH cofactor within the Hyperkinetic subunit and slows the inactivation of the Shaker ion channel complex according to previously published work [94]. To confirm this observation and reinforce the notion that dFB neurons can integrate ROS pressure via altered channel kinetics, the miniSOG protein was selectively expressed in dFB neurons and illuminated the cells with stimulating blue light. Patch clamp experiments were guided by expressing GFP under the dFB-specific R23E10 Gal4 driver. miniSOG was also expressed using this driver to achieve specificity to the dFB neurons.

Activation of miniSOG using blue light created a marked increase in both the fast (τ_1) and slow (τ_2) time constants of A-type current (I_A) inactivation when compared to the inactivation observed just after break-in (t=0 in Fig. 2.1B & C). In contrast to previous publications though there was a small run-down in the peak I_A amplitude before and after miniSOG photostimulation (Fig. 2.1D). Further, previous publication show a significant increase in the membrane resistance (R_m) following photostimulation, this was not observed in these experiments (Fig. 2.1E) and the membrane resistance remained relatively constant throughout the recording. This membrane resistance seen with miniSOG also proved to be noticeably lower to other genotypes (e.g. Fig. 2.3C). Baseline inactivation time constants also appeared slightly elevated compared to previous publication [94] and also subsequent experiments without miniSOG perhaps indicating some premature activation, perhaps from natural light or unintentional activation of miniSOG while visualising GFP. This may also explain why no increase in R_m was observed as this change had already occurred prior to recording. Nevertheless, a significant increase

in the inactivation constants was still observed in-line with previously recorded experiments [94].

2.3 Intracellular 4-ONE slows Shaker inactivation

Having demonstrated miniSOG significant effect on Shaker inactivation and confirmed the role of ROS in the channel's modulation, whole cell voltage clamp electrophysiological trial experiments were then performed. These used a variety of supplements added directly to the intracellular pipette solution. Upon achieving whole cell mode, a period of 10 minutes was used to allow for diffusion throughout the neuron and metabolism of any substrates. Our experimental groups included the LPPs 4-ONE and 4-HNE. Further, controls included normal intracellular solution with no additional supplements (Normal) and the vehicle for the LPPs, 0.15% methyl acetate (MeAc).

Similar to the miniSOG results, 4-ONE inclusion produced a prominent trend towards increased inactivation time, with very little change in either of the control groups (Fig. 2.2A). Furthermore, individual voltage clamp experiments showed a dramatic change in the overall inactivation curve in response to 4-ONE (Fig. 2.2B). 4-HNE elicited no change over the time course of the experiment, suggesting that 4-ONE's effects are specifically due to its interaction with Hyperkinetic as 4-HNE is a reactive LPP which has no affinity for $K_v\beta$. However, off-target effects which may impact recorded results could not be wholly ruled out by this specific experiment, as 4-ONE is more reactive than 4-HNE and the results may in-fact reflect this instead of Hyperkinetic specificity. While this experiment did not reach significance with relatively low sample size, it did set the stage for an encouraging substrate to use for subsequent experiments as a hyperkinetic substrate and a potential conveyor of sleep pressure.

Further characterisation of the effects of 4-ONE revealed that the increase to inactivation time constants was both reproducible and significant. After 10 minutes

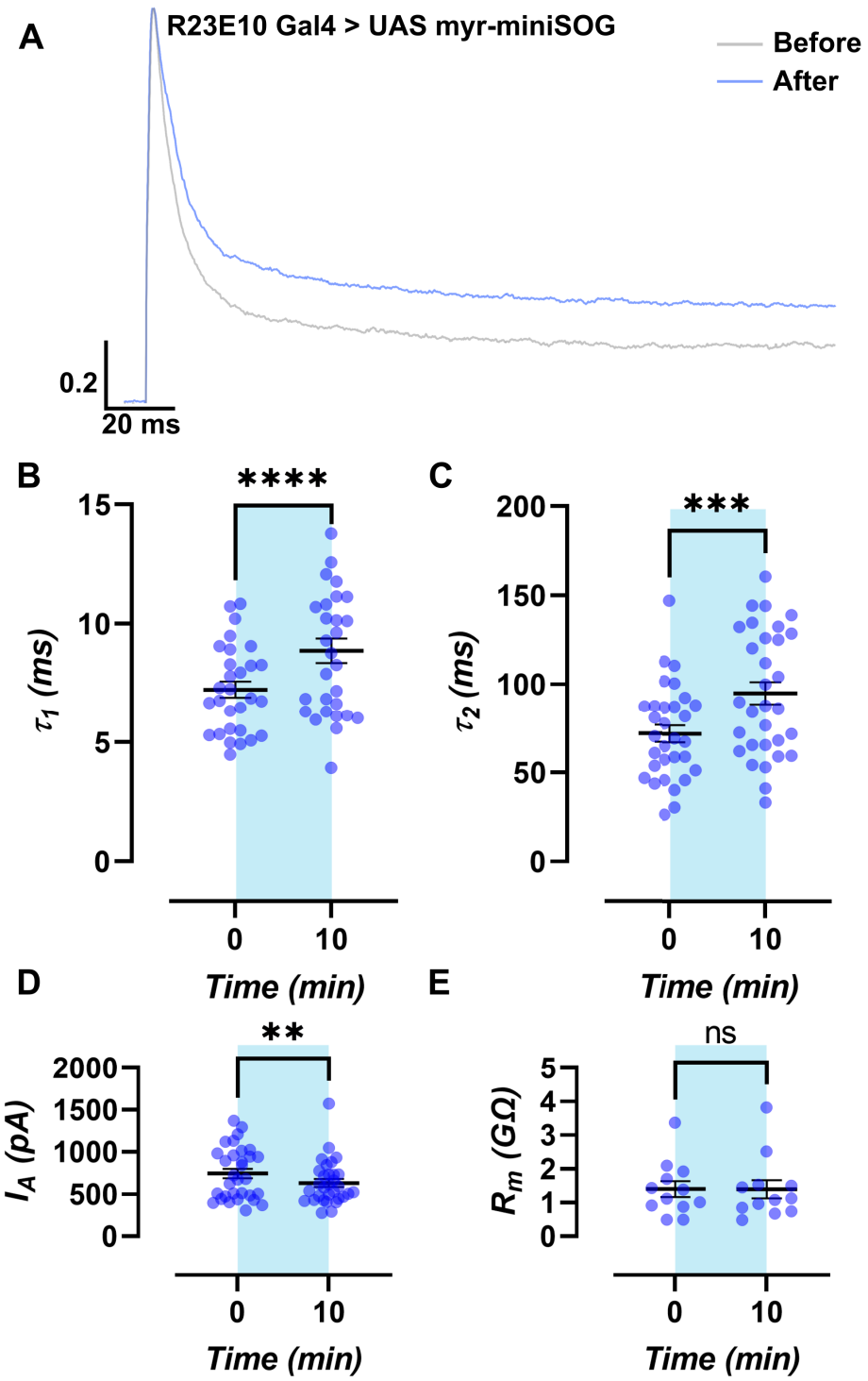


Figure 2.1: Characterisation of dFB neurons expressing the ROS generating miniSOG before (0 min) & after (10 min) photostimulating blue light. Blue background indicates time when blue light was on. **A** Representative normalised trace of I_A current inactivation profile before and after miniSOG stimulation **B** Fast inactivation time constants (τ_1) of I_A in response to miniSOG stimulation, n=29, **C** Slow inactivation time constants (τ_2) of I_A in response to miniSOG stimulation, n=28 **D** Peak I_A measured at the largest depolarising step, n=12 **E** Membrane resistance (R_m) derived from linear fits of the current-voltage relationship, n=12. Bars are mean±SEM. Paired Student's t-test *=p<0.05, **=p<0.01, *** = p<0.001, **** = p<0.0001, ns = no significance.

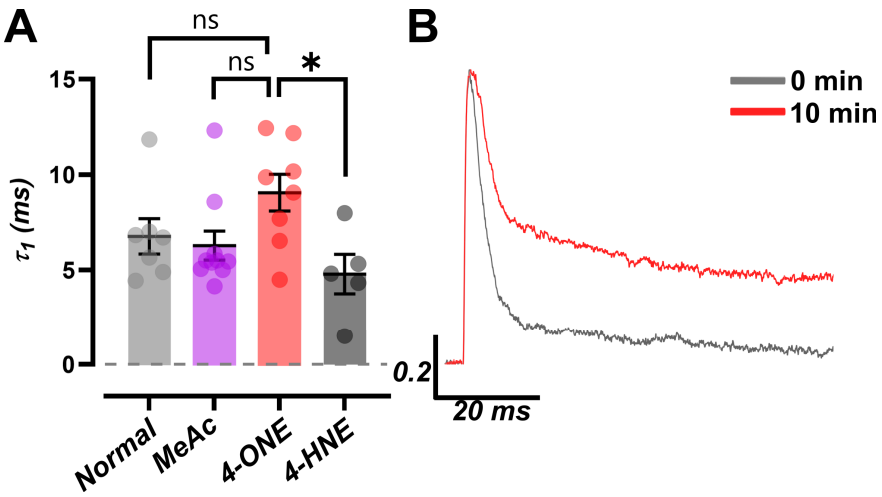


Figure 2.2: **A** Patch clamp experiments quantifying inactivation, τ_1 using potential Hyperkinetic substrates. Bars are mean ± SEM. Data were recorded from dFB neurons after 10 minute of intracellular exposure to an intracellular supplement. **B** Representative normalised trace showing inactivation profile before and after 10 minutes of intracellular 4-ONE exposure in the same neuron. For Normal, MeAc, 4-ONE and 4-HNE groups n= 6, 10, 8 and 5 respectively. One-way ANOVA Tukey's post-hoc. * = p< 0.05, ns = no significance.

4-ONE showed a strong increase in τ_1 (Fig. 2.3A) and an increasing, yet non-significant trend in τ_2 (Fig. 2.3B). Importantly, when merely holding the cell at -80 mV with no further intervention, τ_1 inactivation continues to rise and plateaus between 10 and 20 minutes, with the lion's share of change occurring within approximately the first 10 minutes (Fig. 2.3A). The second, slower time constant of inactivation showed a strong (albeit non-significant) slowing trend throughout the experiment, with a slight lag compared to the increase seen in τ_1 (Fig. 2.3B). There was little to no change in the membrane resistance (Fig. 2.3C). The membrane time constant (τ_m) showed a slight downward trend, however this remained small and non-significant throughout the experiment (Fig. 2.3D). During these extended voltage-clamp recordings, a noticeable drop in numbers occurred over the time-course of the experiment owing to cell death or excessive access resistance drift. These cells were still included in the earlier time-points though and in the case of access resistance, were within acceptable limits.

Further characterisation of the dFB neurons' electrical properties showed that the prominent shaker current exhibited possessed a half-activation and half-inactivation

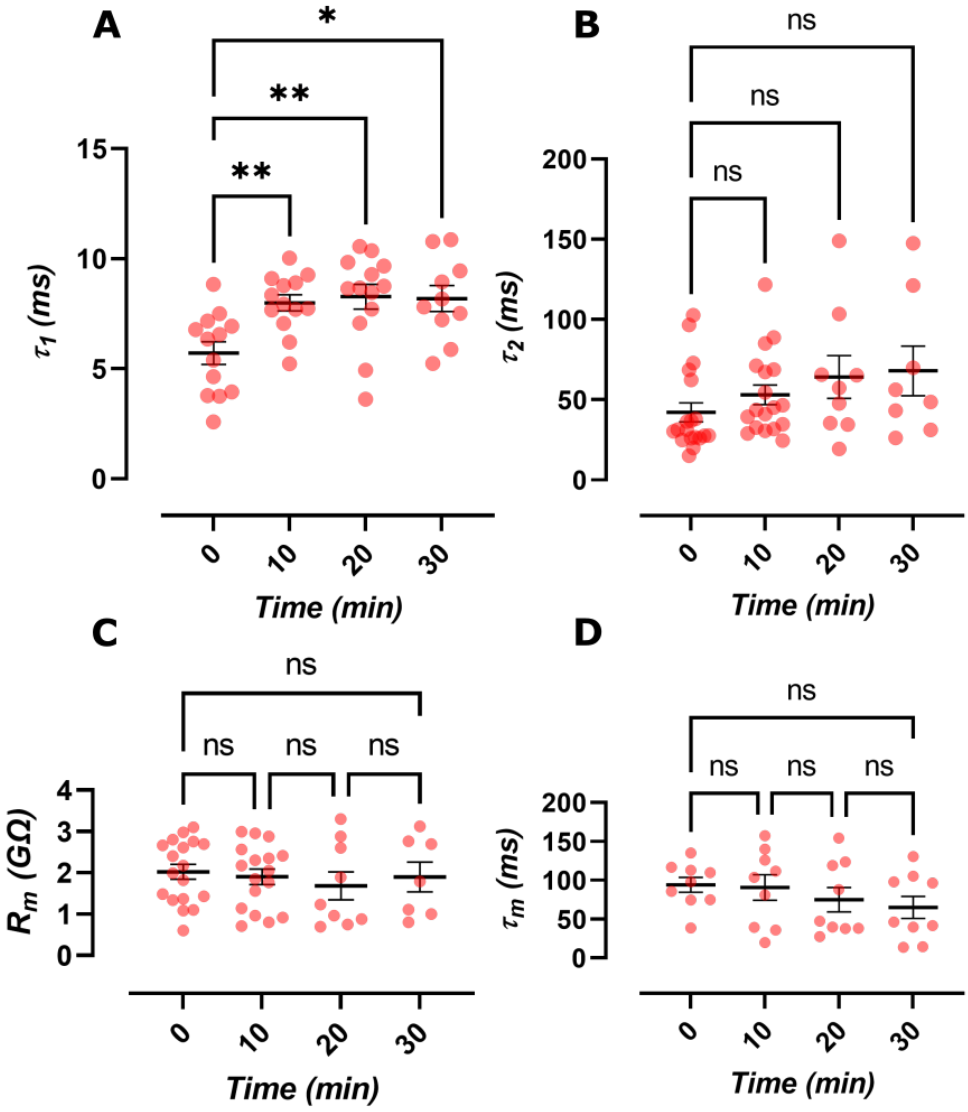


Figure 2.3: Characterisation of the effects of intracellular 4-ONE on dFB neurons. Time-points represent time elapsed since whole-cell mode was achieved. **A** Fast inactivation time constants (τ_1) of I_A in the continuous presence of 4-ONE, n= 20-9 across time-points **B** Slow inactivation time constants (τ_2) of I_A in the continuous presence of 4-ONE, n=19-9 **C** Membrane resistance (R_m) derived from linear fits of the current-voltage relationship in the presence of 4-ONE, n=18-7 **D** Membrane time constant (τ_m), derived from single exponential fits to the decay of depolarising currents, n=18-7. Mixed-effects analysis with Tukey's post hoc * = $p<0.05$, ** = $p<0.01$, ns = no significance.

voltage of -35.04 mV and -8.10 mV at baseline, respectively (Fig. 2.4A). The half-inactivation voltage remained arguably constant after 30 minutes of exposure to 4-ONE (-35.04 to -40.12 mV). However, the half-activation voltage did see some drift towards activation at more hyperpolarised voltages, with a half activation value of -15.42 mV (from -8.10 mV). A small caveat in the half-activation voltage values is that the curve does not plateau at the hyper- and depolarised value which makes estimating a precise figure less accurate. Nevertheless, for the purpose of clarifying any 4-ONE related changes, it is sufficient.

Quantifying the isolated I_A and I_{Non-A} showed that I_{Non-A} was largely unaffected by the exposure to 4-ONE and showed very little variance across all time-points, reinforcing the notion that 4-ONE is producing relatively low levels of off-target effects. However, consistent with the drop-off seen in the peak amplitude of I_A following miniSOG stimulation, there is a clear rundown of measured I_A with time (Fig. 2.4B).

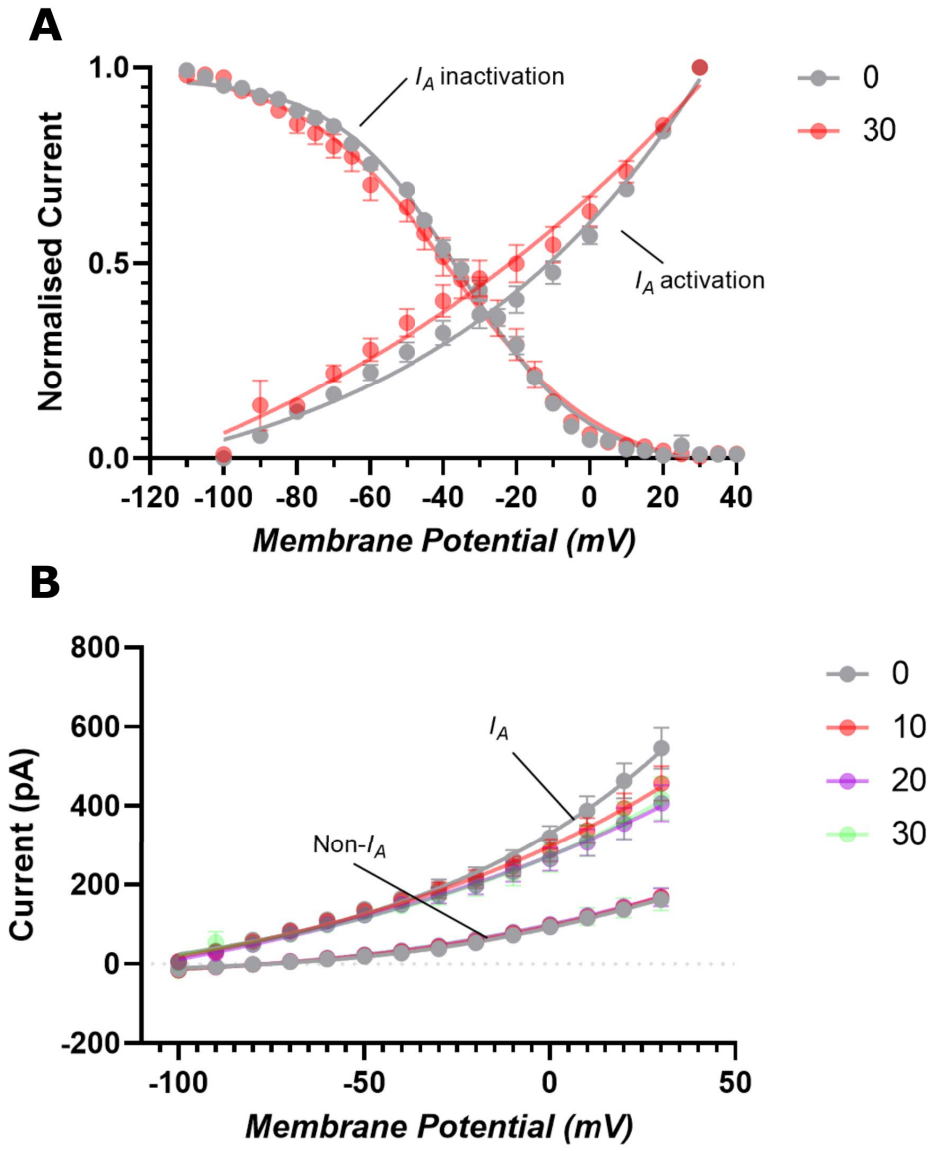


Figure 2.4: Characterisation of the effects of intracellular 4-ONE on dFB neurons. Time-points represent time elapsed since whole-cell mode was achieved. Curves were fitted using the Boltzmann function. Values are mean±SEM, n=21 **A** Activation and inactivation kinetics of Shaker in the dFB neuron at baseline (0) and after 30 minutes (30). Currents are normalised to maximum value individually for each cell **B** Characterisation of I_A and I_{Non-A} amplitude over time.

2.4 The effects of 4-ONE are Hyperkinetic dependent

While these early results showed promise, it was important to constrain this effect to the metabolism of the 4-ONE by Hyperkinetic as opposed to an off-target interaction. To confirm this, functional (Hk^{WT}) or catalytic null mutants (Hk^{K289M}) were introduced into a Hyperkinetic null (Hk^{1}) background. If the effects are specific to Hyperkinetic, then the catalytic null rescue should not be able to metabolise 4-ONE and thus not cause a shift of bound NADPH to $NADP^{+}$ and that could alter the inactivation kinetics. Conversely, the functional Hyperkinetic rescue would be expected to replicate the earlier 4-ONE results (Fig. 2.3).

Whole cell patch clamp experiments of dFB neuron expressing the catalytic null mutant Hk^{K289M} showed no significant change over the same time course as previous experiments (Fig. 2.5A & B) regarding both fast and slow components of the inactivation. However, consistent with previous experiments this also showed a steady trend of decay in I_{Non-A} amplitude (Fig. 2.5E) suggesting that this occurs independently of any interaction with Shaker:Hyperkinetic ion channel complex. It is unlikely that this change is a mere artefact brought on by changes to the patch resistance considering that the membrane resistance (R_m) of the patch remains stable throughout (albeit admittedly with a degree of scatter) and with access resistance was monitored throughout.

Re-introducing a functional Hyperkinetic in lieu of the catalytic null mutant yielded further evidence for the specificity of the effects of 4-ONE for Hyperkinetic. dFB neurons expressing this functional variant completely restored the effects of 4-ONE on the inactivation time constants (Fig. 2.6A & B). Similar to the catalytic null experiment, this exhibited a slight yet consistent decay of I_A amplitude over the course of the experiment (Fig. 2.6D). The input resistances remained constant over the course of the experiments (Fig. 2.6C).

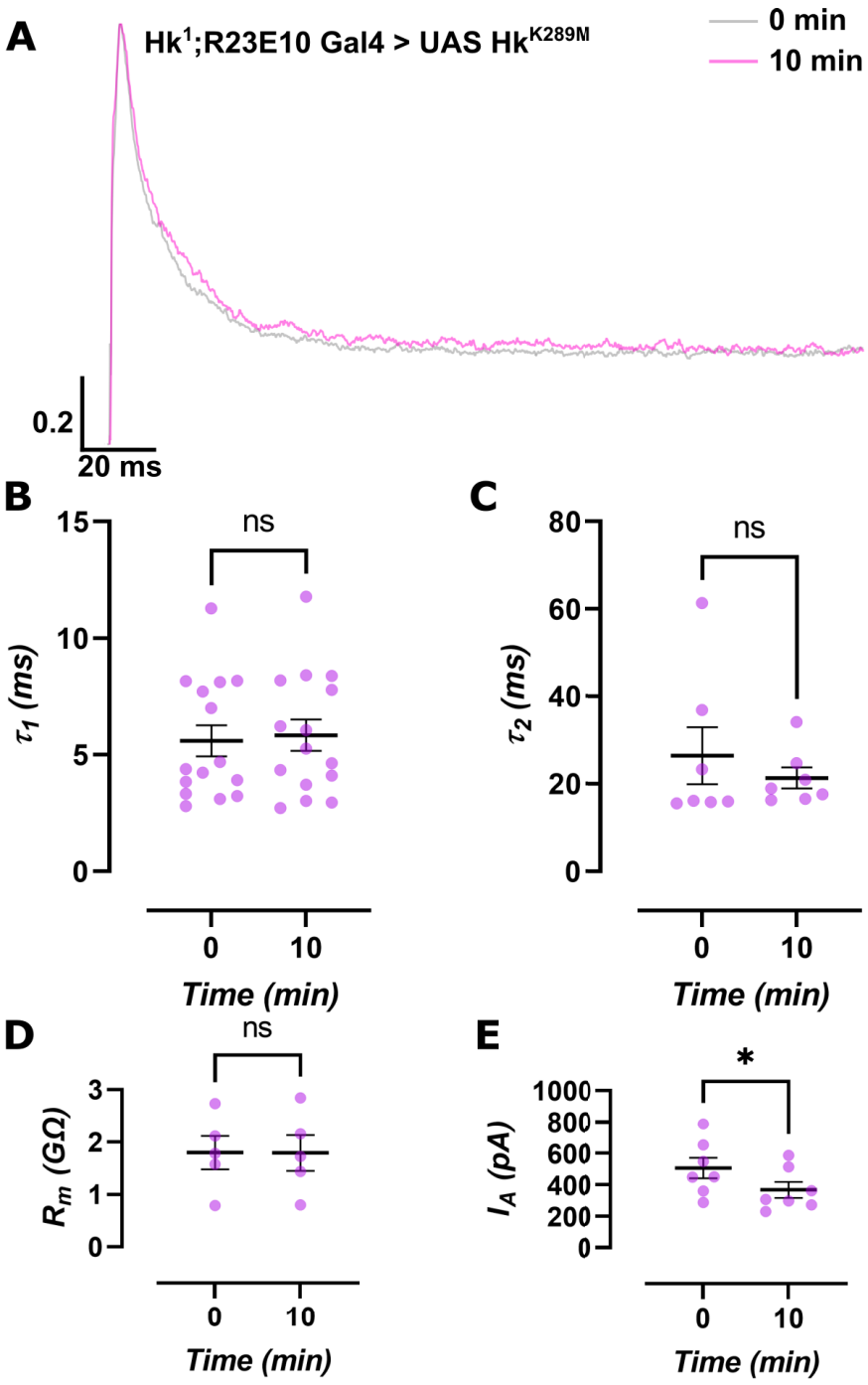


Figure 2.5: Characterisation of electrophysiological properties of dFB neurons expressing a catalytic null variant of Hyperkinetic (Hk^{K289M}) on a Hyperkinetic null background (Hk^1) before and after 10 minutes of intracellular exposure to 4-ONE. **A** Representative normalised trace of I_A before and after 10 minutes of intracellular exposure to 4-ONE in dFB neurons equipped with catalytic null mutants of Hyperkinetic **B** Fast inactivation time constants (τ_1) of I_A, n=15 **C** Slow inactivation time constant (τ_2) of I_A, n=7 **D** Membrane resistance (R_m) extracted from the current-voltage relationship, n=5 **E** Peak I_A measured at the largest depolarising step, n=7. Bars are mean±SEM. Paired Student's t-test * = $p< 0.05$, ns = no significance.

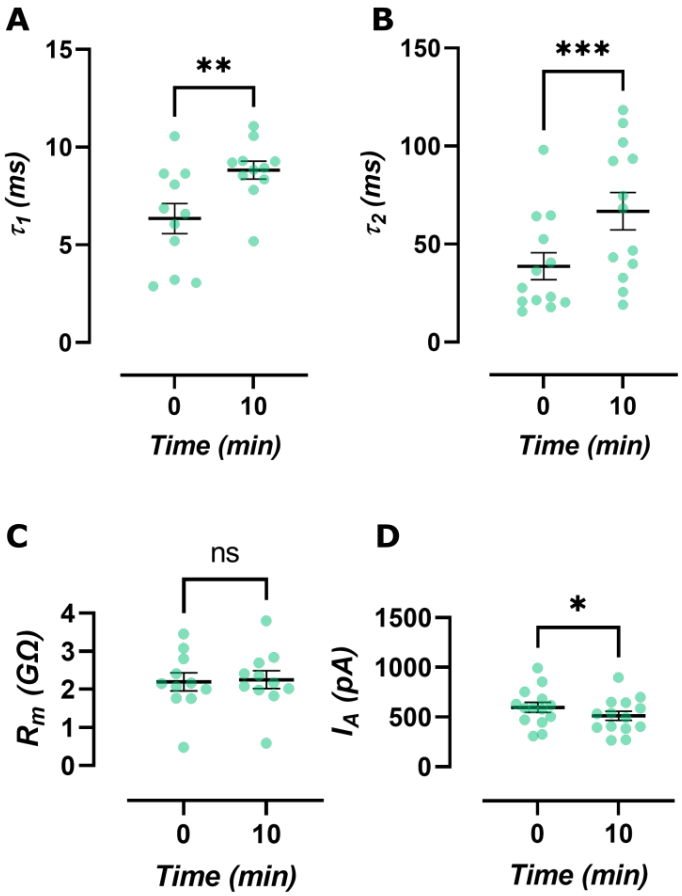


Figure 2.6: Characterisation of electrophysiological properties of dFB neurons expressing a functional variant of Hyperkinetic on a Hyperkinetic null background before and after 10 minutes exposure to intracellular 4-ONE. **A** Fast inactivation time constants (τ_1) of I_A in response to 4-ONE, n=11 **B** Slow inactivation time constant (τ_2) of I_A, n=13 **C** Membrane resistance (R_m) extracted from the current-voltage relationship, n=12 **D** Peak I_A measured at the largest depolarising step, n=13. Bars are mean ± SEM. Paired Student's t-test *** = p< 0.01, **** = p< 0.0001, ns = no significance.

2.5 Summary

In this chapter, I confirmed the efficacy of both 4-ONE and miniSOG on affecting the inactivation of the Shaker:Hyperkinetic channel complex thereby supporting the case that Shaker and Hyperkinetic integrate ROS strain in multiple forms which echoes in the form of slowed channel inactivation. While this has been shown to some extent before in simplified systems [85–87], these experiments represent only the second time this has been performed in-vivo and the first time using potential physiological substrates as opposed to solely using artificial genetic constructs [94]. While the τ_1 and τ_2 time constant are typically inferred to represent N-type and C-type inactivation respectively (also known as the fast and slow component), due to the high degree of overlap of kinetics between the two forms it would be unsuitable to excessively attempt to tease either component apart based purely on these results [63]. However, previous experiments using the oxidative substrate 4-CY on Shaker ion channel complexes including mutated forms of $K_v\beta$ showed that an intact N-terminus was required for the response to oxidative stress on inactivation [106]. It is thus with a degree of certainty that I can conclude excessive intracellular ROS loads significantly slow the Shaker ion channel complex' inactivation as suggested in previous publications, with the main effect likely due to altered kinetics at the N-terminal ball and chain motif [106, 108]. Nevertheless, the possibility of some interaction with the C-terminal inactivation domain can not be wholly ruled out.

The exact mechanism of Hyperkinetic's NADP(H) cofactors control over the channel complex is unknown [86]. However, gradual introduction of amino acid substitutions in the $K_v\beta$ N-terminal outlined 2 small segments that when mutated exhibited a nigh-abolished sensitivity to the redox state of the cofactor; this was termed the redox regulation sequence (RRS) [86]. Specifically, two glutamate-arginine pairs within the RRS were determined as the leading determinants of the effect of NADP(H) redox [86]. In the $NADP^+$ state these pairs interact and restrain the inactivation peptide and hinder channel block hence slowing overall inactivation time [86]. However, this hypothesis comes from mammalian $K_v\beta1$ which in contrast

to Hyperkinetic, possesses its own N-terminal inactivation chain and it is with this tail that the proposed Tail-RRS interaction occurs. Whether the same or a similar mechanism occurs in the case of the Shaker-Hyperkinetic ion channel complex where the N-type inactivation is solely conferred by Shaker's N-terminal is uncertain. It is not unfeasible that the same interaction can occur across proteins i.e. glutamate residues from Hyperkinetic become mobilised/shift due to the oxidation of the NADP(H) and interact with Arginines at the N-inactivation chain of the Shaker protein to restrain inactivation similarly. Especially when considering that the essential glutamate amino acids are conserved between $K_v\beta 1$ and Hyperkinetic [62].

The extended exposure (30 minutes) of dFB neurons to intracellular 4-ONE showed a strong and sustained effect. An integral observation here is that the initial change to inactivation time constants showed no signs of either slowing down or reversing over time, arguing for a prolonged integration of ROS by the channel complex.

The null effect produced by 4-ONE on the catalytically deficient mutant confirmed the suspected specificity of ROS' ability to slow inactivation to the catalytic activity of Hyperkinetic. This is strengthened by the observation that a proven non-compatible substrate such as 4-HNE, an otherwise reactive molecule, had no effect. Further, it is encouraging to observe that, even at elevated concentrations, 4-HNE had no apparent effects despite the risk of off-target effects or direct amino acid modification of the Shaker channel. A common concern while using ROS products in the presence of K_v ion channels are cysteine modifications. These are known to also impact inactivation time constants independent of $K_v\beta$ activity. However, in the case of Shaker this becomes irrelevant due to the non-conservation of these commonly modified cysteines in the *Drosophila* variant [109]. Furthermore, the interaction between $K_v\beta$ and oxidative benzaldehydes are known to be specific to the AKR core and there is no interaction in its absence [86]

The rundown of I_A amplitude was unexpected as previous studies demonstrate that slowed inactivation resulted in a significant increase in current size [85, 86]. A

distinct difference between previous studies and the presented data is the expression system where the environment may impact the recorded effects. Previous studies used *Xenopus laevis* oocytes as a relatively pure expression vessel with little to no other A-type K_v channels present. However, isolating a current in the complexities of the dFB neuron would always present more of a challenge. Beyond the obvious Na^+ and Ca^{2+} channels that can be blocked using toxins, dFB neurons likely express other A-type channels e.g. Shal which have the potential to skew the resultant I_A profile [38]. Considering the lack of effect using catalytic null mutant Hk^{K289M} on the inactivation time constant but the rundown remaining (Fig. 2.5), it is unlikely that the altered kinetics on other channels had any effects on the inactivation changes and also previously published changes to firing rate which were abolished in the absence of functional Hyperkinetic [94]. Furthermore, in the context of sleep regulation, RNAi screens show that dFB neurons expressing $Shal^{RNAi}$ had no effect on sleep, in stark contrast to flies expressing $Shaker^{RNAi}$ where a significant decrease in sleep was observed, reinforcing Shaker's dominant role among the A-type channels in conveying sleep pressure [38]. A simple but perhaps unsatisfying answer to the varying degrees of rundown may come down to simply variations in patch quality and perhaps a non-perfect solution composition. Regardless, while the rundown of I_A amplitude may involve multiple channel types, considering the $Hk K289M$ results and Shaker's prominent role in sleep regulation, it is highly likely that 4-ONE's effect on inactivation is specific to Shaker, especially when considering that Hyperkinetic interacts solely with Shaker and not any of its homologues e.g. Shal, Shab [110]

3

Effects of oxidative by-products are reversible by simulated spiking

Contents

3.1 Introduction **47**
3.2 Simulated spiking facilitates NADP(H) cofactor exchange of Hyperkinetic **48**
3.3 Reversal of Shaker inactivation kinetics by simulated spiking require Hyperkinetic **52**
3.4 Summary **55**

3.1 Introduction

Previous experiments have shown a correlation between altered I_A inactivation time with increased firing in the dFB neurons [94]. Considering 4-ONE's effects on I_A inactivation, 4-ONE should have the same effect on neural activity. It has been proposed that the enzymatic rate of Hyperkinetic is potentially voltage sensitive and intermittent depolarisation resulting from increased firing could give rise to a voltage driven conformational change that facilitates NADP(H) co-factor exchange [82, 86]. Cellular $NADP^+$:NADPH ratio is typically weighted towards the reduced NADPH form [111]. In view of this, any increased turnover of cofactor exchange would be

expected to shift the overall Hyperkinetic population into the NADPH-bound form with "normal" fast inactivation and reverse any shift caused by previous oxidative strain.‘

In this chapter, I attempted to reverse the effects of miniSOG and 4-ONE, by driving simulated spiking reminiscent of the increase in action potential firing expected from the altered channel inactivation. In these experiments, the dFB neurons are exposed to oxidative products via either direct intracellular 4-ONE application or miniSOG stimulation. As a result of this, Shaker inactivation is slowed as demonstrated in the previous chapter. Following this, if the proposed voltage sensitive cofactor exchange hypothesis proves correct, then prolonged membrane depolarisation will mediate cofactor exchange and return the inactivation time constants closer to those seen immediately after patch break-in where presumably the majority of the Hyperkinetic pool is bound to NADPH (illustrated in Fig.3.1).

3.2 Simulated spiking facilitates NADP(H) cofactor exchange of Hyperkinetic

The first set of experiments sought to confirm the results seen previously using 4-ONE, where exposure to Hyperkinetic produced an increase in Shaker inactivation. This effect was reproduced in the next set of experiments, where a significant increase was seen after 10 minutes of intracellular exposure. This was true for both the fast and slow time constants (Fig. 3.2B & C). However, in contrast to previous experiments with no depolarisation (Fig. 2.3B & C), a significant reduction in inactivation occurred after simulated spiking between the time-points of 10 and 30 minutes. This depolarisation protocol effectively reset the time constants to those seen immediately after break-in to the point that there was no significant difference between time-points 0 and 30 minutes (Fig. 3.2B & C).

There were still some similarities between the two experiments, notably the strenuous depolarisation protocol did not appear to affect the membrane time constant (Fig. 3.2E) nor the membrane resistance (Fig. 3.2F).

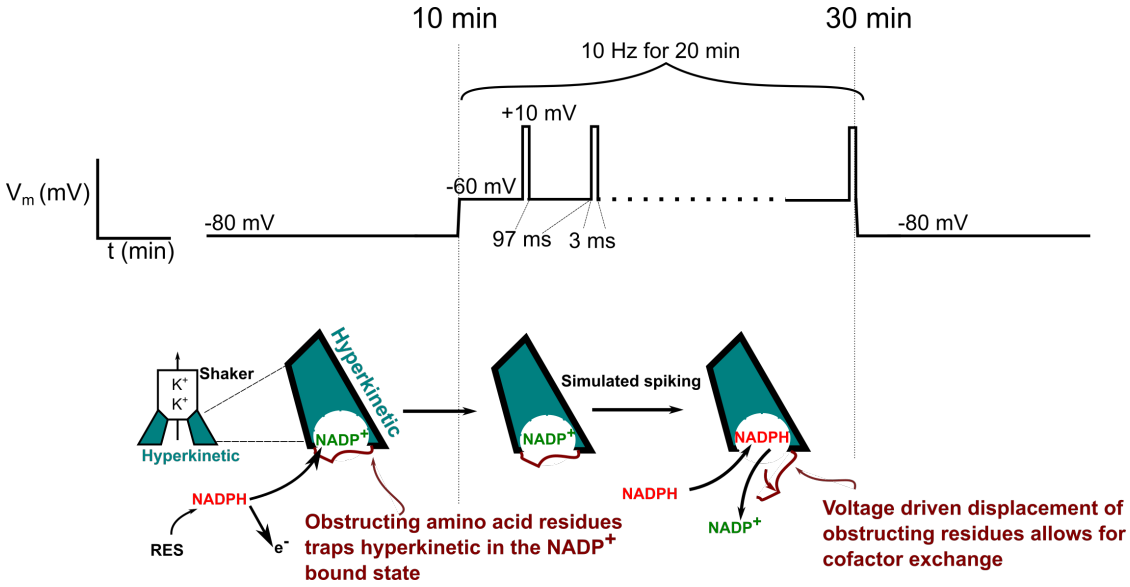


Figure 3.1: Illustration of proposed protocol and hypothesis of voltage driven reversal of ROS-derived changes on the Shaker-Hyperkinetic ion channel complex. In whole-cell mode, 10 minutes of exposure to RES (either 4-ONE or miniSOG-derived ROS) will drive Hyperkinetic into the $NADP^+$ state. This will form a long-lasting effect due to key amino acids blocking the NADP(H) escape route and thus making co-factor exchange exceedingly slow. After 10 minutes, application of a 20-minute simulated spiking protocol consisting of a 97 ms -60 mV baseline interrupted by 10 Hz 3 ms pulses to +10 mV will hypothetically cause voltage driven rearrangement of Hyperkinetic to free up an escape route and allow co-factor exchange with the much more abundant reduced NADPH form and thus resetting the ion channel kinetics.

Despite the reduction in inactivation time following depolarisation, the immediate environment of the Shaker:Hyperkinetic channel complex would still contain a relatively large amount of 4-ONE. If allowed to metabolise this 4-ONE without further depolarisation, the inactivation time constant should return to an elevated state. While in this particular example significance was not reached ($p = 0.09$ for the fast component), there was a clear trend present and with a larger sample significance is likely to be reached.

Similar to previous experiments, there was a noticeable drop-off in sample size as time went on in these long-term experiments. Furthermore, the 20 minute long depolarising protocol proved strenuous. Thus, it became difficult to maintain a high quantity of cells to a high degree of patch quality and thus a fair proportion of cells had to be excluded or were outright lost after a certain time-point as their input

resistance, access resistance or holding current drifted beyond acceptable limits.

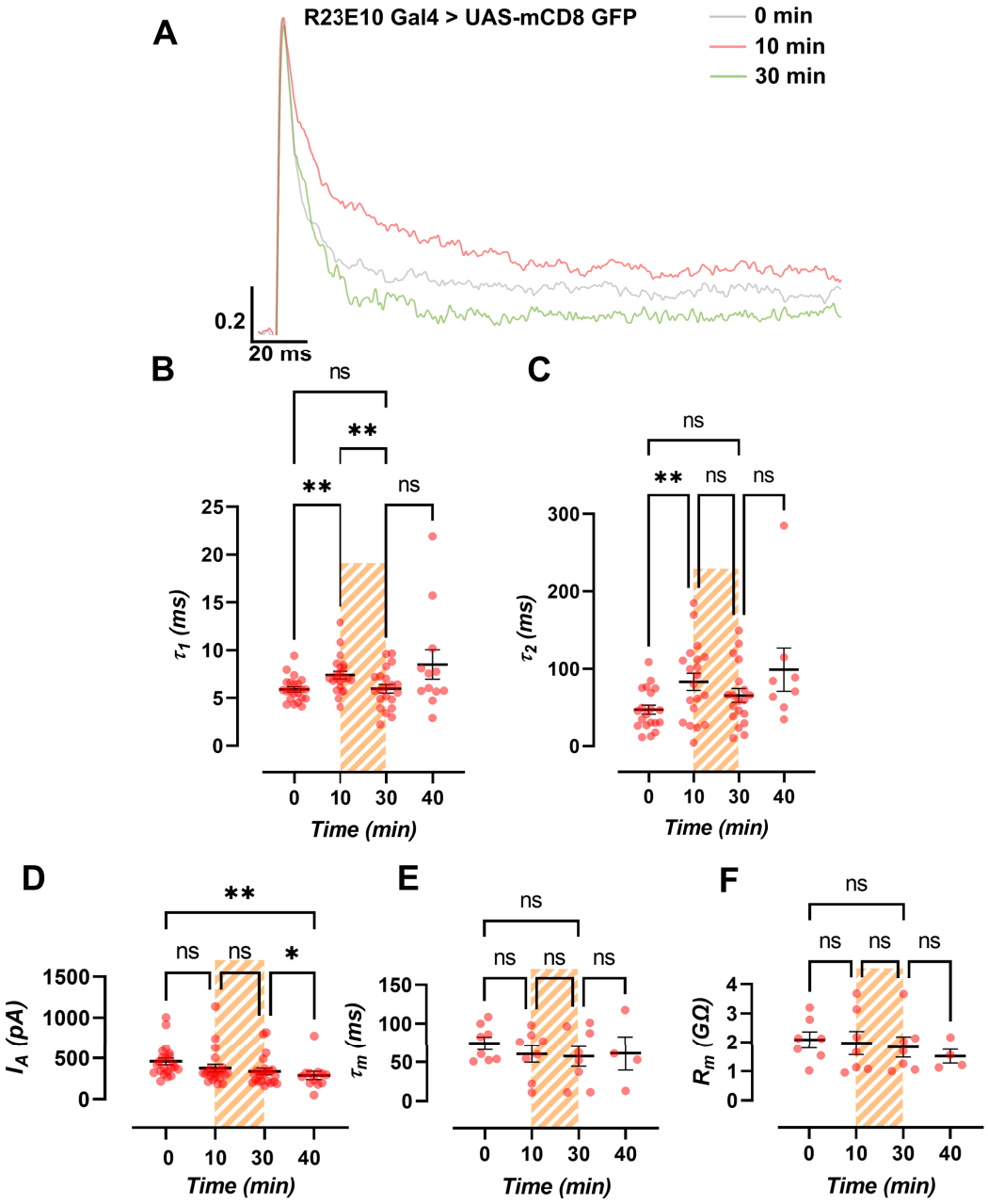


Figure 3.2: Characterisation of GFP expressing dFB neurons exposed to intracellular 4-ONE for 10 minutes followed by a 20 minute 10 Hz simulated spiking protocol (diagonal red stripes). **A** Representative normalised trace demonstrating 4-ONE's initial altering effect on Shaker inactivation (Red Trace) followed by the reversal protocol reverting the inactivation profile or exceeding the initial speed of inactivation (Green Trace) **B** Fast inactivation time constant (τ_1) of I_A **C** Slow inactivation time constant (τ_2) of I_A **D** Peak I_A measured at the largest depolarising step **E** Membrane time constant, T_m **E** Peak I_A measured at the largest depolarising step **F** Membrane resistance R_m. Bars are mean±SEM, mixed effects analysis with Tukey's post hoc. * = p<0.05, ** = p<0.01, ns = no significance.

I next investigated whether this reversal was possible on the less specific application of ROS via miniSOG stimulation. Similar to the previous experiments, miniSOG stimulation reliably produced an increase on the inactivation time of Shaker in both τ_1 and τ_2 (Fig. 3.3B & C). miniSOG induced changes to inactivation also proved to be susceptible to depolarisation. Following initial light stimulation, 20 minutes of depolarisation (at 30 minutes) returned both time constants to non-significance when compared to the baseline seen at the 0 minute time-point. Furthermore, akin to the prolonged presence of 4-ONE driving a resurgence of slowed Shaker inactivation following the depolarisation protocol, driving miniSOG stimulation via blue light a second time was again able to produce an increased inactivation time. The observation that the reversal is itself reversible via further oxidative stress supports the proposition that the effects seen in the reversal are genuine and are due to oxidative strain rather than some unspecific effect or patch deterioration.

3.3 Reversal of Shaker inactivation kinetics by simulated spiking require Hyperkinetic

To confirm the specificity of this reversal to the catalytic activity of Hyperkinetic, the focus returned to using flies expressing catalytic null Hyperkinetic mutants. Using this version of Hyperkinetic, it is expected that the entire population would be bound to the more abundant NADPH and thus exhibit the "normal", faster inactivation. Furthermore, as already shown in Chapter 2, Fig. 2.5, this form would also be unable to metabolise 4-ONE and cause oxidation of its bound NADPH resulting in no altered inactivation kinetics. Due to this, the simulated spiking protocol should also have no effects (increase or decrease) on inactivation time constants as any increase in co-factor exchange would at most lead to an exchange of NADPH with simply another NADPH and thus maintain the same inactivation time constants.

Initial exposure to intracellular 4-ONE had no significant effect, with no discernible trend in either direction for either the fast or slow inactivation component (Fig.

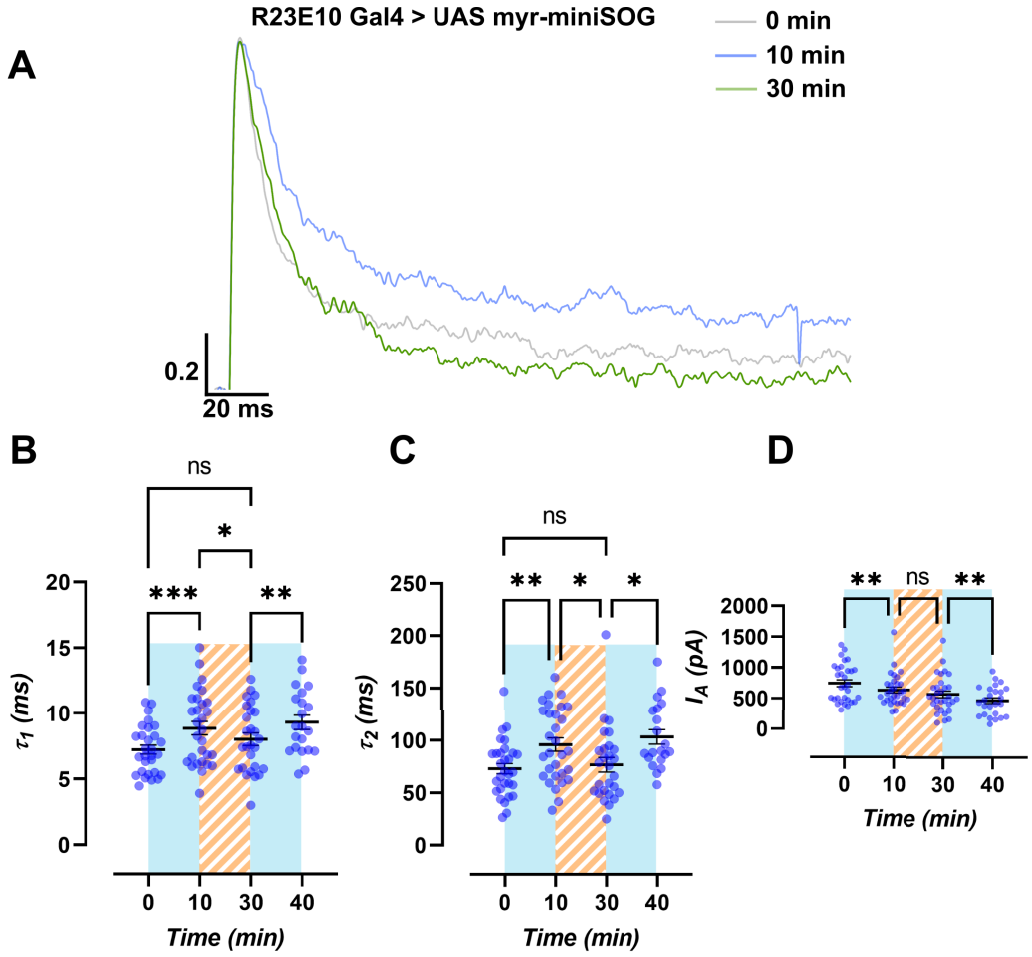


Figure 3.3: Characterisation of I_A in dFB neuron expressing miniSOG. Photostimulating blue light occurred between minutes 0-10 and 30-40 (blue field). Simulated spiking occurred between minutes 10 and 30 (striped red). **A** Representative normalised trace demonstrating miniSOG's modifying effect on Shaker inactivation (Blue Trace) followed by the 20-minute reversal protocol reverting the inactivation profile (Green Trace) **B** Fast inactivation time constant (τ_1) of I_A, n=29-19 **C** Slow inactivation time constant (τ_2) of I_A, n=28-18 **D** Peak I_A measured at the largest depolarising step n=32-25. Bars are mean±SEM, mixed effects analysis with Tukey's post hoc. * = p<0.05, ** = p <0.01, *** = p<0.001, ns = no significance.

3.4B & C). Upon exposure to simulated spiking, these cells still exhibited the same inactivation kinetics. Similar to the 4-ONE and miniSOG experiments, the membrane resistance remained largely constant throughout (Fig. 3.4D). Also, continuing the trend seen in most previous experiments, a run-down in the A-type current over time was again observed (Fig. 3.4E).

In light of the results using Hk^{K289M}, to confirm that this was not merely an

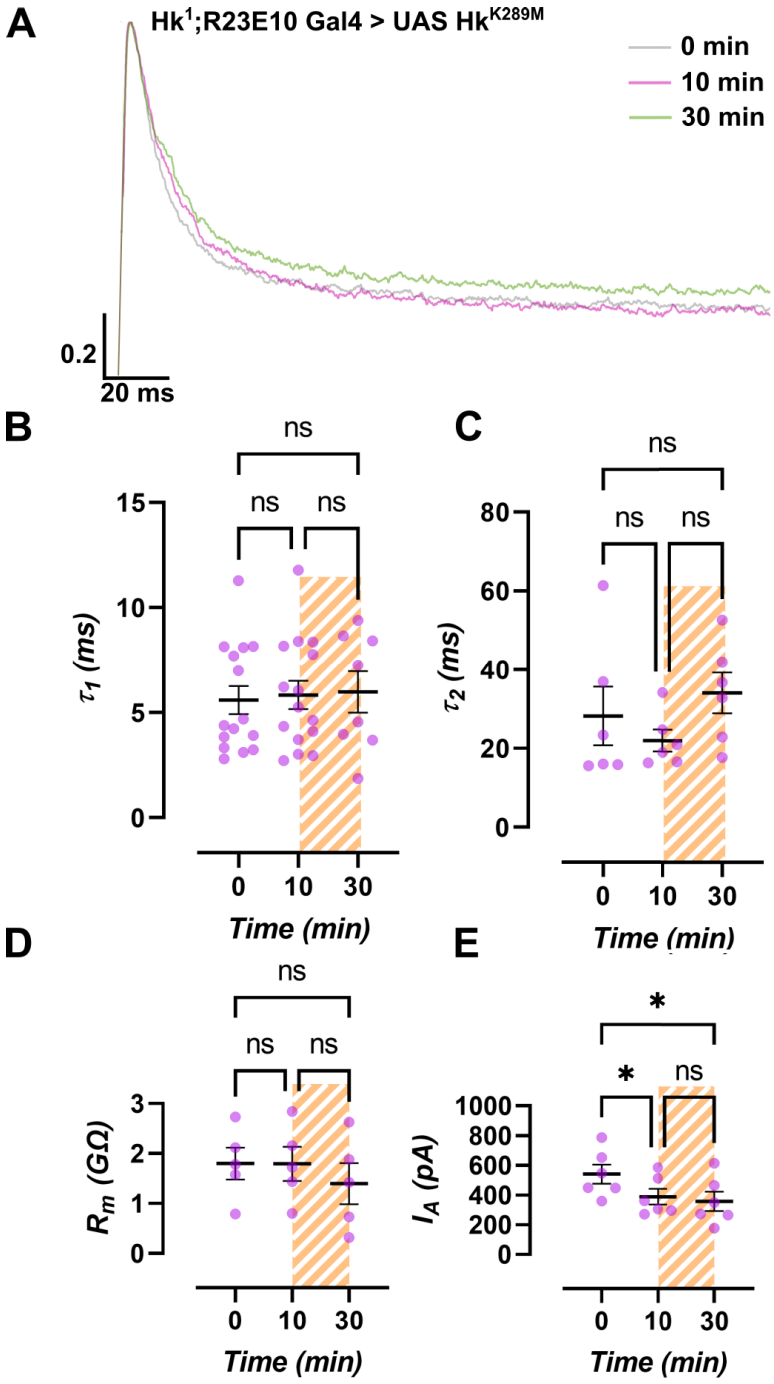


Figure 3.4: Electrophysiological characterisation of dFB neurons expressing only a catalytic null version of Hyperkinetic on a Hyperkinetic null background exposed to intracellular 4-ONE for 10 minutes followed by a 20 minute 10 Hz simulated spiking protocol (diagonal red stripes). **A** Representative normalised trace showing the lack of effect of both 4-ONE application (Pink Trace) and the subsequent simulated spiking on the I_A inactivation profile (Green Trace) in dFB neurons equipped with a catalytic null mutants of Hyperkinetic (Hk^{K289M}) **B** Fast inactivation time constant (τ_1) of I_A, n=8 **C** Slow inactivation time constant (τ_2) of I_A, n=6 **D** Membrane resistance, R_m, n=5 **E** Peak I_A measured at the largest depolarising step, n = 6. Values are mean±SEM. Mixed effects analysis with Tukey's post hoc, ns = no significance, * = $p<0.05$.

artefact of the Hyperkinetic null background, a functional Hyperkinetic form, Hk^{WT}, was reintroduced selectively into dFB neurons in flies of the same background and the same protocol was run. With the functional Hyperkinetic, the response to 4-ONE returned. Since Hyperkinetic is now able to metabolise 4-ONE and reach a state of slower inactivation due to bound $NADP^+$, the effect of simulated spiking should also return. After a 4-ONE mediated increase in inactivation time, simulated spiking reverses this effect to the point of non-significance compared to the baseline time seen directly after break-in at time-point 0 (Fig. 3.5B & C). The membrane resistance remained constant throughout (Fig. 3.5C), with the slight rundown in peak currents still present (Fig. 3.5D).

3.4 Summary

Here, I demonstrate, for the first time in vivo, the proposed bidirectional relationship of membrane potential and the catalytic activity of the complex. Previous literature either directly or indirectly advocates for the notion that simulated spiking induces a voltage driven conformation change in the channel structure and allows for faster $NADP^+$:NADPH exchange [82, 86, 106, 109]. This confirms a long suspected biophysical quirk of Hyperkinetic, which has hitherto only been indirectly tested in-vitro on the mammalian counterpart $K_v\beta1$ [86]. The fact that miniSOG induced channel inactivation modulation was also reversible by simulated spiking support the idea that miniSOG derived ROS and 4-ONE both act by the same pathway i.e. Hyperkinetic.

The reversal protocol would occasionally drive the inactivation time constants lower than the baseline levels. If the original hypothesis holds true and this time constant is an indirect measure of cumulative oxidative and thereby sleep pressure, this potentially demonstrates the dispersal of not only the oxidative strain imposed by 4-ONE/miniSOG application, but also the physiologically sourced pressure already integrated by the channel complex in the individual dFB neuron.

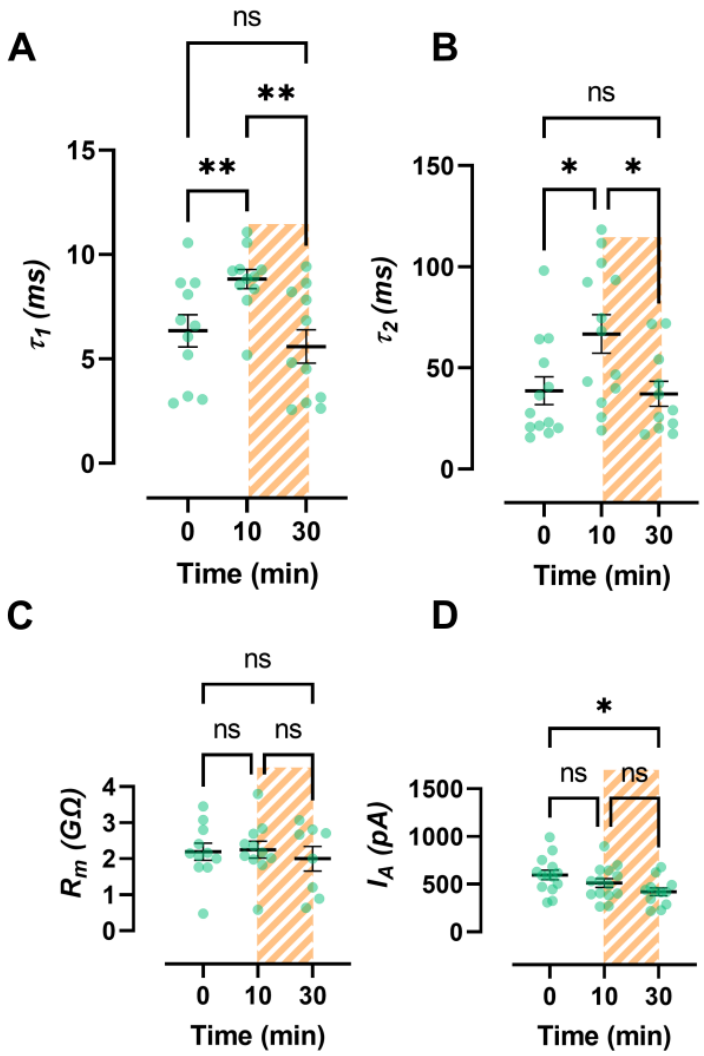


Figure 3.5: Electrophysiological characterisation of dFB neurons expressing a rescuing functional version of Hyperkinetic on a Hyperkinetic null background exposed to intracellular 4-ONE for 10 minutes followed by a 20 minute 10 Hz simulated spiking protocol (diagonal red stripes). **A** Fast inactivation time constant (τ_1) of I_A, n= 11 **B** Slow inactivation time constant (τ_2) of I_A, n = 11 **C** Membrane resistance, R_m, n =11-9 for final time-point **D** Peak I_A measured at the largest depolarising step, n = 14. Values are mean±SEM. RM one-way ANOVA (except for R_m for which a mixed-effects analysis was done) with Tukey's post hoc, ns = no significance, * = $p<0.05$, ** = $p<0.01$.

In the proposed sleep model, the reversal procedure represents the rapid dissipation of sleep pressure. While flies realistically require more than 20 minutes of sleep to recover from homeostatic sleep pressure, it is noteworthy that the above protocol simulates spiking at 10 Hz while physiological spontaneous rates would not exceed 1-3 Hz (Fig. 4.9A) and the reversal protocol at these lower rates would presumably also require a significantly longer period of time to effectively reverse any effects of oxidative by-products.

A central question that remains regarding Hyperkinetic's role as a ROS integrator is how the simulated spiking is able to impart its control over the channel subunits. Furthermore, structures developed of $K_v\beta$ show only the structure when the co-factor is in the oxidised form and thus preventing structural comparison between states [82]. Similarly, it is also difficult to predict the degree of structural conformational change around the NADP(H) binding site in response to depolarising voltage as no structure shows a comparison between a resting hyperpolarised environment and a depolarised environment. Encouragingly, it is likely that the voltage sensitivity and thereby effects of the simulated spiking are specific to the catalytic function of Hyperkinetic. Especially when considering the lack of effect in Fig. 3.4B & C using the catalytic null Hyperkinetic.

Whether the depolarisation caused by the 10 Hz 3 ms depolarising pulses (or the action potentials it attempts to emulate) are truly sufficient to actually drive a conformational change is not yet proven, but one can speculate on the probable effectiveness of this protocol. The 3 ms depolarisation at 10 Hz may seem exceedingly short, especially when considering that only 3% of the total time of the reversal protocol is actually depolarising. Furthermore, the voltage dependent gating decay time constant of Shaker is fairly rapid (approximately 3-5 ms) [112–114]. However, considering that the membrane time constant of dFB neurons are demonstrated here as lying on a timescale of between approximately 60-100 ms (Fig. 2.3D & 3.2E), the effects of an even transient application of voltage may in fact be maintained for a sufficient period of time for mediating co-factor exchange.

4

Do 4-ONE related changes influence spiking in dFB neurons?

Contents

4.1 I_A current and neuronal activity 59
4.2 Investigating baseline excitability 60
4.3 Investigating spontaneous spiking rate and pattern . . 66
4.4 Summary 71

4.1 I_A current and neuronal activity

The previous chapters have shown that ROS, via either miniSOG stimulation or direct application of the hyperkinetic substrate 4-ONE, produced a robust and consistent effect on the inactivation of Shaker mediated I_A. The outward flow of K^+ ions of I_A might initially seem as a counter-productive activity in producing action potentials, as it would appear to act to hyperpolarise the neuronal membrane. However, I_A constitute the essential repolarisation force following an action potential and enables repetitive firing [39]. Furthermore, abolished I_A in dFB neurons via RNA^i targeting Shaker, reduces neuronal firing frequency and increases average interspike intervals (ISI) [38]. Moreover, increased Shaker inactivation time constants

(and thereby more sustained I_A) has an enhancing effect on spiking in dFB neurons [94]. On the other hand, there's also evidence that reducing I_A in certain neural circuits can in fact increase neuronal excitability, observed as a reduced spike latency in response to depolarising current as well as increased overall firing rate [115, 116]. Increasing I_A had the exact opposite effect[115, 116]. These later studies, however, theorise that the reduced excitability observed is in fact due to 'premature' activity K_v channels (such as Shaker) at the resting membrane potential of the neurons where the repolarising force of I_A is continuously opposing the depolarisation required for an action potential cascade to form, thus I_A's removal logically resulted in a more excitable neuron. The studies supporting I_A's role in enhancing activity suggests that the premature activity of I_A-channels seen elsewhere, in the case of dFB neurons, is not applicable due to a more hyperpolarised resting potential and thus the function of I_A can change depending on cellular circumstances.

In the physiological context of my original hypothesis where spiking drives this reversal process, if 4-ONE is a sleep pressure messenger, 4-ONE should also increase the baseline spiking rate as a direct effect of the altered Shaker inactivation. I suspected that 4-ONE's effect on Shaker inactivation could generate a more sustained, repolarising I_A current following action potentials. This would repolarise the neuron and restore the molecular machinery (e.g. Na_V channels) to their ready state more rapidly and able to produce another action potential, and thereby increase the overall firing rate of a neuron when stimulated.

4.2 Investigating baseline excitability

To investigate baseline excitability, I probed whether any changes in output spiking could be observed in response to depolarising current injection in a whole cell patch clamp setup. The experimental design followed a simple protocol of gradually increasing depolarising currents in 5 pA increments and the firing rate determined at every step from a holding of -60 mV. The conditions included normal intracellular solution (control), vehicle control (MeAc) and my molecule of interest, 4-ONE. As

before, 4-ONE was directly supplemented to the intracellular solution of the patch pipette and allowed 10 minutes for solution exchange and any potential enzymatic conversions.

This produced little significant change to the overall spiking frequency of dFB neurons over the observed time period for any conditions. All groups showed a slight, yet non-significant, increase over the time-course of the experiments (4.1A-C). However, comparing all conditions after 10 minutes of intracellular exposure, all conditions remained comparable (4.1D). The interspike interval (ISI) distribution also showed no significant change between vehicle and 4-ONE groups (Fig. 4.2)

Quantifying the underlying input resistance of the average traces (Fig. 4.1E) showed a predominantly insignificant, yet clearly present, drift in input resistance for all groups between the 0 and 10 minute time-point. It also highlighted the large diversity in input resistance across the overall dFB population, perhaps reflecting the different states the neuron can exist in. Considering that the typical experimental protocols for generating IF curves uses constant input currents regardless of input resistance, there was some concern that any differences between groups in excitability could perhaps be obscured (or created) by the changing input resistance, as voltage deflection would invariably change with the resistance and affect spiking at each current injection step. It is unlikely that a change in input resistance is wholly due to the effects of either the vehicle or 4-ONE, as this increase is observed in the control groups as well, albeit to a smaller extent. Furthermore, a proportion of neurons experienced depolarisation block at the higher current injection steps and were rendered silent, thus making it impossible to gauge any spike rate changes for those cells and if included in bulk analysis could potentially have a concealing effect. I attempted to correct for this by calibrating the size of the input current to the input resistance measured immediately before running my experimental protocol so that for each cell, the current injected would cause a 5mV deflection at -60 mV. Using this correction, any increases previously observed (Fig. 4.3A) were abolished

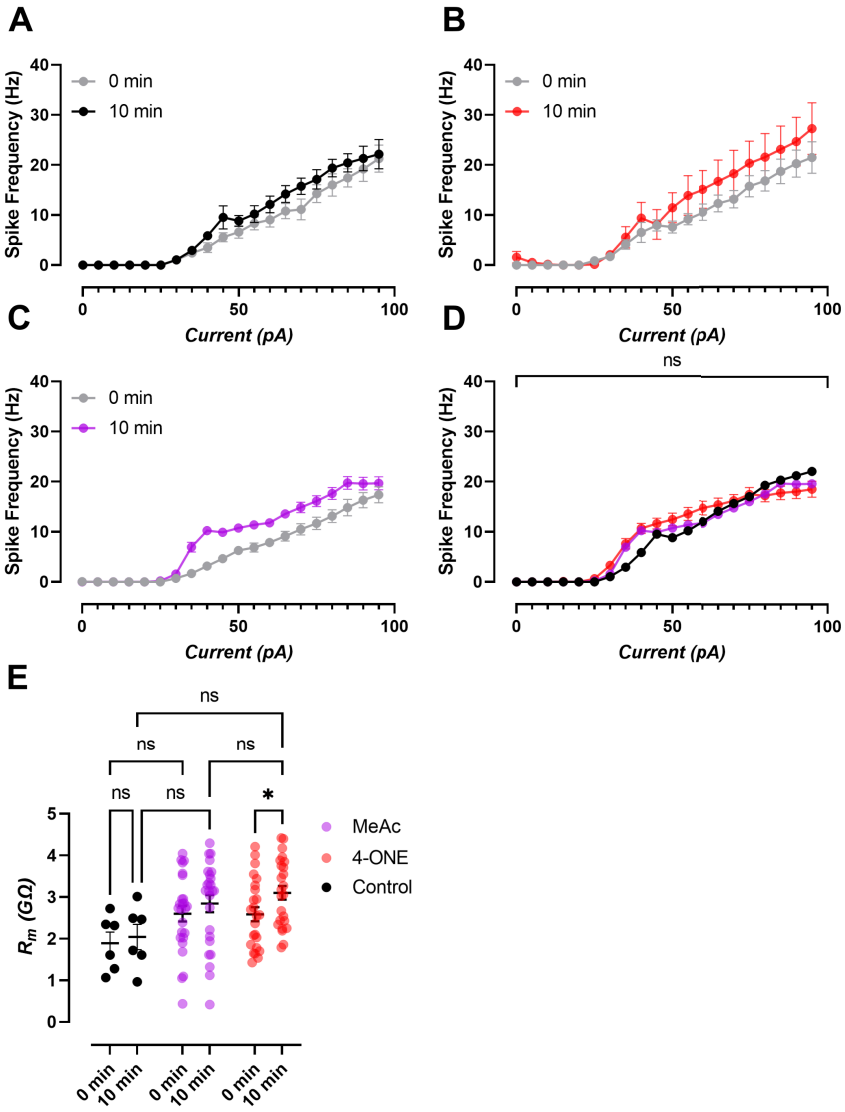


Figure 4.1: Current-Frequency (IF) curves and membrane resistance (R_m) of dFB neurons measured by step-wise current injection pulses. **A-C** Spiking frequency of dFB neurons when subjected to a series of depolarising current injections of 5 pA increments from a -60 mV holding potential while simultaneously exposed to either intracellular non-supplemented control, 4-ONE or MeAc respectively. **D** Overlaid traces of groups in A-C at the 10 minute time-point **E** R_m of cells from A-C. Values are mean±SEM. numbers of cells (A-C & E) = 6, 32, 39 respectively. Mixed effects analysis with Tukey's post hoc, * = $p<0.05$, ns = no significance.

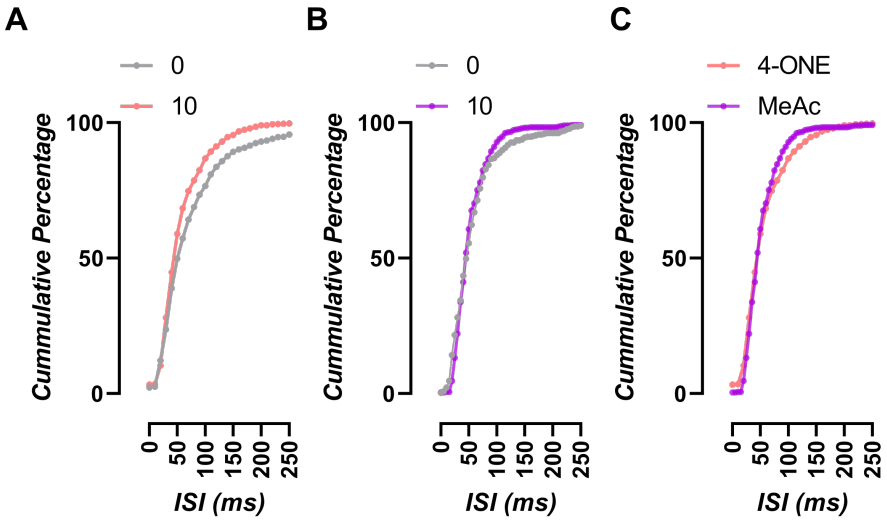


Figure 4.2: **A & B** Cumulative interspike intervals (ISI) distribution derived from depolarising currents applied to dFB neurons while presented with either intracellular 4-ONE or MeAc vehicle, n=32 & 39 respectively. **C** Overlaid traces of groups in A & B at the 10 minute time-point.

(Fig. 4.3B) suggesting that the previous increases in firing frequency were indeed due to a tendency towards increasing input resistance across all groups.

When considering the firing rate in terms of fold-change between the 0 and 10 time-points, an interesting characteristic of dFB neurons became apparent. The baseline firing rate at 0 minute appeared to determine whether there was space for any further increases in firing rate (Fig. 4.4A). At baseline firing frequencies above approximately 15-20 Hz, the cells were very unlikely to see any increase in their firing in the time-course of the experiment. Meanwhile, cells peaking at a firing rate of approximately 10 Hz during the initial IF curves saw possibilities of many-fold increases. Similar to the input resistance, this may be reflecting the different possible states the dFB neurons can occur in. This implied that in the case of cells above a firing rate of 15-20 Hz at the highest current injection, these were already saturated in terms of firing rate and any manipulations were unlikely to increase it further. In view of this, the concern that these "static" cells would obscure any results led me to look into whether filtering cells with a frequency of 15 Hz and above from my analysis might reveal any hitherto obfuscated effect (grey dotted line in Fig. 4.4A). Applying this reasoning to my previous datasets of 4.1

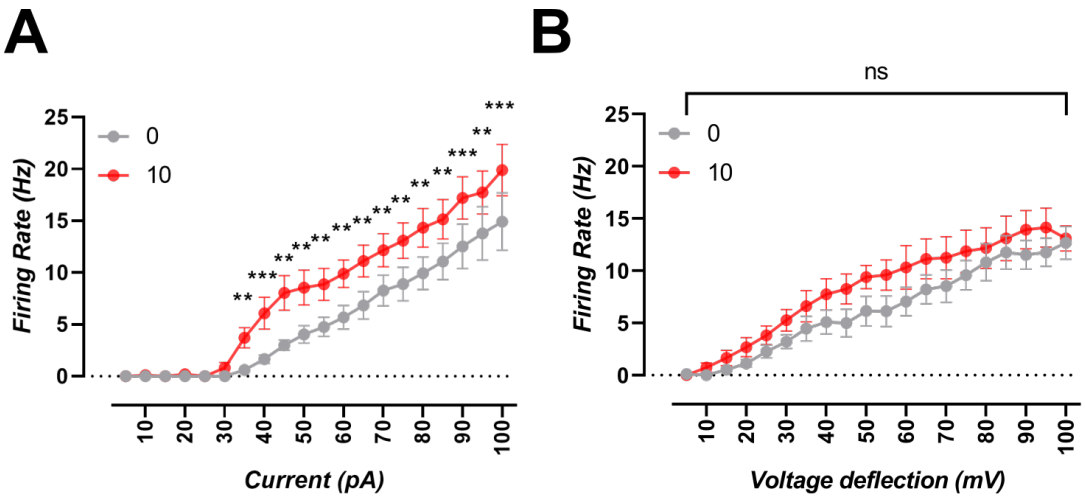


Figure 4.3: Current-Frequency (IF) curves of the same dFB neurons using two different variations of the experimental protocol while exposed to intracellular 4-ONE. **A** Spiking frequency of dFB neurons using normal experimental protocol of gradually increasing depolarising current injection in 5pA increments **B** Spiking frequency dFB neuron exposed to intracellular 4-ONE using normal experimental protocol using a corrected protocol where each current injection corresponds to a 5 mV voltage deflection from -60 mV rather than a set 5 pA current increment. Values are mean spiking frequency ±SEM, n = 14. Two-way RM ANOVA with Tukey's post hoc *p<0.05,**p<0.01, ***p<0.001, ns = no significance.

revealed, perhaps unsurprisingly, a widening gap between the baseline firing rate and the later firing rate for both 4-ONE and my vehicle group (4.4B & C) where the former had an apparent larger increase in the timespan of the experiment compared to its baseline firing. However, overlaying the later time-points from both groups show no significant difference between the 2 groups (4.4D).

The final set of analyses performed on induced spiking looked at whether the time delay to spiking and the minimum spiking voltage (rheobase) in response to an ascending ramp of depolarising current were affected in either of my experimental groups. There was a small apparent vehicle effect in the rheobase values, where the MeAc vehicle appeared to have a slightly reduced excitability, i.e. requires a higher voltage to produce an action potential (4.5A). However, considering the lack of any significant effect in any of the other analyses to suggest an altered excitability in this group it is unlikely that MeAc truly has an anti-excitable effect. In terms of spike latency, there was no change in either group (Fig. 4.5B).

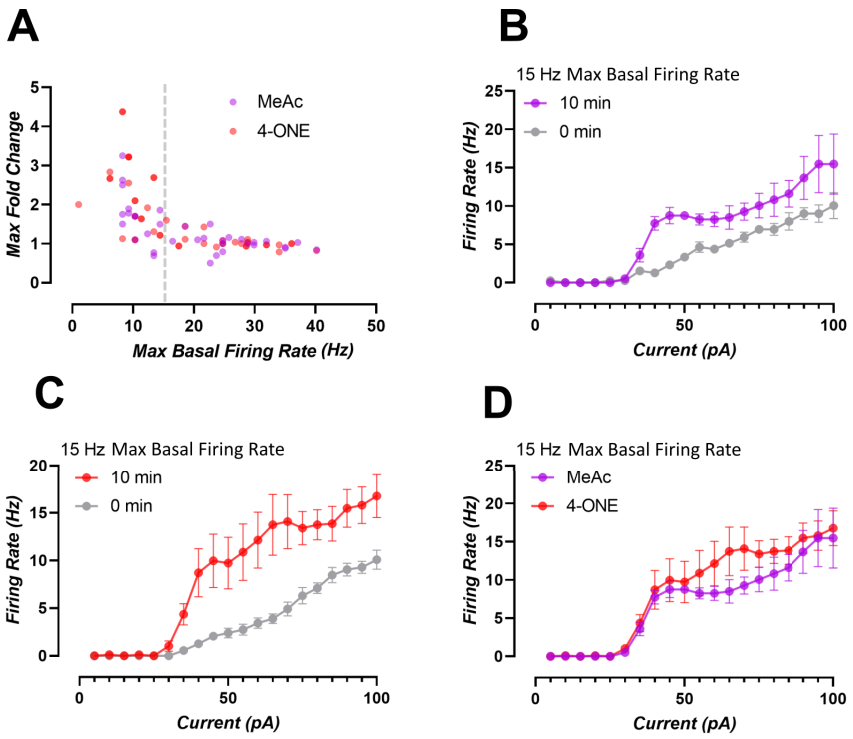


Figure 4.4: **A** Plot showing the max calculated fold change between the IF curves of dFB neurons at time-points 0 and 10 minute versus the max firing rate seen at time-point 0 (basal firing rate) **B-C** IF curve for dFB neurons exposed to intracellular MeAc or 4-ONE from 4.1. Analysis was restricted to cells with a baseline firing rate of less than 15 Hz. **D** Overlaid traces of MeAc and 4-ONE group at the 10 minute time-point. Values are mean±SEM, n = 14.

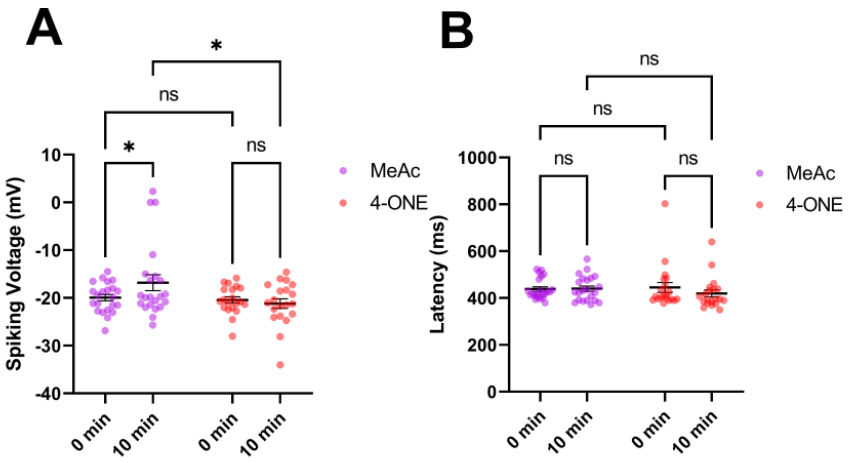


Figure 4.5: **A** Rheobase and **B** spike latency of dFB neurons exposed to intracellular MeAc or 4-ONE in response to ramp of depolarising current. Values are mean±SEM, n = 21 for both groups. Two-way RM ANOVA with Tukey's post hoc *p<0.05, ns = no significance.

4.3 Investigating spontaneous spiking rate and pattern

In parallel to assessing the firing capabilities of a neuron in response to depolarising current protocols, spontaneous activity of the neurons were also investigated. In these cases, no current was injected, and only spontaneous firing was recorded. The lack of notable changes in response to 4-ONE regarding elicited spiking led me to assess whether, if there truly was an interaction between 4-ONE and neuronal activity, could it manifest itself instead as an alteration in spike shape and spiking patterns (i.e. bursty versus tonic) rather than purely firing rate terms?

The spike shape was described by the maximal rate of increase in the rise phase and the maximal rate of decline in the decay phase. The mean of every spike per cell is represented as a single data point, and the combined mean of every cell was used for analysis. The rise and decay rates were collected from the maxima and minima respectively of the differential plot derived from the voltage traces of each action potential. Similar to previous analyses, there were consistent trends of change between the two measured time-points. In the rise rate there was a small increase in both the experimental and vehicle group (Fig. 4.6A). Conversely, a decrease was observed in the rate of decay in the falling phase (Fig. 4.6B). These changes were statistically non-significant compared with their corresponding earlier time point. However, the 4-ONE group, for both action potential rise and decay, showed a significant difference to the MeAc control. Further breakdown of this data into frequency distribution of each individual action potential highlighted underlying differences. In the action potential rise rates, the 4-ONE at 0 minutes had a condensed distribution around ∼5000 mV/s compared to the much broader distribution of the corresponding MeAc control at 0 minutes which showed a peak at the lower rate of ∼4000 mV/s. Over time, the MeAc group remained largely unchanged while the 4-ONE group's distribution became wider (Fig. 4.6C) . Apparent differences also appeared in the decay phase of action potentials where for both time points, the MeAc group showed a high representation at the ∼2000

mV/s peak. Conversely, the 4-ONE group, while still having a peak at the same rate exhibited a much broader distribution of rates which ultimately translated to a higher average rate of decay in action potentials (Fig. 4.6D)

Next, while the overall shape of action potentials were indistinguishable between groups, the possibility of whether the pattern of spiking was affected was investigated. Unclamped current clamp recordings of dFB neurons revealed a wide variety in spiking patterning ranging from tonic firing to consistently bursting cells (Fig. 4.7). In the context of bursting cells, these showed a wide variation in both frequency of the oscillations of bursts and also the strength of these burst i.e. how many action potentials occurs within the burst window. These variations also existed between multiple dFB neurons in the same brain.

The calculated ISI from spontaneous data was exceptionally different from those derived from the IF curves of induced spiking. The overall length of ISI was considerably longer and the spread in distribution increased (Fig. 4.8). Both groups saw some change between the 0- and 10-minute time-point (Fig. 4.8A & B). No significant difference was discernible between the two groups however regarding ISI (Fig. 4.8C). Again, the large variation in population distribution of ISI may reflect the high variability of the states that the dFB neurons can exist in. Further, quantifying the mean ISI of spontaneous firing showed no difference for any group. The coefficient of variation (C_V) of the spontaneous spiking ISI was then calculated to determine the width between spike trains (Equation 7.3 in Method). Using C_V of ISI, a $C_V < 1$ indicates that a spike train is more regular than a Poisson distribution i.e. tonic firing [117]. Conversely, a $C_V > 1$ typically indicates a more irregular process but is also characteristic of an intrinsically bursting neuron [117]. C_V quantification again showcased a diverse population of both regular firing (typically tonic firing neurons. Example: top panel in Fig. 4.7) and more intrinsically bursting neurons (bottom panels of Fig. 4.7) with an average mean C_V value of approximately 1.1.

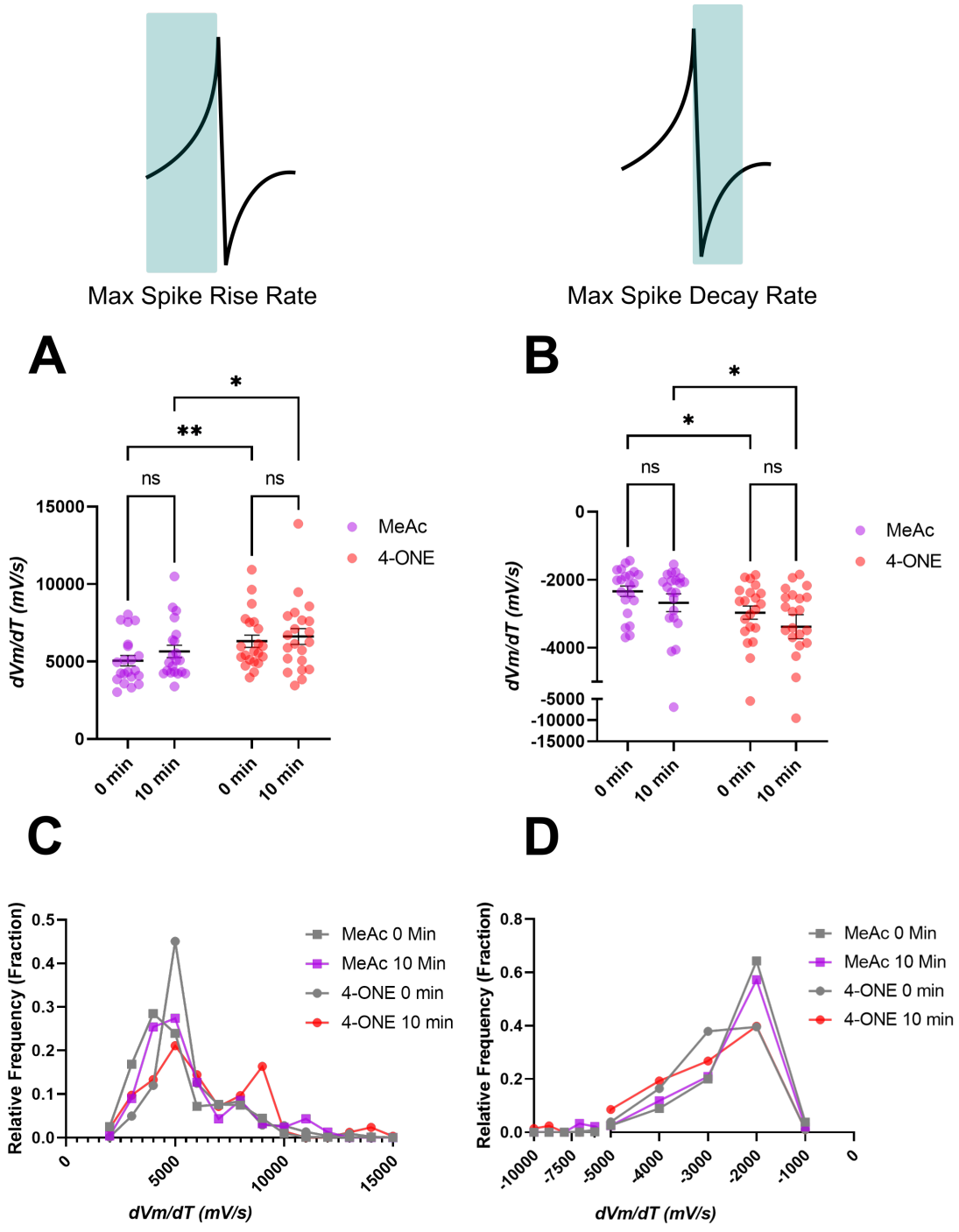


Figure 4.6: Maximal rate of change of the **A** rise and **B** decay, respectively, of action potentials in dFB neurons' spontaneous activity when exposed to intracellular 4-ONE or MeAc vehicle. Each data point is the mean of the max rate of rise/decay derived from the differential plot of every action potential in an individual cell from a 20-second bin of spontaneous activity. MeAc and 4-ONE n = 22, 20 respectively. Values are mean±SEM. Mixed effects model with Tukey's post hoc. *=p<0.05, **p<0.01, ns = no significance **C-D** Relative frequency distribution of all action potential's rise and decay across all cells.

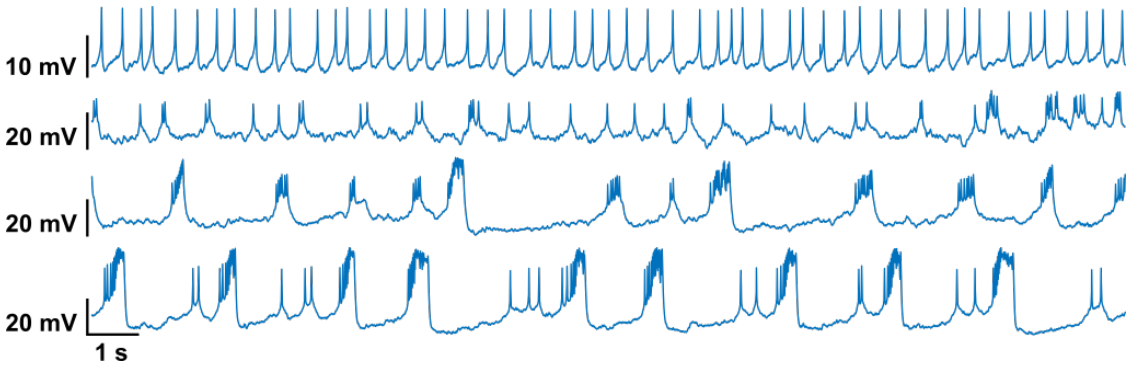


Figure 4.7: 4 representative sample cells demonstrating the wide variety in spontaneous activity patterns of dFB neurons when unclamped, ranging from highly burst prone neurons to others that exhibited purely tonic firing.

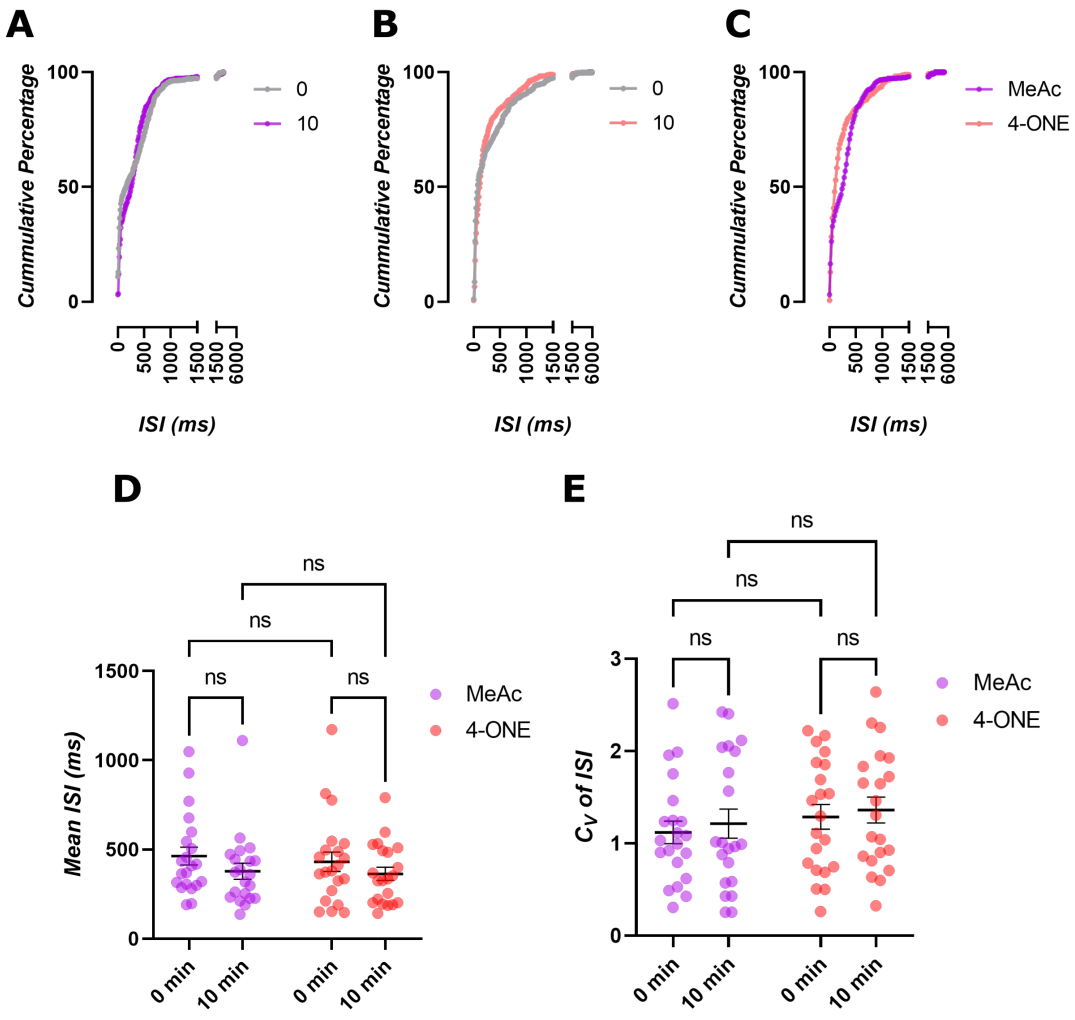


Figure 4.8: **A-B** Cumulative ISI distribution curves of spontaneous activity of dFB neurons exposed to intracellular MeAc or 4-ONE over time. **C** Compared ISI distributions of spontaneous activity from both groups at the 10-minute time-point. **D** Quantified mean ISI of all groups **E** Calculated coefficient of variation of ISI. Values are mean±SEM. For all groups n=21. Two-way RM ANOVA with Tukey's post hoc ns = no significance.

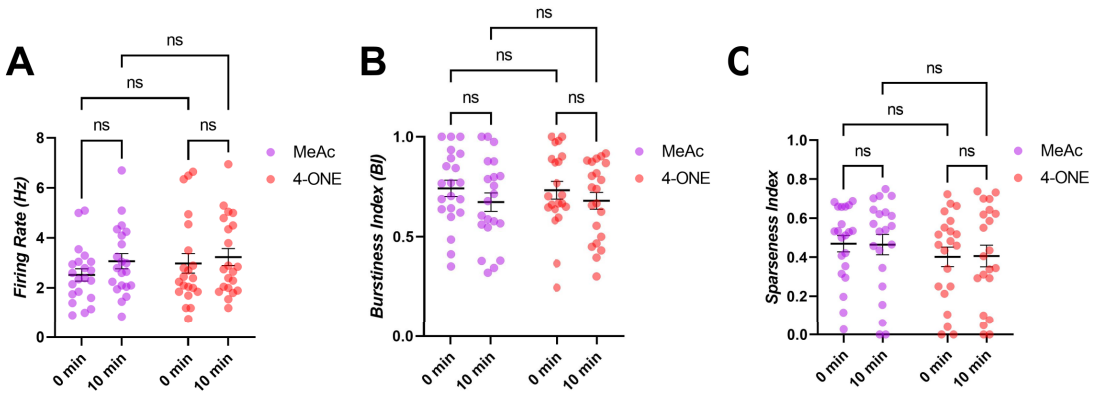


Figure 4.9: A dFB spontaneous firing rate **B-C** Burstiness Index (BI) and Sparseness Index (SI) of spontaneous spiking in dFB neurons across different time-points for 4-ONE or MeAc vehicle. Indices calculated as described in Fig. 7.2. Values are mean±SEM, n = 21. Two-way RM with Tukey's post hoc ANOVA ns = no significance.

Quantifying the raw firing rate of the spontaneous activity showed no significant drift for either group. A small insignificant up-tick in firing rate is apparent (Fig. 4.9A). However, these changes appeared to be non-specific to any group and likely reflect the earlier tendency towards excitability observed in the earlier IF curves (Fig. 4.1).

While ISI frequency distribution can give clues to whether spiking patterns have changed, it is not always ideal for detecting more subtle changes. Attempting to quantify potential changes in spiking patterning involved calculating two separate indices which have previously been used to assess the degree of burstiness or sparseness seen in the spontaneous activity, hereafter "Sparseness Index" (SI) and "Burstiness Index" (BI) [118](Equation. 7.2 in Methods). These additional descriptors of dFB spiking activity attempt to assess the proportion of spiking occurring within set time bins: in a bursty cell, most spikes would occur within fewer bins while with tonic firing the action potentials would be dispersed evenly throughout all time bins. However, these did not give any further suggestion that 4-ONE affected spiking. In both indices, the results mirrored those of previous figures where a slight change occurred in both groups between the two time-points; however, these were non-significant (4.9). Further, no significant change was detected between the MeAc vehicle and 4-ONE at either time-point for either index.

4.4 Summary

At this juncture, I have exhaustively demonstrated that 4-ONE has little or no apparent effect on the spiking dynamics of the dFB neurons and any alterations observed in the 4-ONE group were also present in either the normal intracellular control or the vehicle control. As previously discussed, the function of altered I_A is dependent on environmental circumstances. In the context of 4-ONE and its lack of effect on spiking, it seems that either the alteration to I_A was not sufficient in terms of degree of inactivation change or I_A in this system does not function to enhance spiking frequency. In previous studies, comparable changes to τ_1 were shown to be coupled with increased firing [94]. It is possible that increased inactivation time constants are not always coupled to an increase in overall amplitude, which may in fact be the actual essential component required to enhance activity as opposed to the degree of sustained current. In previous chapters, most experiments, including controls, saw a slight but significant run-down in overall I_A amplitude suggesting perhaps a small imperfection in the methodology of the patch clamp. This imperfection may also explain why all cells had a slight increase in baseline firing between time-points, as it is unlikely this change is due to natural variations over time since I would then also expect to see decreases in firing rate which was rarely observed. It is noteworthy that in a previous study, the amplitude of I_A remained constant while inactivation slowed yet spike rate was still enhanced [94]. It is therefore unlikely that any relevant, crucial changes to I_A amplitude were missed. Nevertheless, it is also important to note that under no experimental conditions did the firing rate decrease, which would otherwise be expected if the I_A amplitude was the main contributor to this role. This would also be expected in cases where altered inactivation kinetics of I_A were truly a counter-productive force in producing repetitive spiking in the dFB neuron [115, 116].

The lack of any notably change was a surprise, as previous studies have clearly shown a correlation between alterations to Shaker inactivation and neuronal activity [38, 94]. One possibility is that the dosage of 4-ONE was insufficient or was not

allowed sufficient time to produce an effect. The latter is unlikely considering that around the 10-minute mark the vast majority of change to Shaker inactivation had already occurred, thus any potentially coupled changes to firing would presumably also already be applied. The dosage proved difficult to increase without including an excessive amount of vehicle. I investigated whether resuspending the 4-ONE in a smaller volume of MeAc to increase the effective concentration by evaporating the initial vehicle under an inert nitrogen stream, taking efforts to avoid excessive contact with atmospheric oxygen. In current clamp experiments, using a four-fold increase in working concentration while maintaining a less than 0.15% MeAc proportion did not produce any further effects (data not shown). While some efficacy may have been lost due to excessive oxidation during the resuspension procedure, this suggested that the working concentration is likely not a limiting factor in producing any effect on firing frequency. Furthermore, increasing the length of the experiments did not produce any noticeable trend in either direction regarding firing rate.

Concerning the significant differences in the rise and decay kinetics of action potentials between the 4-ONE and MeAc groups, it was surprising that any differences would be apparent at the 0-minute mark. While one could perhaps argue that the time elapsed to perform the whole suite of recordings is sufficient for 4-ONE to have an effect (approximately 2-3 minutes) hence why even the 'baseline' activity is altered, it is unlikely since this is not reflected in any other criteria assessed. This includes the voltage clamp experiments where a clear baseline can still be observed within 1-2 minutes after break-in suggesting that this small period of time is insufficient. The underlying distribution of rates in the rising phase of the action potentials shows clearly that the theoretically similar baselines of MeAc and 4-ONE at the 0-min time point are in fact not comparable (Fig. 4.6C). The exact reason for this is unclear. It is unlikely that this is an early effect of 4-ONE as after 10 minutes of presumable effect of 4-ONE, the distribution begins to more resemble that of the MeAc group at 10 min (albeit with a slight shift towards higher rates) rather than enhancing the apparent differences seen at the 0-minute time point.

Curiously, while the vehicle MeAc and 4-ONE also had clear differences in the decay of action potentials, these differences were more or less consistent throughout the experiments with a small drift towards increased decay rates in both groups (Fig. 4.6B & D). If the slowed A-type current inactivation demonstrated in Chapters 2 & 3 affect spike shape by enhancing repolarising forces, it would be expected that the decay rate (i.e. repolarisation following an action potential) would also accelerate. If this indeed is a true effect of 4-ONE then it invites the question as to why the overall neuronal activity is not affected. A potential explanation for this is that the enhanced post-spike repolarisation only speeds up overall action potential if the mean firing rate of a neuron exceeds a certain threshold where the actual repolarisation of the membrane becomes the rate-limiting step and only then would the enhanced repolarisation contribute to an even higher firing rate.

Considering the previously shown effects of miniSOG in the dFB neuron system on enhanced activity and the correlated increased sleep, it is possible that it is precisely due to the lower specificity of $^1O_2$ generated via miniSOG that they are able to have an effect. This is in contrast to the relative specificity of 4-ONE to the shaker-hyperkinetic ion channel complex. An alternative and perhaps contradictory suggestion would posit that the diffusion speed and high reactivity of the 4-ONE limits the distance it can travel in a reasonable period of time. Perhaps the changes I incur on Shaker inactivation kinetics are only occurring exclusively in or very proximal to the soma. This would explain why I observe a significant effect on inactivation from both 4-ONE and the depolarisation reversal protocol, but this effect is not widespread enough throughout the projections of the neurons, specifically at the axon-initial segment (AIS) where action potentials arise, to affect the overall spiking dynamics both in terms of raw action potential output but also in terms of spike shape (i.e. rate of rise and decay) and pattern (bursty versus tonic). Furthermore, it would also explain why the previously publicised effects of miniSOG would occur readily as ROS would be generated throughout the neuronal projections and thus any effect on Shaker would be certain to occur at sites of action potential generation [94]. To resolve this, further study is required into the

exact localisation of Shaker, which at this time remains uncertain. Some studies suggest a purely axonal localisation [119], however, others propose expression at both the pre- and post-synapse [120]. Further, it is also likely that subcellular localisation may vary depending on cell type and thus translating observations at, e.g. the neuromuscular junction (NMJ), would have questionable validity in terms of elucidating expression within the dFB neuron.

As already alluded to, the spiking analyses have however highlighted an interesting high degree of variability of responses within the dFB population with a highly variable basal excitability, spontaneous firing rate and firing pattern. Whether this reflects the individual sleep need of the host fly or whether this perhaps hints at a heterogeneity within the dFB population or, more likely, both, presents an interesting question for future studies.

5

Is it possible to generate a "forgetful" Hyperkinetic?

Contents

5.1 Introduction 75
5.1.1 Hyperkinetic residues of interest 76
5.2 Sleep characteristics of new constructs 77
5.3 Summary 81

5.1 Introduction

In previous chapters I describe how Hyperkinetic can integrate ROS pressure over time due to the low exchange rate of the NADP(H) co-factor. It is postulated that the root cause of the low turnover and one of the main characteristic which sets $K_v\beta$s apart from conventional AKRs, is the nigh complete burying of the cofactor within the structure to the extent where only the reactive nicotinamide ring is exposed [82]. Considering this, it is theorised that it would be possible to create an essentially "forgetful" version of Hyperkinetic. This Hyperkinetic would be mutated in such a way that the NADPH turnover would drastically increase and would shift the Hyperkinetic population into the NADPH bound form, regardless of

relative abundance of substrate. In this case, selective expression of these forms of Hyperkinetic in the dFB neurons on a Hyperkinetic null background should produce a similar behavioural phenotype to catalytic null mutants (K289M) i.e. reduced sleep [58, 94]. Here we attempt to synthesise a "forgetful" version of Hyperkinetic determined and assess any potential sleep pattern alterations.

5.1.1 Hyperkinetic residues of interest

Candidate residues for mutations were either derived from literature review or procured from analysis of the β-subunit structure for residues potentially blocking access to the active site. This section outlines the chosen amino acid residues and the rationale for their selection.

The amino acid Trp-403 forms part of the NADPH binding pocket in Hyperkinetic and constitutes a bulky steric block of NADPH exchange [109]. Furthermore, the glutamine residues at positions 414, 505 and 508 form an overarching loop across the NADPH binding site which again is proposed to trap NADPH within the structure. These residues were mutated into the significantly smaller amino acid alanine which would potentially allow for improved cofactor exchange. In the case of Trp-403, a common concern is that the unique properties of tryptophan often makes any substitution detrimental to the overall structure, especially when replaced by the dissimilar alanine [121]. To attempt to mitigate this, I also included a substitution with tyrosine to preserve the aromatic properties, which in some cases can preserve the overall structure of the protein [121].

His-256 constitutes an outlying residue of interest as it was selected due to its non-conserved status between Hyperkinetic and mammalian $K_v\beta$ rather than structural significance. As a matter of curiosity, it was included to observe what the effects of its substitution to a tyrosine (like in the mammalian variants) would be.

Arg-349 constitutes a semi-conserved residue in AKRs where it is a member of the substrate binding site alongside a tyrosine partner. When replaced with glycine

(R349G) in the equivalent position within AKR5C3, the enzyme showed a marked increase in turnover rate for substrates with longer aliphatic chains [122].

Finally, Asp-251, when replaced with alanine (D251A) in the equivalent position in AKR5C3 indirectly affects the positioning of two tryptophan residues in the NADPH binding pocket; while maintaining the overall protein structure, this rotates the NADPH binding pocket and alters NADPH binding affinity and should affect enzyme catalysis [122]. Indeed, this substitution has a demonstrated significantly increased metabolic rate with a benzaldehyde substrate [122]. Furthermore, an Asp-Asp (D251D) mutation was also done to control for any potential side effects of the mutagenesis protocol on the protein and beyond this should act as a negative control - i.e. sleep patterns should be normal.

The location of these residues on $K_v\beta$ are highlighted in Fig. 5.1 (note equivalent residues are shown on the published structure of $K_v\beta 2$ [81])

These constructs were kindly developed by P. Liu and integrated into the fly germline under the control of a UAS enhancer [123]. The constructs were then selectively expressed in the dFB neurons on a Hk null background ($Hk^{-/-}$) using R23E10-Gal4 [32]. Subsequent sleep behaviour was monitored for each construct.

5.2 Sleep characteristics of new constructs

First, to validate the control groups, I assessed the sleep of a selection of fly lines: Cs (a commonly used "wildtype" of *Drosophila* due to a reportedly low degree of genetic drift [124]), Homo- and heterozygous null mutants of Hyperkinetic ($HK^{-/-}$ & $Hk^{-/+}$) and a Gal4 control to account for non-specific effects of Gal4 protein aggregates ($Hk^{-/-}$ R23E10). Cs and $Hk^{-/+}$ flies exhibited a high amount of sleep relative to the rest of the control groups (Fig. 5.2). Flies equipped only with mutated null forms of Hyperkinetic exhibited reduced total sleep relative to normal sleepers. Isolating the total sleep into the light and dark periods in a 24-hour bin revealed the main contributing factor came from a nigh-abolished day-time sleep in Hyperkinetic null mutants (Fig. 5.2B). Nighttime sleep was unaffected across groups

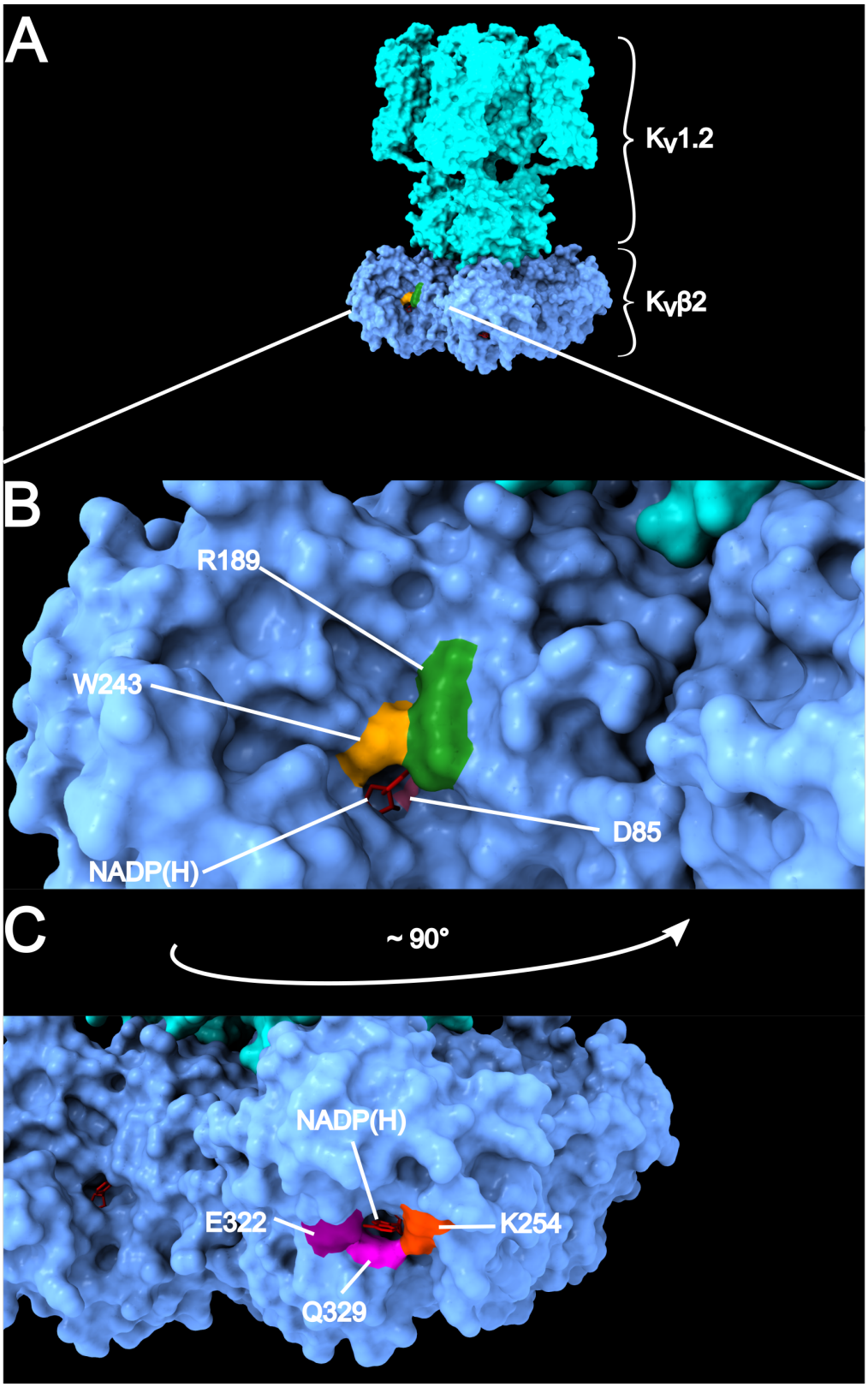


Figure 5.1: Highlighted equivalent residues of interest on the $K_v1.2$-$K_v\beta2$ structure [81]. **A** Full structure of ion channel complex, α-subunit in cyan and β in blue. **B** Close-up of NADP(H) binding site within β subunit highlighting residues R189, W243 and D85 (R349, W403 and D251 in Hyperkinetic respectively) displaying the overarching loop formed by R189 and W243. **C** Rotation of 90° to show E322, K254 and Q329 (Q508, Q414 and Q505 in Hyperkinetic respectively), again, highlighting potentially blocking residues.

(Fig. 5.2C). While heterozygous null Hyperkinetic flies ($Hk^{-/+}$) had comparable total and nighttime sleep, in day-time sleep, where differences for other groups were at their most apparent, the heterozygous flies appeared to show a partially deficient phenotype (Fig. 5.2B). Further break-down of the sleep profiles of the control flies into the number of sleep bouts and their average length highlighted further differences. CS flies and $Hk^{-/+}$ had comparable total sleep, however, the CS flies' sleep profile was highly fragmented compared to the $Hk^{-/+}$ flies, exhibiting almost twice as many sleep bouts (Fig. 5.2E). This change is compensated for by an increased length of each sleep bout. While the reduced sleep bout count remained consistent with Hyperkinetic null flies, the compensatory sleep was not always so, which underscored a further curious difference. $Hk^{-/-}$ flies exhibited a compensatory increase in sleep bout length to account for the reduced sleep episodes while the additional presence of a R23E10 Gal4 driver removed this compensatory increase to the point of being non-significant with the CS group resulting in the shortest sleeping fly group among the controls (Fig. 5.2F).

After establishing the sleep characteristics of our control groups, the next step involved introducing the engineered Hyperkinetic constructs and observing, if any, rescue effects this has on a Hyperkinetic null background. These constructs produced a variety of degrees of rescue, presumably reflecting the relative efficiency of the expressed Hyperkinetic protein. These ranged from a highly effective rescue seen with $Hk^{-/-}$ D251D-R23E10 to the negligible change of $Hk^{-/-}$ H256Y-R23E10. Quantifying these profiles again revealed that the vast majority of changes in sleep profile occurred in day-time sleep (Fig. 5.4A) while nighttime sleep was largely unaffected (Fig. 5.4B)

An important further comparison within the introduced construct comparison is the $Hk^{-/-}$ D251D-R23E10 group which represents the reintroduction of a functional "wildtype" form of Hyperkinetic. This would be expected to perform as well as the CS and $Hk^{-/+}$ group. The 2 latter groups slept 15.5 and 15.0 hours respectively in a 24-hour period while $Hk^{-/-}$ D251D-R23E10 expressing flies slept on average

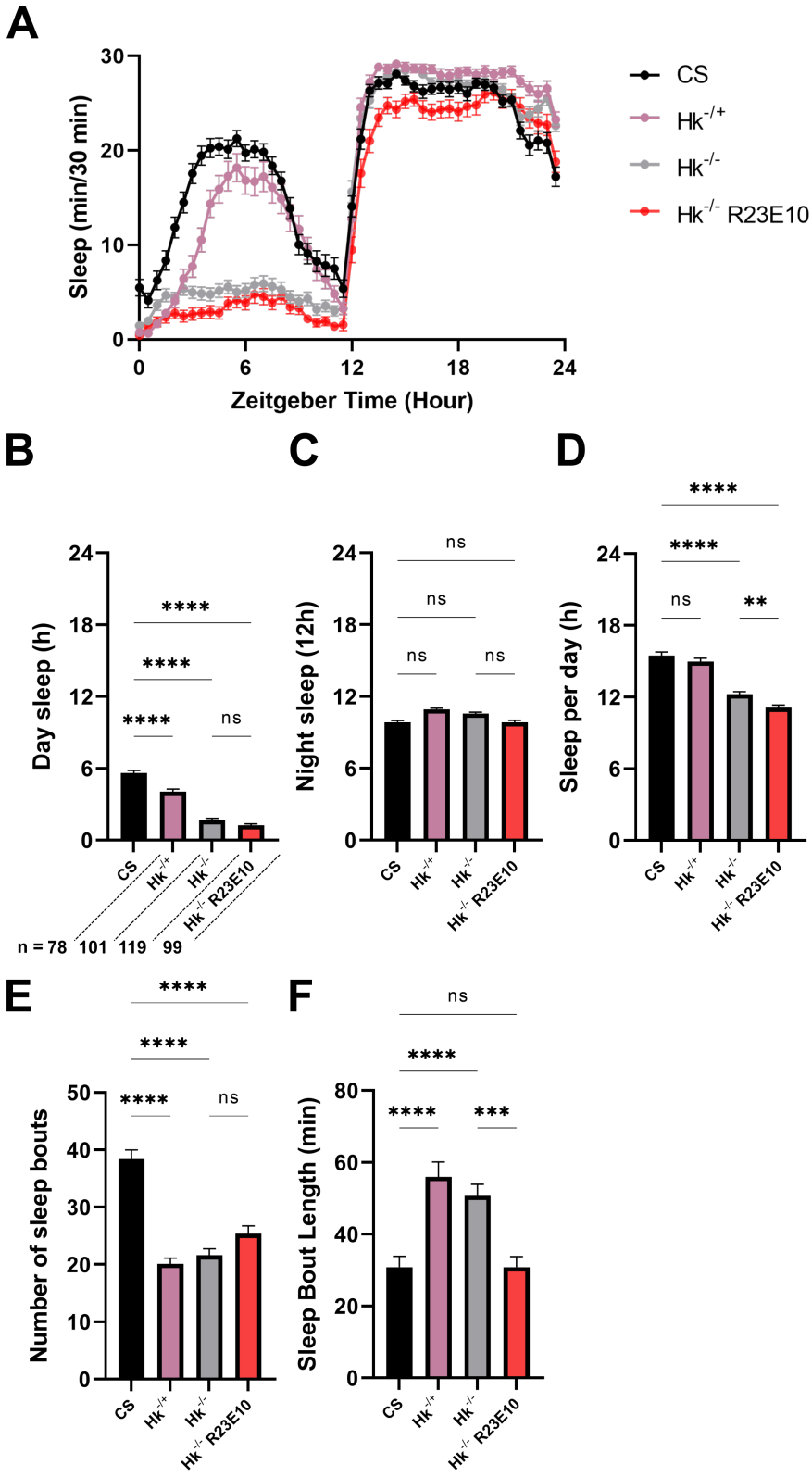


Figure 5.2: Characterisation of sleep in control groups. **A** Sleep per 30 minute bin in a 24-hour period **B** Average sleep during light hours (day) **C** Average sleep during dark hours (night) **D** Average total sleep in a 24-hour period **E** Average amount of sleep bouts in a 24-hour period **F** Average sleep bout length. Values are mean±SEM. n numbers displayed in panel **B** are consistent throughout. One-way ANOVA. *=p<0.05, **=p<0.01,***p=<0.001, ****p<0.0001.

only 11.4 hours in the same 24-hour period. In fact, this actually makes the rescue comparable to the Hk null Gal-4 control ($Hk^{-/-}$ R23E10, 11.1 hours). However, the 11.4 hours of the $Hk^{-/-}$ D251D-R23E10 still represents a significant rescue of a sleep deficient phenotype. The same fly lines without the driven constructs ($Hk^{-/-}$ D251D) exhibit an even more sleep-deprived pattern (approximately 8.5-8.9 hours per 24 hours, Fig. 5.4C).

Consistent with the results in the control group, reintroduction of Hyperkinetic mutants such as the D251D construct suggests that expressing functional hyperkinetic results in more sleep bouts with varying degrees of rescue depending on the specific mutation introduced. There was no significant compensatory change in sleep bout length for any construct.

Of the 8 constructs introduced specifically into dFB neurons on a Hyperkinetic null background (other than $Hk^{-/-}$ D251D-R23E10), 5 produced a significant rescue in day-time sleep and all constructs had at least some degree of rescuing trend compared to their un-driven controls (Grey in Fig. 5.4A). Similar to the control groups (Fig. 5.2B), nighttime sleep appeared to be unaffected by the absence and reintroduction of Hyperkinetic and no construct showed any significant difference from its relative control (Fig. 5.4B). In terms of total sleep, only 2 of the constructs produced a significant rescue compared to its un-driven control (Q505A and W403Y). For constructs D251A and H256Y, the rescuing trend seen during day-time sleep disappeared as a compensatory decrease in nighttime sleep erased this

5.3 Summary

In this chapter I observed a wide variety of sleep profiles in flies without a functional Hyperkinetic or equipped with a plethora of different Hyperkinetic constructs in dFB neurons. The wide range in effective rescue for each construct was encouraging. This implied that while the mutations are clearly affecting the activity of Hyperkinetic, they are still conferring varying degrees of function to the dFB neuron.

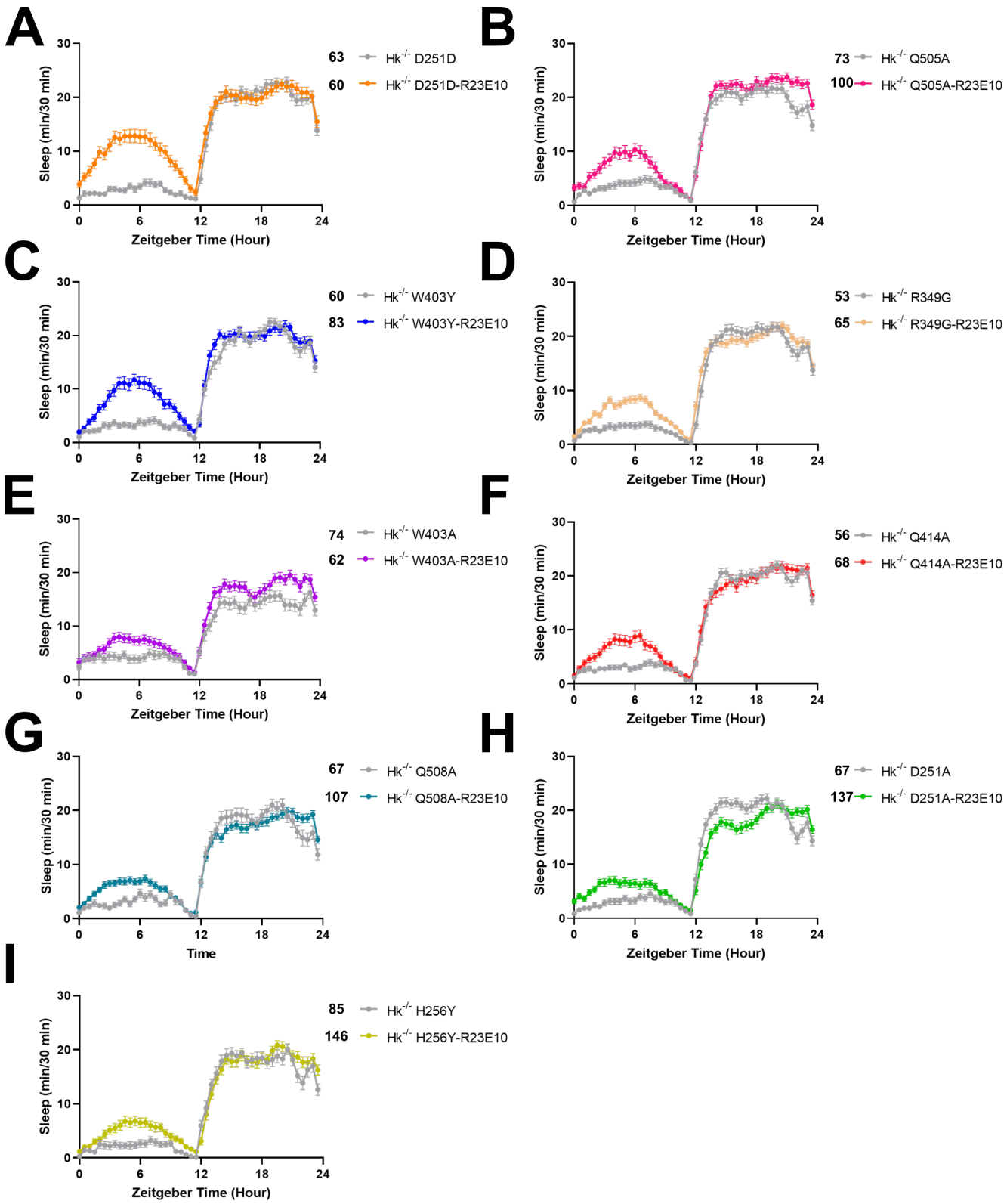


Figure 5.3: Collected traces showing sleep per 30 minute bin in a 24-hour period from flies expressing Hyperkinetic mutants on a Hyperkinetic null background compared to their respective non-'rescue' control. Values are mean±SEM. n numbers are indicated next to the relevant genotype.

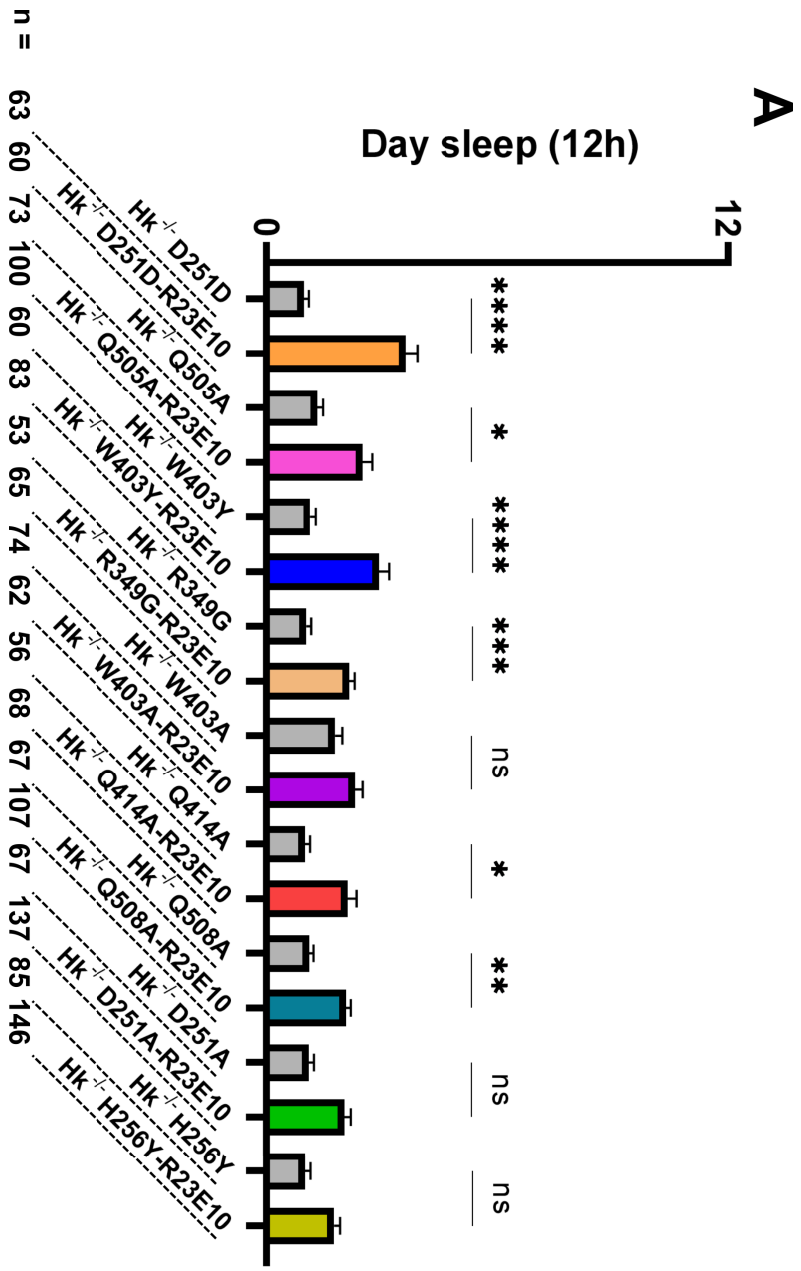


Figure 5.4: Characterisation of sleep in flies expressing Hyperkinetic mutants on a Hyperkinetic null background. **A** Average sleep during light hours (day) **B** Average sleep during dark hours (night) **C** Average total sleep in a 24-hour period. Values are mean±SEM. One-way ANOVA. *=p<0.05, **=p<0.01,***p=<0.001, ****p<0.0001, ns = no significance.

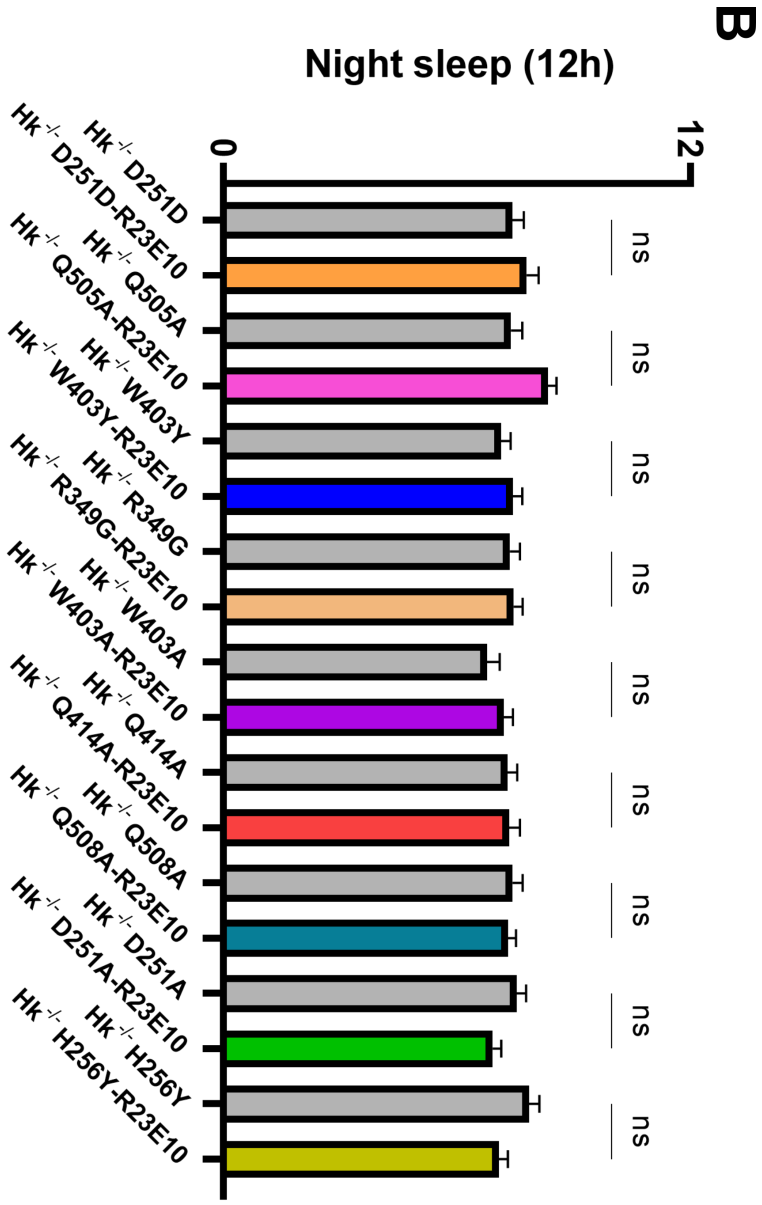


Figure 5.4: Characterisation of sleep in flies expressing Hyperkinetic mutants on a Hyperkinetic null background. **A** Average sleep during light hours (day) **B** Average sleep during dark hours (night) **C** Average total sleep in a 24-hour period. Values are mean±SEM. One-way ANOVA. *=p<0.05, **=p<0.01,***p=<0.001, ****p<0.0001, ns = no significance.

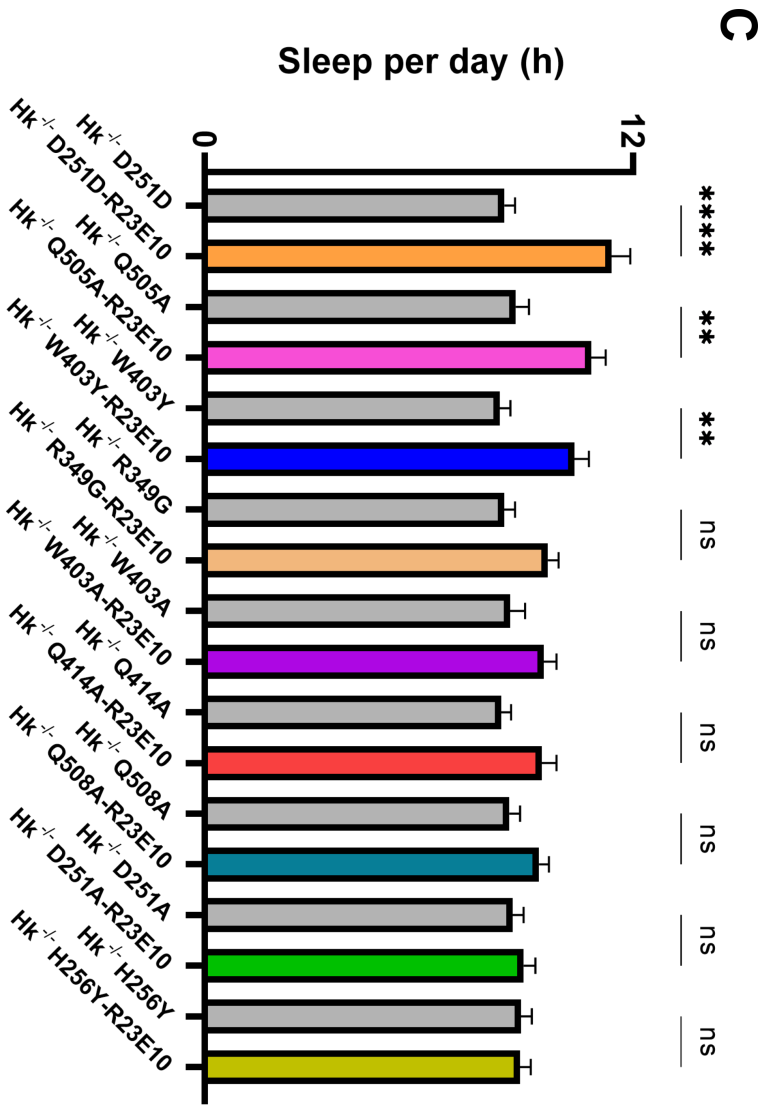


Figure 5.4: Characterisation of sleep in flies expressing Hyperkinetic mutants on a Hyperkinetic null background. **A** Average sleep during light hours (day) **B** Average sleep during dark hours (night) **C** Average total sleep in a 24-hour period. Values are mean±SEM. One-way ANOVA. *=p<0.05, **=p<0.01,***p=<0.001, ****p<0.0001, ns = no significance.

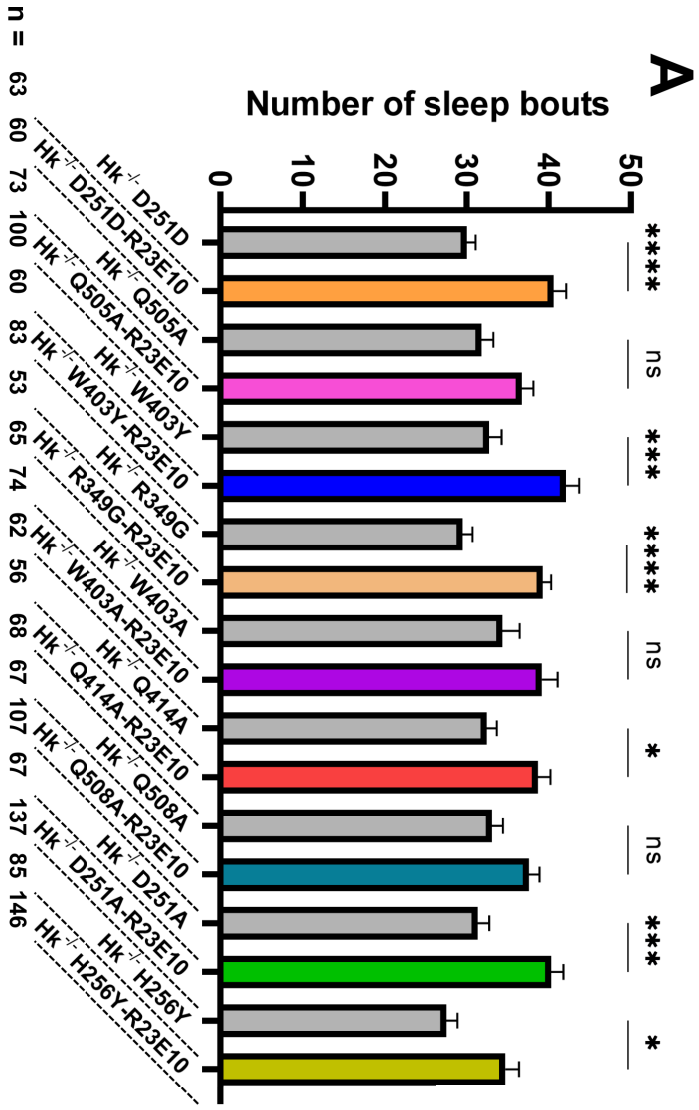


Figure 5.5: Quantified sleep structure of flies expressing Hyperkinetic mutants in the dFB neurons on a Hyperkinetic null background. **A** Average amount of sleep bouts in a 24-hour period **B** Average sleep bout length. Values are mean±SEM. One-way ANOVA. *=p<0.05, **=p<0.01,***p=<0.001, ****p<0.0001, ns = no significance.

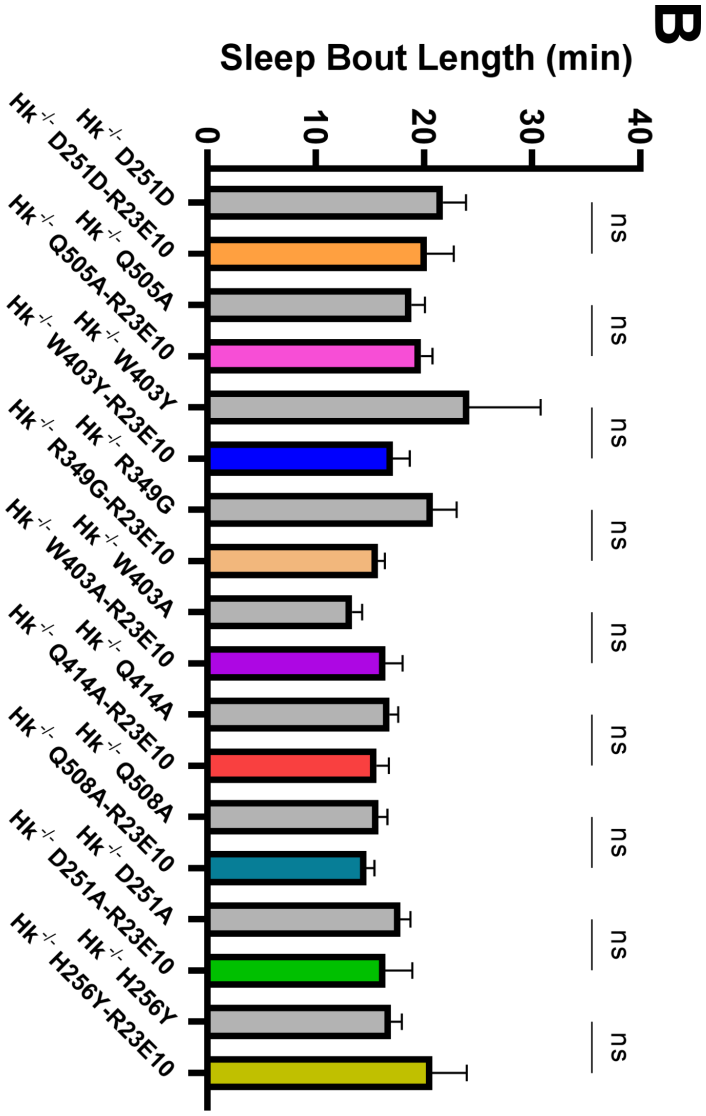


Figure 5.5: Quantified sleep structure of flies expressing Hyperkinetic mutants in the dFB neurons on a Hyperkinetic null background. **A** Average amount of sleep bouts in a 24-hour period **B** Average sleep bout length. Values are mean±SEM. One-way ANOVA. *=p<0.05, **=p<0.01,***p=<0.001, ****p<0.0001, ns = no significance.

A major consideration to these experiments which also somewhat limit what firm conclusions can be drawn from them is whether these results are due to the actual turnover of NADPH as opposed to directly impairing the catalytic activity, protein folding or membrane trafficking. However, the fact that previous studies have shown that some of these mutations can be performed without adverse effects in similar proteins suggests that at least some chosen constructs should be tolerated in the protein folding e.g. D251A and R349G [122]. To confirm whether catalytic activity remains requires expression of these constructs in a simplified system and measuring NADPH conversion into $NADP^+$ using UV absorption and an assay to ensure that expression and formation of the channel complex at the membrane are still taking place at normal levels. Another possible method would be a simple electrophysiological characterisation; the presence of a functional β subunit will always impart an increase in I_A. As such, a simple comparison in current amplitude should be sufficient to give an outline of the degree of folding and effective transport to the membrane. While important to this chapter and relevant to this work, it forms the basis of a distinct independent project and is not investigated further here. One further final consideration is that some constructs were derived from mutations in the equivalent residues in other proteins and thus, while likely to have the same effect, conclusions must be drawn with caution. Nevertheless, based on the presented sleep data and structural information it is still possible to propose the underlying root of the presented behavioural phenotype.

The complete lack of rescue of the H256Y construct was unexpected. It was assumed that the Histidine performed the same function as the Tyrosine in Hyperkinetic. This particular residue is conserved as a tyrosine throughout mammalian $K_v\beta$ and AKRs [109]. It is possible that we have either perturbed the structure or completely removed the catalytic function of Hyperkinetic, similar to the K289M constructs used in previous chapters [58]. This tyrosine in $K_v\beta$ forms a critical residue in the hydride transfer of the NADP(H) cofactor [109]. It was therefore surprising that its substitution in lieu of histidine (which is able to perform the same transfer) perturbed the function of Hyperkinetic to such a degree.

The W403A and W403Y constructs aspired to speed up turnover by removing a potentially overarching loop that trapped the NADPH co-factor. The alanine substitution aimed to remove the loop completely while the tyrosine substitution aimed to resolve whether the tryptophan, typically a difficult residue to mutate without adverse side effects, could be safely mutated into a different yet more similar amino acid. Considering this, it is encouraging that the sterically more distinct alanine substitution resulted in a non-rescue phenotype in both sleep length and in sleep episode breakdown. The W403Y on the other hand, which we hoped would still behave similar to the wildtype protein, has a comparable rescue to the effective wildtype D251D construct. The substitutions Q505A, Q414A and Q508A all attempted to achieve similar effects as the W403A with the similar underlying idea of unblocking the NADP(H) binding site. The Q505A substitution appeared to not achieve this goal as its expression was comparable to the effect of the D251D rescue. In contrast, the Q414A and Q508A both showed a diminished rescue effect comparable to the W403A substitution. These 3 constructs, if shown to facilitate NADP(H) cofactor exchange compared to the wildtype protein, would further demonstrate Hyperkinetic's and the redox state of this cofactor's role in modulating sleep pressure and strengthen previous publications' conclusions [38, 94]. However, to contrast this original prediction it is worthwhile to note that in functional AKRs with elevated catalytic rates, the Try-403 residue is substituted with a tyrosine suggesting that perhaps the presence of tryptophan or even a tyrosine is not, in fact, a rate limiting factor for Hyperkinetic's catalytic rate [109].

The D251A mutation represented one of the few constructs to have been tested previously in-vitro where an increase, albeit a modest 27%, in catalytic turnover rate was demonstrated on AKR enzymes [122]. It was thus unexpected that this modest change in enzymatic rate would result in an essential inability for Hyperkinetic (again, if indeed properly folded and expressed) to integrate homeostatic sleep pressure in the dFB neuron. However, if this increased turnover is confirmed to indeed be the case in in-vitro studies, it would lend support that even modest increases to catalytic turnover can lead to drastic changes to the dFB neuron's

homeostatic integration capabilities. Furthermore, it would also strengthen the assumption that voltage facilitated NADP(H) cofactor exchange which previously has been shown to impose an approximately 2-fold increase in cofactor exchange may in fact be sufficient to play a role in dissipating accumulated sleep pressure within the dFB neuron [106].

Curiously, while sleep was indeed significantly impaired in the absence of Hyperkinetic, these experiments highlighted a significant divergence from previous publications using the same lines. Previously, the Hyperkinetic null lines saw a reduction in both nighttime and day-time sleep [93, 94]. However, here, night sleep appears to be largely unaffected and remains comparable to the controls (Fig. 5.2B) and instead day sleep shows a very noticeable divergence between groups as null mutants exhibit virtually no sleep during day-time (Fig. 5.2A). The apparent increase in sleep consolidation in Hyperkinetic mutants (Fig. 5.2E & F) was surprising as it has been shown previously that the opposite effect would be expected [93]. Typically, such a dramatic change from previous publications are caused by genetic drift occurring as generations progress or by differences in parental backgrounds. Indeed, even varying laboratory background of the canonical wildtype CS line has been shown to be highly variable in terms of sleep behaviour despite being theoretically identical [125]. It is possible that while the Hyperkinetic null mutant was indeed effective in earlier generations at affecting both day and nighttime sleep, this mutation may only affect a single or some of the Hyperkinetic splice variants and over generations a partial rescue occurs via the upregulation of another unaffected splice variant which attenuates the effect of the null mutant.

Consistent with the previous results in the control group, our rescue experiments suggest that expressing functional Hyperkinetic results in more sleep bouts. However, in contrast to the CS group, none of the reintroduced Hyperkinetic constructs, including the proposed rescue showed any compensatory changes in sleep bout length (Fig. 5.5A & B). This suggests that the role of Hyperkinetic in sleep and subsequently the action of dFB neurons is not to consolidate existing sleep but to promote sleep

induction and hence more episodes to increase total sleep. Whether the intensity of sleep was affected was not assessed in these experiments but either conceptually simple arousal assays or more technically challenging electrophysiological LFP measurements would help answer this question. In contrast, previous experiments using short-sleeping Hyperkinetic or Shaker mutants in flies showed no increase in sleep fragmentation [92, 93].

The electrophysiological characteristics of these constructs present an enticing trove of information. This is however currently beyond the scope of this project. Speculatively though, the ideal dynamics of a truly forgetful Hyperkinetic would appear to be insensitive to the actions of either 4-ONE or miniSOG stimulation as the enzymatic turnover and co-factor exchange rate would be so fast as to obscure the effects that oxidation of the co-factor might have on both the inactivation time constants and the overall spiking of the neuron. It is however unlikely that this would realistically manifest itself in this manner. It is probable that the sheer ROS load of either 4-ONE or miniSOG experiments would still lead to the overall Hyperkinetic bound NADPH to be in oxidised form. Perhaps the time to reach the plateau in effects would instead take longer and the time required for persistent depolarisations to reverse oxidative effect reduced. In terms of miniSOG experiments, it would be interesting to see whether 10-minute light stimulation was still sufficient to produce a reliable effect. The above speculations all hinge on the assumption that the mutated versions of Hyperkinetic are otherwise properly folded and functional. Yet, as already alluded to, it is probable that few of the mutations had any adverse effects on the overall protein structure as almost all of their expression on a Hyperkinetic null background produced some degree of rescue of sleep deficiency (though not always significantly), likely due to reintroducing some degree of ROS sensitivity and altered Shaker inactivation to the dFB neurons.

6

Reflections & further directions

Contents

6.1 Main Findings 93
6.2 Discussion 95
6.3 Potential Future Directions 99

6.1 Main Findings

In this project I have confirmed the potential role of LPPs acting as physiological substrates of Hyperkinetic. Furthermore, I demonstrated for the first time in-vivo an interesting biophysical quirk of the Shaker Hyperkinetic channel complex, namely the voltage sensitivity of the co-factor exchange. This alone forms an interesting finding regardless of whether this has a direct impact on sleep regulation within the dFB neurons. However, the question that remains is what specific pathway/conformational change of the channel complex actually occurs to mediate the voltage-driven reversal of NADP(H) oxidation occurs.

Considering 4-ONE's effect on the inactivation of the Shaker-Hyperkinetic complex and previous publications [39, 94], I expected 4-ONE to increase neuronal excitability. Yet ultimately there was little observed effect from our chosen lipid peroxidation

product on the spiking of dFB neurons. This lack of effect could either be due to experimental limitations e.g. lack of trafficking of 4-ONE throughout the neural projections or the previously published ROS response on firing rate occurs via alternate pathways that still involves ROS but independently of Hyperkinetic. The latter remains unlikely however since the effects of miniSOG are specific to Hyperkinetic and therefore presumably any effect 4-ONE may have had on neuronal firing would also be Hyperkinetic dependent [94]. It is possible that 4-ONE and its interaction with the Hyperkinetic only represents one piece of the puzzle. It may in fact be a required component of the ROS sensitivity pathway but may not be sufficient to cause the overall increase in neuronal excitability. In this case, the lack of specificity from the miniSOG method may result in multiple pathways being engaged (including Hyperkinetic's) which act in conjunction to bring about sleep promotion via increased dFB neuron activity. This proposition is strengthened when considering that miniSOG's generally broad application of ROS still requires Hyperkinetic for its sleep promoting effects [94]. Nevertheless, there remains several pathways to explore however to determine whether ROS molecules (and specifically LPPs) have an impact on neuronal activity which are discussed in more detail in subsequent sections.

The sleep experiments in this project aimed to produce forms of Hyperkinetic that possessed a reduced hold on its NADP(H) cofactor and thus facilitating its exchange and perhaps give some insight to which residues are moved in order to facilitate the voltage driven mediation of cofactor exchange. The reduced hold on NADP(H) would translate as an impaired ability to integrate sleep pressure via Hyperkinetic's role in conveying this within the dFB neurons. The sleep assay highlighted a few promising residue substitutions for further characterisations (e.g. D251A & W403A). The assumptions made on these constructs still hinge on the premise that protein folding and trafficking occur as normal and only catalytic activity is affected.

6.2 Discussion

In this project we propose a model of integrating and dissipating sleep pressure. However, dFB neurons are not the sole integrator of homeostatic sleep pressure and ROS is likely not the sole messenger of said pressure. Homeostatic pressure has also been shown to accumulate at the previously mentioned R5 neuron [41]. A prominent alternative theory of homeostatic sleep pressure integration is the synaptic homeostasis hypothesis (SHY) which proposes that wakefulness is characterised by a propensity for synaptic upscaling during wakefulness and analogous pruning during sleep [4, 126], a pattern demonstrated in both mice and flies [4, 127]. In SHY the increased synaptic connectivity would equate to increased SWA power following extended wakefulness [4]. Indeed, this proposal has been demonstrated to have promise in mouse cortical recordings [128]. Furthermore, neuronal populations within the *Drosophila* brain such as the LNvs and the γ KCs of the mushroom body show an upregulation in synaptic size and number, demonstrating a potential translatability of SHY across different model organisms [127]. How sleep pressure would be dissipated in SHY is unclear, but one suggestion proposes that the resultant long term 1-Hz oscillations seen during NREM sleep may induce long-term depression (LTD) of synaptic connections [47, 93]. Another prevalent theory of sleep homeostasis refers to the balance of brain adenosine and glycogen stores [129]. Simplifying, repetitive metabolism of ATP results in serial removal of phosphate groups until only the residual adenosine remains. The abundance of adenosine can therefore be said to reflect both an increase in energy demand and reduced supply of said energy [130]. Here, the function of sleep would be to reduce demand and replenish stores. Similar to SHY, there is evidence to support this theory. Specific brain regions after extensive wakefulness accumulate adenosine and see a reduction during sleep [48]; caffeine, an adenosine receptor antagonist, results in decreased SWA and NREM sleep and increased overall wakefulness [131]. While caffeine has the equivalent effect in *Drosophila*, in contrast to mammals, this occurs without the interaction with adenosine receptors [132, 133]. Instead, in flies, caffeine acts via Dopamine, a neurotransmitter known for its wake promoting role [132, 133]. In

mammals, adenosine acts on a group of neurons in the hypothalamus, analogous to the dFB neurons of the central complex in *Drosophila* [134]. Specifically, these are predominantly GABAergic and galaninergic neurons of the ventral lateral preoptic (VLPO) area and the medial preoptic nucleus (MnPN); activity here is correlated with homeostatic sleep pressure and resulting activity induces sleep and inhibits arousal circuits [135]. However, the effects of adenosine are complex, and its effects are observed throughout several sleep centres in the mammalian brain. Adenosine acts via 4 distinct receptors for either an inhibitory and excitatory effect where the expression of these receptors varies with brain region to modulate adenosine's effect [136, 137]. Furthermore, sleep deprivation is associated with build-up of adenosine in several sleep-promoting centres of the brain such as the hippocampus, cortex and nucleus accumbens of the basal forebrain [137]. Additionally, the neuroglial astrocytes have also been shown to play a role in adenosine signalling: astrocytes release ATP which is rapidly hydrolysed into adenosine [138]. Inhibition of this release from astrocytes attenuates SWA and thus implies impaired sleep pressure accumulation [139]. While these represent examples of alternative theories, it would be premature to assume that these theories are competing and that the function and regulation of sleep are always mutually exclusive. In the case of SHY, it is assumed one of the major detriments of abundant synaptic connectivity is not only the competition for space of synaptic connections, but also the large increase in metabolic strain [4]. This project's common foundation in neuronal energy demand links the multiple hypotheses together. Furthermore, considering dFB neurons' demonstrated role operating as the sleep switch in *Drosophila*, it becomes likely that some components of these hypotheses would unify. Similar to SHY, this represents another self-regulating model of homeostatic sleep pressure building and dissipating. While the role of adenosine is not as clear in *Drosophila*, considering sleep's highly conserved role throughout the animal kingdom it is not unlikely that a similar signalling pathway exists within flies possibly using a different sleep promoting molecule to perform the same role.

To what degree the results presented here can be translated into other species forms an interesting question. Almost all the relevant preceding literature regarding Shaker-family channels and the related β subunit on which this project was based on were performed with mice homologues [85, 86, 109, 140]. Only a few used the actual *Drosophila* forms and even fewer investigated the enzymatic efficacy of Hyperkinetic [63, 65, 76, 94]. The work presented here represents only the second time that the catalytic activity of *Drosophila* Hyperkinetic and its effect on channel inactivation is demonstrated [94]. Considering the conserved nature of the mammalian enzymatic effects in *Drosophila* Hyperkinetic, one can with some certainty also presume that the role it plays as a ROS sensor is conserved. Whether the ROS sensitivity of $K_v\beta$ has a role in sleep regulation as is suggested in *Drosophila* is less clear. However, taking into account that the model proposed herein, the SHY and the adenosine balance hypotheses all have a foundation in metabolic stress (from which invariably ROS molecules will develop from) it would not be unexpected if the same function is conserved between *Drosophila* and mammals [51, 98]. An elegant unifier would be the monitoring of ROS levels via $K_v\beta$. However, the potential role of ROS and $K_v\beta$ in mammalian sleep is yet to be tested. There is some evidence to both support and oppose this notion. First, $K_v1.2$ knockout mice, a mammalian homologue of Shaker, show a significant decrease in overall sleep [141]. Further, other members of the K_v family also show a sleep phenotype when knocked down e.g. $K_v3.2$ and have an involvement in generating the SWA typical of NREM sleep [142]. However, the latter $K_v3.2$ knockdown effect on EEG activity is independent of sleep and thus its role in homeostatic sleep regulation is more tenuous [141, 143]. Knockout of the Hyperkinetic homologue $K_v\beta2$ showed no apparent phenotype (although sleep pattern and underlying brain oscillation was seemingly not assessed) [144]. The uncertainty in the results in mammalian knockdowns highlights the perks of the relative simplicity of the *Drosophila melanogaster* model. In contrast to *Drosophila*, the large variety of mammalian K_v and $K_v\beta$ subunits (which can additionally form heterotetramers for additional intricacies) adds an enormous amount of complexity in predicting a singular subunits' precise role in a mammalian model regarding any

function. For instance, the lack of apparent phenotype for $K_v\beta 2$ knockdown may simply be due to a degree of redundancy where other members of the families may see a compensatory upregulation and may be able to some degree, fulfil the same role.

The heavy focus within this thesis on Shaker and Hyperkinetic stems from previous work that strongly implicated their involvement in ROS sensitivity and sleep homeostasis [38, 93, 94]. Whether other channels e.g. voltage-gated calcium channels (Ca_v) and calcium-activated potassium channels (K_{Ca}) play a role remains undetermined. For instance, dFB neurons often display burst-prone activity where approximately 75% exhibit some form of burst-like activity. Within such activity, K_{Ca} channels repolarise membranes following bursts after being activated by the cumulative increase in intracellular Ca^{2+} stemming from the repetitive action potentials [113]. In the context of dFB neurons it is thus likely that these channels oppose burst-like activity or at least fine-tune their temporal presence and thus likely also tune any sleep promotion stemming from such activity. It is therefore surprising that the K_{Ca} channel, Slowpoke (slo), when mutated throughout the fly, maintain normal sleep behaviour [93]. Further, high-voltage active (HVA) Ca_v such as the Ca-α1 family are driven to activation by repetitive action potential firing and maintain depolarisations by allowing a constant depolarising influx of calcium ions. If the dFB sleep promotion requires more complex activity such as altered burstiness rather than simple "on/off" properties, it is highly likely that both K_{Ca} and Ca_v channels play a role and interference with their expression would thus likely influence dFB activity and any resulting sleep behaviour. The demonstrated lack of effect from mutating *slo* (for which the details of the mutations are sparse i.e. nonsense versus missense etc.) may in fact be due to compensatory mechanisms in either expression levels of a partially impaired channel or another channel replacing it in its function all together e.g. small conductance-K_{Ca}-class (SK) channels. There's even potential that the increased excitability from altered Shaker inactivation [39, 94] permits for the channel activation cascade leading to repetitive action potential bursts, as the increased action potential firing rate and correlated increase in depolarisation time

recruits further Ca_v. This would still be in agreement with the proposed model of this project where the prolonged periods of depolarisation resulting from burst activity would in fact produce more opportunity for co-factor exchange than simply faster tonic firing. While Hyperkinetic's interactions are not exclusive to Shaker and readily interact with another channel, eag, it is an important aside that the sleep reducing effect of Hyperkinetic mutation is solely through its interaction with Shaker as it does not produce any additional sleep deficient effects when ablated in the absence of functional Shaker suggesting that they impact the same pathway. Meanwhile, eag knockdown had only a modest reduction on sleep compared to Shaker knockdown [93].

6.3 Potential Future Directions

The lack of notable effects in terms of 4-ONE's effect on spiking highlights a potential limitation in the application protocol in these experiments. To eliminate the concern that there is perhaps restricted diffusion throughout the projections of the dFB neurons the ideal solution would be to produce a direct application of 4-ONE throughout the whole neuron in a manner similar to the miniSOG experiments where ROS was synthesised uniformly within the neuron. Halo-tag targetable RES which release its payload in response to photostimulating light presents an interesting solution [145]. In this scenario Hyperkinetic would be either directly Halo-tagged or free-floating halo-tags would be used. These would be loaded with 4-ONE for proximal release to Hyperkinetic. Furthermore, this method would assist in establishing an accurate baseline of both Shaker inactivation and neuronal firing due to the temporal control afforded by this system. For this project I synthesised several versions of these constructs in the hope of using this technique. Although, at the time of writing this method does not allow for the loading of 4-ONE and has hitherto mostly been used with 4-HNE which is comparable in structure to 4-ONE but as demonstrated in Fig. 2.2, 4-HNE is regrettably not a substrate of Hyperkinetic. Regardless, this method still holds a lot of promise for potential future experiments. Based on enzymatic assays of $K_v\beta$, 4-ONE is likely not the sole

substrate of Hyperkinetic [87]. It is therefore potentially possible to use this system with another LDE or adapt the technique to accommodate the additional reactive group of the 4-ONE [145].

Another avenue to potentially pursue involves a similar experiment to previous experiments using AOX [94], only this time restrict the antioxidant enzyme's targeting to LDEs. The *Drosophila* gene *sniffer* encodes a short chain dehydrogenase/reductase (SDR) that has a demonstrated strong affinity for 4-ONE (and interestingly nil affinity for 4-HNE) [146]. Interference with this gene results in a reduced lifespan in flies with associated accelerated age-related neurodegeneration [147]. Its overexpression increases average lifespan under normal conditions and imparts a protective effect against pro-oxidant environments and diminishes its detrimental effects on life-span [146]. Studies investigating this protein have hitherto not assessed *sniffer*'s role in sleep and do not give details about whether the age-related neurodegeneration is associated with reduced sleep. Specific overexpression of *sniffer* in the dFB neuron would give additional clues about the specific identity of ROS signalling molecules. Furthermore, an additional interesting question would be whether, in *sniffer* mutants, artificially induced sleep via either thermo- or optogenetic activation of dFB neurons would rescue the reduced life-span phenotype. If so it would again strengthen the case that sleep is a neuroprotective measure against ROS.

While perhaps somewhat tangential in the context of this project's original aim, the current clamp experiments of Ch.4 highlighted a fascinating diversity within the population of the dFB neurons when observing input resistance, spiking frequency and spiking patterning i.e. tonic versus bursty. Preliminary in-house data from single cell mRNA sequencing suggests that the dFB neuron population can be further subdivided into smaller groups based on their neuropeptide complement (beyond the almost ubiquitous AstA-R expression). A very enticing, yet relatively simple experiment would be to characterise the spiking dynamics of these subpopulations and further investigate, based on sleep history, any altered activity to increased

sleep pressure. In terms of the ROS-Hyperkinetic interaction, all cells for the patch clamp were selected at random and thus it is likely that cells from all of the above subpopulations were included. 4-ONE's effect on Shaker inactivation appeared to be consistent however, and no distinct distributions appear in any of the voltage clamp data sets suggesting the effect applied uniformly on all cells regardless of which subgroup of dFB neurons may have been patched.

7

Materials and Methods

Contents

7.1 Fly Strains 103
7.2 Sleep measurements 104
7.3 Electrophysiology 104
7.4 Statistical analysis 107
7.4.1 Statistical tests 107
7.4.2 Equations 107
7.5 Miscellaneous contributions 109

7.1 Fly Strains

All flies were reared on medium consisting of sucrose, yeast, molasses and agar on a 12:12h dark:light cycle at 25 °C. Cell type specificity was achieved using the commonly used GAL4:UAS expression system [31]. In all experiments, transgenes were introduced specifically to dFB neurons using the R23E10-GAL4 driver line [123]. dFB neurons were labelled for patch clamp experiments via the fluorescent label, UAS-mCD8-GFP [148]. In experiments using miniSOG, the experimental flies were heterozygous for the UAS-miniSOG transgene [104]. Experiments using either catalytic null mutant (Hk^{K289M}) or functional rescue Hk^{WT} forms of Hyperkinetic were reared in a Hyperkinetic null background (Hk^{1})[58]. All custom Hyperkinetic

mutant constructs for sleep experiments were developed by P. Liu using the Hyperkinetic isoform E (Hyperkinetic_RE) as a template, a Q5 Site-Directed Mutagenesis Kit (New England Biosciences) was used to insert single nucleotide mutations at the desired loci. Constructs were integrated into fly germline by BestGene Inc.

7.2 Sleep measurements

2-5 day old females were loaded into 65 mm glass tubes and loaded into Drosophila Activity Monitors (DAM, Trikinetics). Sleep was assessed exclusively in female flies due to flies exhibiting sexual dimorphism regarding sleep amounts and patterns which made it unsuitable to mix genders in datasets. Female flies' sleep is mostly constrained to nighttime and, overall, has a slightly lower duration [149, 150]. Sleep studies were performed under a 12h:12h light:dark cycle. Continuous periods of inactivity of 5 or more minutes were quantified as sleep. This assumption has previously been shown to strongly correlate with the actual behavioural state, crucially flies with more than 5 minutes of inactivity show raised arousal threshold to stimuli, a hallmark of sleep [21, 25]. Flies which exhibited little or no activity (<2 beam breaks) in any 24-hour test period were excluded from further analysis. Sleep behaviour was quantified using the MATLAB script Sleep and Circadian Analysis MATLAB Program (SCAMP) developed by the Vecsey Lab [151]. Flies were allowed one night to adapt to the new environment and the following 2 24-hour periods were used for analysis.

7.3 Electrophysiology

Adult female flies 2-6 days post eclosion were head fixed on custom mounts using eicosane (Sigma). Flies were generally patched during mornings and afternoons when presumably sleep pressure was low-to-moderate. In the presence of extracellular solution, the cuticle, trachea, excess adipose tissue and the perineural sheath were removed using forceps [152, 153]. Extracellular solution contained 103 mM NaCl, 3

mM KCl, 5 mM N-TRIS (TES), 8 mM trehalose, 10 mM glucose, 7 mM sucrose, 26 mM NaHCO3, 1 mM NaH2PO4, 1.5 mM $CaCl_2$ and 4 mM $MgCl_2$, 275 mOsM, pH 7.3 with 5% CO2: 95% O2. Labelled cells were visualised using an Axioskope 2 FS mot microscope (Zeiss) equipped with a 60 × 1.0 NA water-immersion objective (LUMPLFLN60XW, Olympus) and illuminated using a pE-300white LED (CoolLED). Recordings were made at room temperature with a MultiClamp 700B amplifier, lowpass-filtered at 10 kHz, and sampled at either 20 or 50 kHz using a Digidata 1440A & 1550B digitizer controlled through pCLAMP 10 & 11 (Molecular Devices). Patch pipettes (9-11 MOhm) were pulled using a PC-10 Puller (Narishige) or a DMZ-Universal-Electrode-Puller (Zeitz-Instruments) and filled with intracellular solution containing 140mM potassium aspartate, 10 mM HEPES, 1 mM KCl, 4mM MgATP, 0.5 mM Na_3GTP, 1 mM EGTA, pH 7.3, 265 mOsM. When present, 4-oxo-2-nonenal (4-ONE, 50 µM, Cayman Chemical), 4-hydroxynonenal (4-HNE, 200 µM, Cayman Chemical) were directly supplemented into the intracellular solution. 4-ONE and 4-HNE were suspended in methyl acetate (MeAc) and ethanol, respectively and were not allowed to surpass 0.15% of total volume. miniSOG photo stimulation was performed using a 455-nM LED (Thorlabs, M455L3) with a collimator lens controlled by a T-Cube LED Driver (Thorlabs), power was set to 3.5-5 mW/cm2 at the sample.

All voltage clamp experiments were performed in the presence of tetrodotoxin (TTX, Tocris) and cadmium to block sodium and calcium currents respectively. I_A was measured by holding neurons at a potential of either -10 or -110 mV and then stepped to a test pulse in 10 mV increments from -100 mV to +30 mV. Stepping from the -110 mV pre-pulse produces the total potassium current (I_{Tot}) mediated by a plethora of various K^+ channels including Shaker. Meanwhile, a -10 mV holding induces inactivation in K_v channels such as Shaker and produces only non A-type currents (I_{Non-A}) when stepping to the test pulse. I_A was thus derived from digitally subtracting I_{Non-A} from the I_{Tot} recordings. To obtain values for the fast and slow decay constants (τ_1 and τ_2 respectively), a double exponential curve was fit to the subtracted traces (Example shown in Fig. 7.1). All fits were performed to the

highest depolarising step (i.e. +30 mV). In cases where a consistent fit for the second time constant was unachievable, only the fast component was included for analysis. Spiking was simulated by holding at -60 mV for 95 ms and depolarising the cells for 3 ms to +10 mV. This protocol was repeated at 10 Hz for 20 minutes. The digital subtraction and subsequent curve fitting were done using the NeuroMatic package [154] in Igor Pro (WaveMetrics).

Input resistance (R_m) was calculated from a linear fit of 5 1-second hyperpolarising current injections in 5 pA increments, starting from -20 pA, from a resting membrane potential of -60±5 mV. Membrane time constants (τ_m) were calculated by fitting a single exponential curve to the voltage deflection of a -5 pA hyperpolarising current injection from a resting membrane potential of -60±5 mV.

Current-Frequency (IF) curves were generated from a series of depolarising current injections from a membrane potential of -60±5 mV in 5 pA increments. Spikes were detected from the derivative of the membrane potential trace with a custom spike detection script within Igor Pro. The interspike interval values generated from all current injections were pooled for analysis.

The spike rise and decay rate were calculated using custom MATLAB scripts. Every individual spike was assessed for each cell recorded in a 20-second bin of only spontaneous activity. Each spike was converted into a differential plot and the maxima and minima were extracted. The mean values for all spikes formed 1 data point per cell.

Appropriate whole cell capacitance and bridge balance were used in voltage and current clamp, respectively. Access resistance (R_a) was monitored throughout experiments, cells which exceeded 50 MOhm R_a were excluded from analysis. The common cut-off standard of no more than 20% change proved unviable for *Drosophila* whole cell patching, likely due to the very small patch pipettes compared to other systems, (e.g. HEK cell patching) where such a standard is relatively easy to abide by. Therefore, a set value was used instead to avoid excessive detrimental effects of access resistance.

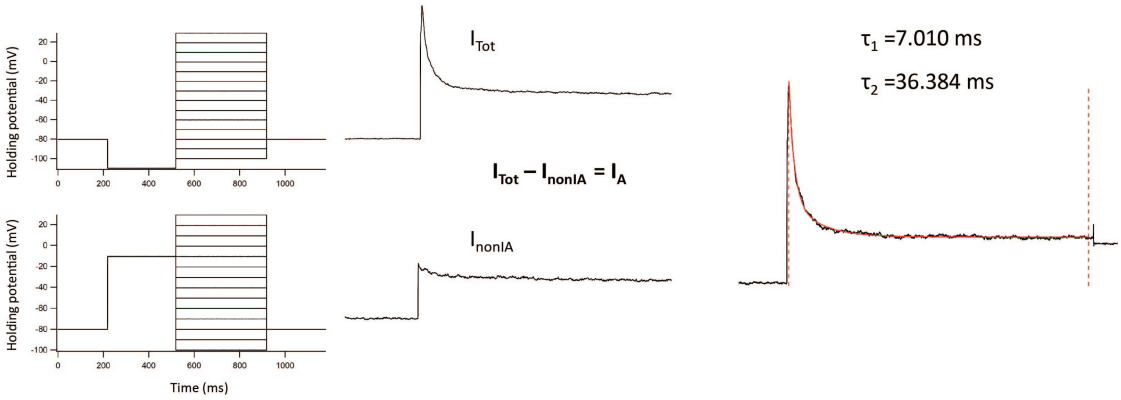


Figure 7.1: A-type current measured by running 2 distinct protocols with different pre-pulses (either -110 mV or -10 mV). This results in the total current, (I_{Tot}) and total current excluding A-type currents (I_{Non-A}), respectively. Subtracting the latter from the former results in the isolated A-type current, to which a double exponential decay curve can be fitted to retrieve inactivation time constants. In this case, these are 7.0 ms and 36.3 ms for the fast and slow inactivation time constants respectively.

7.4 Statistical analysis

7.4.1 Statistical tests

Data was analysed using Prism 9 (GraphPad). All voltage clamp experiments with two time-points used paired Student's t-test. For experiments with multiple time points repeat measured 1-way ANOVA were used with a Tukey's multiple comparison post hoc. In cases where multiple groups were compared over several time points, i.e. IF curve comparisons, repeated measure 2-way ANOVAs were used with Tukey's post hoc. If there were a reduction in n numbers as the experiment progressed, as certain protocols were prone to this (typically long duration voltage clamp experiments), a mixed-effects model with Tukey's post hoc was used instead. A p-value of less than 0.05 was considered significant for all of the above tests. Unless stated otherwise, each data point represents a single cell.

7.4.2 Equations

For calculating the indices describing the degree of burstiness of spontaneous activity, 60-second recordings of unclamped cells were used to record spontaneous activity. The cells were allowed 40 seconds to settle into a recurring rhythm. Once activity had settled and the neuron's activity had become uniform, the last 20 seconds of

these recordings were used. For indices calculation, these 20 second of spontaneous activity were further subdivided into 0.2 second bins.

The burstiness index (BI) was derived from [118]. The formula to calculate the BI of dFB neurons was:

$$B.I = \frac{Sum\ of\ spikes\ in\ top\ 15\%\ of\ bins}{Sum\ of\ spikes\ in\ all\ bins} \tag{7.1}$$

A value of 1 would indicate that all spikes are located within the top 15% of bins. A value closer to 0.15 indicates tonic firing.

The formula to calculate the SI of dFB neurons was:

$$S.I = 1 - \frac{Sum\ of\ spikes\ in\ all\ bins}{Sum\ of\ square\ of\ each\ individual\ bin} \tag{7.2}$$

Using SI, a value closer to 0 indicates sparse firing, while a value closer to 1 indicates more burstiness.

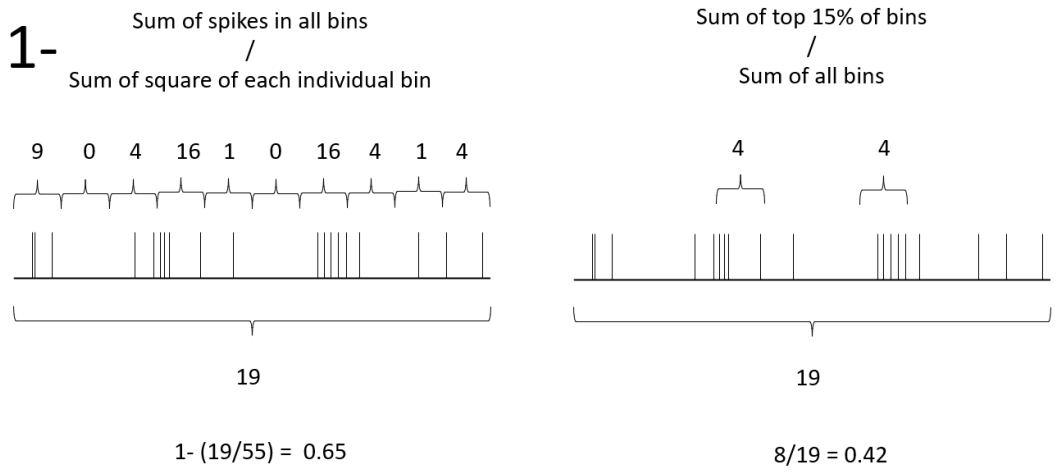


Figure 7.2: Example of methods of determining SI and BI derived from a representative 20s recording, SI and BI on the left and right respectively. Each vertical line represents one action potential and the value above represents the sum of action potential counts either in the top 15% of bins or the square of each individual bin for either BI or SI respectively. The value below represents the total amount of spikes throughout the complete timeline.

The coefficient of variation (C_v) of ISI was calculated as previously described [117] using the equation:

$$C_v = \frac{\Delta t}{t} \tag{7.3}$$

where Δt is the standard deviation of the collected ISI times for all cells and t is the mean ISI times of the same cells.

7.5 Miscellaneous contributions

The plasmid's used for embryo injections were developed and kindly donated by Patrick Liu, a fellow member of the Miesenböck lab. All sleep experiments of Ch.5 were done in collaboration with P. Liu.

References

1. Hill, V. M. *et al.* A Bidirectional Relationship between Sleep and Oxidative Stress in Drosophila. *PLoS biology* **16,** e2005206 (2018).
2. Walker, M. P. & Stickgold, R. Sleep-Dependent Learning and Memory Consolidation. *Neuron* **44,** 121–133 (Sept. 2004).
3. Kuhn, M. *et al.* Sleep Recalibrates Homeostatic and Associative Synaptic Plasticity in the Human Cortex. *Nature Communications* **7,** 12455 (Aug. 2016).
4. Tononi, G. & Cirelli, C. Sleep and the Price of Plasticity: From Synaptic and Cellular Homeostasis to Memory Consolidation and Integration. *Neuron* **81,** 12–34 (Jan. 2014).
5. Weiss, J. T. & Donlea, J. M. Sleep Deprivation Results in Diverse Patterns of Synaptic Scaling across the Drosophila Mushroom Bodies. *Current Biology* **31,** 3248–3261.e3 (Aug. 2021).
6. Dement, W. C. The Study of Human Sleep: A Historical Perspective. *Thorax* **53,** S2 (1998).
7. Zordan, M., Costa, R., Macino, G., Fukuhara, C. & Tosini, G. Circadian Clocks: What Makes Them Tick? *Chronobiology International* **17,** 433–451 (Jan. 2000).
8. Loomis, A. L., Harvey, E. N. & Hobart, G. A. Cerebral States during Sleep, as Studied by Human Brain Potentials. *Journal of Experimental Psychology* **21,** 127–144 (1937).
9. Blake, H. & Gerard, R. W. Brain Potentials during Sleep. *American Journal of Physiology-Legacy Content* **119,** 692–703 (July 1937).
10. Aserinsky, E. & Kleitman, N. Regularly Occurring Periods of Eye Motility, and Concomitant Phenomena, during Sleep. *Science* **118,** 273 (1953).
11. Dement, W. & Kleitman, N. The Relation of Eye Movements during Sleep to Dream Activity: An Objective Method for the Study of Dreaming. *Journal of Experimental Psychology* **53,** 339–346 (1957).
12. Konopka, R. J. & Benzer, S. Clock Mutants of Drosophila Melanogaster. *Proceedings of the National Academy of Sciences* **68,** 2112 (1971).
13. Sehgal, A., Price, J. L., Man, B. & Young, M. W. Loss of Circadian Behavioral Rhythms and per RNA Oscillations in the Drosophila Mutant Timeless. *Science (New York, N.Y.)* **263,** 1603–1606 (Mar. 1994).
14. Allada, R., White, N. E., So, W. V., Hall, J. C. & Rosbash, M. A Mutant Drosophila Homolog of Mammalian Clock Disrupts Circadian Rhythms and Transcription of Period and Timeless. *Cell* **93,** 791–804 (May 1998).

15. Rutila, J. E. *et al.* CYCLE Is a Second bHLH-PAS Clock Protein Essential for Circadian Rhythmicity and Transcription of Drosophila Period and Timeless. *Cell* **93,** 805–814 (May 1998).

16. Tataroglu, O. & Emery, P. Studying Circadian Rhythms in Drosophila Melanogaster. *Methods (San Diego, Calif.)* **68,** 140–150 (June 2014).

17. Helfrich-Förster, C. The Period Clock Gene Is Expressed in Central Nervous System Neurons Which Also Produce a Neuropeptide That Reveals the Projections of Circadian Pacemaker Cells within the Brain of Drosophila Melanogaster. *Proceedings of the National Academy of Sciences of the United States of America* **92,** 612–616 (Jan. 1995).

18. Renn, S. C. P., Park, J. H., Rosbash, M., Hall, J. C. & Taghert, P. H. A Pdf Neuropeptide Gene Mutation and Ablation of PDF Neurons Each Cause Severe Abnormalities of Behavioral Circadian Rhythms in Drosophila. *Cell* **99,** 791–802 (Dec. 1999).

19. Ewer, J., Frisch, B., Hamblen-Coyle, M., Rosbash, M. & Hall, J. Expression of the Period Clock Gene within Different Cell Types in the Brain of Drosophila Adults and Mosaic Analysis of These Cells' Influence on Circadian Behavioral Rhythms. *The Journal of Neuroscience* **12,** 3321–3349 (Sept. 1992).

20. Welsh, D. K., Logothetis, D. E., Meister, M. & Reppert, S. M. Individual Neurons Dissociated from Rat Suprachiasmatic Nucleus Express Independently Phased Circadian Firing Rhythms. *Neuron* **14,** 697–706 (Apr. 1995).

21. Shaw, P. J., Cirelli, C., Greenspan, R. J. & Tononi, G. Correlates of Sleep and Waking in Drosophila Melanogaster. *Science* **287,** 1834–7 (2000).

22. Sehgal, A. & Mignot, E. Genetics of Sleep and Sleep Disorders. *Cell* **146,** 194–207 (2011).

23. Cirelli, C. The Genetic and Molecular Regulation of Sleep: From Fruit Flies to Humans. *Nature Reviews Neuroscience* **10,** 549–60 (2009).

24. Van Alphen, B., Yap, M. H. W., Kirszenblat, L., Kottler, B. & van Swinderen, B. A Dynamic Deep Sleep Stage in Drosophila. *Journal of Neuroscience* **33,** 6917–6927 (Apr. 2013).

25. Hendricks, J. C. *et al.* Rest in Drosophila Is a Sleep-like State. *Neuron* **25,** 129–38 (2000).

26. Yap, M. H. W. *et al.* Oscillatory Brain Activity in Spontaneous and Induced Sleep Stages in Flies. *Nature Communications* **8,** 1815 (2017).

27. Raccuglia, D. *et al.* Network-Specific Synchronization of Electrical Slow-Wave Oscillations Regulates Sleep Drive in Drosophila. *Current Biology* **29,** 3611–3621.e3 (Nov. 2019).

28. Cirelli, C. & Bushey, D. Sleep and Wakefulness in Drosophila Melanogaster. *Annals of the New York Academy of Sciences* **1129,** 323–329 (2008).

29. Kirszenblat, L. & van Swinderen, B. in *Handbook of Behavioral Neuroscience* (ed Dringenberg, H. C.) 333–347 (Elsevier, Jan. 2019).

30. Borbely, A. A. A Two Process Model of Sleep Regulation. *Human Neurobiology* **1,** 195–204 (1982).

31. Brand, A. H. & Perrimon, N. Targeted Gene Expression as a Means of Altering Cell Fates and Generating Dominant Phenotypes. *Development* **118,** 401–15 (1993).

32. Donlea, J. M., Thimgan, M. S., Suzuki, Y., Gottschalk, L. & Shaw, P. J. Inducing Sleep by Remote Control Facilitates Memory Consolidation in Drosophila. *Science* **332,** 1571–1576 (June 2011).

33. Kume, K. Dopamine Is a Regulator of Arousal in the Fruit Fly. *Journal of Neuroscience* **25,** 7377–7384 (2005).

34. Andretic, R., van Swinderen, B. & Greenspan, R. J. Dopaminergic Modulation of Arousal in Drosophila. *Current biology: CB* **15,** 1165–1175 (July 2005).

35. Liu, Q., Liu, S., Kodama, L., Driscoll, M. R. & Wu, M. N. Two Dopaminergic Neurons Signal to the Dorsal Fan-shaped Body to Promote Wakefulness in Drosophila. *Current biology : CB* **22,** 2114–2123 (Nov. 2012).

36. Denholm, B. *et al.* Crossveinless-c Is a RhoGAP Required for Actin Reorganisation during Morphogenesis. *Development (Cambridge, England)* **132,** 2389–2400 (May 2005).

37. Donlea, J. M., Pimentel, D. & Miesenböck, G. Neuronal Machinery of Sleep Homeostasis in Drosophila. *Neuron* **81,** 860–872 (Feb. 2014).

38. Pimentel, D. *et al.* Operation of a Homeostatic Sleep Switch. *Nature* **536,** 333–337 (Aug. 2016).

39. Connor, J. A. & Stevens, C. F. Prediction of Repetitive Firing Behaviour from Voltage Clamp Data on an Isolated Neurone Soma. *The Journal of Physiology* **213,** 31–53 (1971).

40. Donlea, J. M. *et al.* Recurrent Circuitry for Balancing Sleep Need and Sleep. *Neuron* **97,** 378–389.e4 (Jan. 2018).

41. Liu, S., Liu, Q., Tabuchi, M. & Wu, M. N. Sleep Drive Is Encoded by Neural Plastic Changes in a Dedicated Circuit. *Cell* **165,** 1347–1360 (2016).

42. Holland, C. Sleep Homeostasis in *Drosophila* : A Window on the Vital Function of Sleep. *Bioscience Horizons: The International Journal of Student Research* **11** (Jan. 2018).

43. Kottler, B. *et al.* A Sleep/Wake Circuit Controls Isoflurane Sensitivity in Drosophila. *Current biology: CB* **23,** 594–598 (Apr. 2013).

44. Sherin, J. E., Elmquist, J. K., Torrealba, F. & Saper, C. B. Innervation of Histaminergic Tuberomammillary Neurons by GABAergic and Galaninergic Neurons in the Ventrolateral Preoptic Nucleus of the Rat. *The Journal of Neuroscience: The Official Journal of the Society for Neuroscience* **18,** 4705–4721 (June 1998).

45. Ni, J. D. *et al.* Differential Regulation of the Drosophila Sleep Homeostat by Circadian and Arousal Inputs. *eLife* **8** (eds Ramaswami, M. & Marder, E.) e40487 (Feb. 2019).

46. Thomas, C. W., Guillaumin, M. C., McKillop, L. E., Achermann, P. & Vyazovskiy, V. V. Global Sleep Homeostasis Reflects Temporally and Spatially Integrated Local Cortical Neuronal Activity. *eLife* **9,** e54148.

47. Tononi, G. & Cirelli, C. Sleep Function and Synaptic Homeostasis. *Sleep Medicine Reviews* **10,** 49–62 (Feb. 2006).

48. Porkka-Heiskanen, T., Strecker, R. E. & McCarley, R. W. Brain Site-Specificity of Extracellular Adenosine Concentration Changes during Sleep Deprivation and Spontaneous Sleep: An in Vivo Microdialysis Study. *Neuroscience* **99,** 507–517 (2000).

49. Reimund, E. The Free Radical Flux Theory of Sleep. *Medical Hypotheses* **43,** 231–233 (Oct. 1994).

50. Cadet, J. L. Free Radical Mechanisms in the Central Nervous System: An Overview. *The International Journal of Neuroscience* **40,** 13–18 (May 1988).

51. Parvez, S., Long, M. J. C., Poganik, J. R. & Aye, Y. Redox Signaling by Reactive Electrophiles and Oxidants. *Chemical Reviews* **118,** 8798–8888 (2018).

52. D'Almeida, V. *et al.* Sleep Deprivation Induces Brain Region-Specific Decreases in Glutathione Levels. *Neuroreport* **9,** 2853–2856 (Aug. 1998).

53. Kerksick, C. & Willoughby, D. The Antioxidant Role of Glutathione and N-Acetyl-Cysteine Supplements and Exercise-Induced Oxidative Stress. *Journal of the International Society of Sports Nutrition* **2,** 38 (Dec. 2005).

54. Cirelli, C., Shaw, P. J., Rechtschaffen, A. & Tononi, G. No Evidence of Brain Cell Degeneration after Long-Term Sleep Deprivation in Rats. *Brain Research* **840,** 184–193 (Sept. 1999).

55. D'Almeida, V. *et al.* Absence of Oxidative Stress Following Paradoxical Sleep Deprivation in rats1These Results Have Been Presented as an Oral Communication during the 13th European Congress on Sleep Research, Brussels, Belgium, 1996.1. *Neuroscience Letters* **235,** 25–28 (Oct. 1997).

56. Vaccaro, A. *et al.* Sleep Loss Can Cause Death through Accumulation of Reactive Oxygen Species in the Gut. *Cell* **181,** 1307–1328.e15 (June 2020).

57. Catsch, A. Eine Erbliche Storung Des Bewegungsmechanismus Bei Drosophila Melanogaster. *Z. Indukt. Abstammungs. Verebungsl.,* 64–66. (1944).

58. Kaplan, W. D. & Trout W. E., 3. The Behavior of Four Neurological Mutants of Drosophila. *Genetics* **61,** 399–409 (1969).

59. Tempel, B. L., Papazian, D. M., Schwarz, T. L., Jan, Y. N. & Jan, L. Y. Sequence of a Probable Potassium Channel Component Encoded at Shaker Locus of Drosophila. *Science* **237,** 770 (1987).

60. Iverson, L. E., Tanouye, M. A., Lester, H. A., Davidson, N. & Rudy, B. A-Type Potassium Channels Expressed from Shaker Locus cDNA. *Proceedings of the National Academy of Sciences* **85,** 5723–5727 (1988).

61. Zagotta, W. N. & Aldrich, R. W. Voltage-Dependent Gating of Shaker A-type Potassium Channels in Drosophila Muscle. *Journal of General Physiology* **95,** 29–60 (1990).

62. Chouinard, S. W., Wilson, G. F., Schlimgen, A. K. & Ganetzky, B. A Potassium Channel Beta Subunit Related to the Aldo-Keto Reductase Superfamily Is Encoded by the Drosophila Hyperkinetic Locus. *Proceedings of The National Academy Of Sciences Of The United States Of America* **92,** 6763–7 (1995).

63. Hoshi, T., Zagotta, W. N. & Aldrich, R. W. Two Types of Inactivation in Shaker K+ Channels: Effects of Alterations in the Carboxy-Terminal Region. *Neuron* **7,** 547–556 (1991).

64. Choi, K. L., Aldrich, R. W. & Yellen, G. Tetraethylammonium Blockade Distinguishes Two Inactivation Mechanisms in Voltage-Activated K+ Channels. *Proceedings of the National Academy of Sciences* **88,** 5092–5095 (1991).

65. Hoshi, T., Zagotta, W. & Aldrich, R. Biophysical and Molecular Mechanisms of Shaker Potassium Channel Inactivation. *Science* **250,** 533–538 (1990).

66. Demo, S. D. & Yellen, G. The Inactivation Gate of the Shaker K+ Channel Behaves like an Open-Channel Blocker. *Neuron* **7,** 743–753 (1991).

67. Jiang, X., Bett, G. C. L., Li, X., Bondarenko, V. E. & Rasmusson, R. L. C-Type Inactivation Involves a Significant Decrease in the Intracellular Aqueous Pore Volume of Kv1.4 k + Channels Expressed in Xenopus Oocytes. *The Journal of Physiology* **549,** 683–695 (2003).

68. Bett, G. C. L., Dinga-Madou, I., Zhou, Q., Bondarenko, V. E. & Randall. A Model of the Interaction between N-Type and c-Type Inactivation in Kv1.4 Channels. *Biophysical Journal* **100,** 11–21 (2011).

69. Pongs, O. Voltage-Gated Potassium Channels: From Hyperexcitability to Excitement. *FEBS Letters* **452,** 31–35 (1999).

70. Axelrod, J., Burch, R. M. & Jelsema, C. L. Receptor-Mediated Activation of Phospholipase A2 via GTP-binding Proteins: Arachidonic Acid and Its Metabolites as Second Messengers. *Trends in Neurosciences* **11,** 117–123 (1988).

71. Doyle, D. A. The Structure of the Potassium Channel: Molecular Basis of K+ Conduction and Selectivity. *Science* **280,** 69–77 (1998).

72. Villarroel, A. & Schwarz, T. Inhibition of the Kv4 (Shal) Family of Transient K+ Currents by Arachidonic Acid. *The Journal of Neuroscience* **16,** 1016–1025 (1996).

73. Oliver, D. Functional Conversion between A-Type and Delayed Rectifier K+ Channels by Membrane Lipids. *Science* **304,** 265–270 (2004).

74. Kruse, M., Hammond, G. R. V. & Hille, B. Regulation of Voltage-Gated Potassium Channels by PI(4,5)P2. *Journal of General Physiology* **140,** 189–205 (2012).

75. Morales, M. J., Castellino, R. C., Crews, A. L., Rasmusson, R. L. & Strauss, H. C. A Novel β Subunit Increases Rate of Inactivation of Specific Voltage-gated Potassium Channel α Subunits. *Journal of Biological Chemistry* **270,** 6272–6277 (1995).

76. Zagotta, W. N., Hoshi, T. & Aldrich, R. W. Gating of Single Shaker Potassium Channels in Drosophila Muscle and in Xenopus Oocytes Injected with Shaker mRNA. *Proceedings of the National Academy of Sciences* **86,** 7243–7247 (1989).

77. Parcej, D. N., Scott, V. E. & Dolly, J. O. Oligomeric Properties of Alpha-Dendrotoxin-Sensitive Potassium Ion Channels Purified from Bovine Brain. *Biochemistry* **31,** 11084–11088 (Nov. 1992).

78. Rehm, H. & Lazdunski, M. Purification and Subunit Structure of a Putative K+-Channel Protein Identified by Its Binding Properties for Dendrotoxin I. *Proceedings of the National Academy of Sciences* **85,** 4919–4923 (July 1988).

79. Rettig, J. *et al.* Inactivation Properties of Voltage-Gated K+ Channels Altered by Presence of β-Subunit. *Nature* **369,** 289–294 (1994).

80. Heinemann, S. H., Rettig, J., Graack, H. R. & Pongs, O. Functional Characterization of Kv Channel Beta-Subunits from Rat Brain. *The Journal of Physiology* **493,** 625–633 (1996).

81. Long, S. B., Tao, X., Campbell, E. B. & MacKinnon, R. Atomic Structure of a Voltage-Dependent K+ Channel in a Lipid Membrane-like Environment. *Nature* **450,** 376–382 (Nov. 2007).

82. Long, S. B., Campbell, E. B. & Mackinnon, R. Crystal Structure of a Mammalian Voltage-Dependent Shaker Family K+ Channel. *Science* **309,** 897–903 (2005).

83. Penning, T. M. The Aldo-Keto Reductases (AKRs): Overview. *Chemico-biological interactions* **234,** 236–246 (June 2015).

84. Tipparaju, S. M., Saxena, N., Liu, S.-Q., Kumar, R. & Bhatnagar, A. Differential Regulation of Voltage-Gated K+ Channels by Oxidized and Reduced Pyridine Nucleotide Coenzymes. *American Journal of Physiology-Cell Physiology* **288,** C366–C376 (Feb. 2005).

85. Weng, J., Cao, Y., Moss, N. & Zhou, M. Modulation of Voltage-Dependent Shaker Family Potassium Channels by an Aldo-Keto Reductase. *Journal of Biological Chemistry* **281,** 15194–200 (2006).

86. Pan, Y., Weng, J., Cao, Y., Bhosle, R. C. & Zhou, M. Functional Coupling between the Kv1.1 Channel and Aldoketoreductase Kvbeta1. *Journal of Biological Chemistry* **283,** 8634–42 (2008).

87. Tipparaju, S. M., Barski, O. A., Srivastava, S. & Bhatnagar, A. Catalytic Mechanism and Substrate Specificity of the β-Subunit of the Voltage-Gated Potassium (Kv) Channel. *Biochemistry* **47,** 8840–8854 (Aug. 2008).

88. Ikeda, K. & Kaplan, W. D. Patterned Neural Activity of a Mutant Drosophila Melanogaster. *Proceedings of the National Academy of Sciences* **66,** 765–772 (July 1970).

89. Stern, M. & Ganetzky, B. Altered Synaptic Transmission in Drosophila Hyperkinetic Mutants. *Journal of Neurogenetics* **5,** 215–228 (Aug. 1989).

90. Yao, W.-D. & Wu, C.-F. Auxiliary Hyperkinetic β Subunit of K+Channels: Regulation of Firing Properties and K+ Currents in Drosophila Neurons. *Journal of Neurophysiology* **81,** 2472–2484 (May 1999).

91. Bähring, R. *et al.* Coupling of Voltage-Dependent Potassium Channel Inactivation and Oxidoreductase Active Site of Kvbeta Subunits. *The Journal of Biological Chemistry* **276,** 22923–22929 (June 2001).

92. Cirelli, C. *et al.* Reduced Sleep in Drosophila Shaker Mutants. *Nature* **434,** 1087–92 (2005).

93. Bushey, D., Huber, R., Tononi, G. & Cirelli, C. Drosophila Hyperkinetic Mutants Have Reduced Sleep and Impaired Memory. *Journal of Neuroscience* **27,** 5384–93 (2007).

94. Kempf, A., Song, S. M., Talbot, C. B. & Miesenbock, G. A Potassium Channel Beta-Subunit Couples Mitochondrial Electron Transport to Sleep. *Nature* **568,** 230–234 (2019).

95. Shi, G. *et al.* Beta Subunits Promote K+ Channel Surface Expression through Effects Early in Biosynthesis. *Neuron* **16,** 843–852 (Apr. 1996).

96. Fogle, K. J. *et al.* CRYPTOCHROME-mediated Phototransduction by Modulation of the Potassium Ion Channel β-Subunit Redox Sensor. *Proceedings of the National Academy of Sciences* **112,** 2245–2250 (Feb. 2015).

97. Laker, R. C. *et al.* A Novel MitoTimer Reporter Gene for Mitochondrial Content, Structure, Stress, and Damage in Vivo*. *Journal of Biological Chemistry* **289,** 12005–12015 (Apr. 2014).

98. Balaban, R. S., Nemoto, S. & Finkel, T. Mitochondria, Oxidants, and Aging. *Cell* **120,** 483–495 (Feb. 2005).

99. Brand, M. D. Uncoupling to Survive? The Role of Mitochondrial Inefficiency in Ageing. *Experimental Gerontology. Biological Aging - Euroconference on Molecular, Cellular and Tissue Gerontology* **35,** 811–820 (Sept. 2000).

100. Murphy, M. P. How Mitochondria Produce Reactive Oxygen Species. *Biochemical Journal* **417,** 1–13 (Dec. 2008).

101. Cirelli, C. & Tononi, G. Uncoupling Proteins and Sleep Deprivation. *Archives Italiennes De Biologie* **142,** 541–549 (July 2004).

102. May-Zhang, L. S. *et al.* Modified Sites and Functional Consequences of 4-Oxo-2-Nonenal Adducts in HDL That Are Elevated in Familial Hypercholesterolemia. *The Journal of Biological Chemistry* **294,** 19022–19033 (Dec. 2019).

103. Maxwell, D. P., Wang, Y. & McIntosh, L. The Alternative Oxidase Lowers Mitochondrial Reactive Oxygen Production in Plant Cells. *Proceedings of the National Academy of Sciences* **96,** 8271–8276 (July 1999).

104. Shu, X. *et al.* A Genetically Encoded Tag for Correlated Light and Electron Microscopy of Intact Cells, Tissues, and Organisms. *PLoS biology* **9,** e1001041 (2011).

105. Torra, J. *et al.* Tailing miniSOG: Structural Bases of the Complex Photophysics of a Flavin-Binding Singlet Oxygen Photosensitizing Protein. *Scientific Reports* **9,** 2428 (Feb. 2019).

106. Pan, Y., Weng, J., Levin, E. J. & Zhou, M. Oxidation of NADPH on Kvbeta1 Inhibits Ball-and-Chain Type Inactivation by Restraining the Chain. *Proceedings of The National Academy Of Sciences Of The United States Of America* **108,** 5885–90 (2011).

107. Esterbauer, H., Schaur, R. J. & Zollner, H. Chemistry and Biochemistry of 4-Hydroxynonenal, Malonaldehyde and Related Aldehydes. *Free Radical Biology and Medicine* **11,** 81–128 (Jan. 1991).

108. Hardin, P. E., Hall, J. C. & Rosbash, M. Circadian Oscillations in Period Gene mRNA Levels Are Transcriptionally Regulated. *Proceedings of the National Academy of Sciences* **89,** 11711 (1992).

109. Gulbis, J. M., Mann, S. & MacKinnon, R. Structure of a Voltage-Dependent K+ Channel Beta Subunit. *Cell* **97,** 943–52 (1999).

110. Wang, J. W. & Wu, C.-F. In Vivo Functional Role of the Drosophila Hyperkinetic F3 Subunit in Gating and Inactivation of Shaker K+ Channels. *Biophysical Journal* **71,** 10 (1996).

111. Veech, R. L., Eggleston, L. V. & Krebs, H. A. The Redox State of Free Nicotinamide-Adenine Dinucleotide Phosphate in the Cytoplasm of Rat Liver. *The Biochemical Journal* **115,** 609–619 (Dec. 1969).

112. Lacroix, J. J., Labro, A. J. & Bezanilla, F. Properties of Deactivation Gating Currents in Shaker Channels. *Biophysical Journal* **100,** L28–L30 (Mar. 2011).

113. Hille, B. *Ion Channels of Excitable Membranes* Third Edition (Oxford University Press, Oxford, New York, July 2001).

114. Ding, S. & Horn, R. Effect of S6 Tail Mutations on Charge Movement in Shaker Potassium Channels. *Biophysical Journal* **84,** 295–305 (Jan. 2003).

115. Harris-Warrick, R., Coniglio, L., Barazangi, N., Guckenheimer, J. & Gueron, S. Dopamine Modulation of Transient Potassium Current Evokes Phase Shifts in a Central Pattern Generator Network. *The Journal of Neuroscience* **15,** 342–358 (Jan. 1995).

116. Harris-Warrick, R. M. *et al.* Distributed Effects of Dopamine Modulation in the Crustacean Pyloric Networka. *Annals of the New York Academy of Sciences* **860,** 155–167 (1998).

117. Gerstner, W., Werner, M. K., Naud, R. & Paninski, L. *Neuronal Dynamics: From Single Neurons to Networks and Models of Cognition* (2014).

118. Wagenaar, D. A., Madhavan, R., Pine, J. & Potter, S. M. Controlling Bursting in Cortical Cultures with Closed-Loop Multi-Electrode Stimulation. *Journal of Neuroscience* **25,** 680–8 (2005).

119. Wu, M. N. *et al.* SLEEPLESS, a Ly-6/Neurotoxin Family Member, Regulates the Levels, Localization and Activity of Shaker. *Nature Neuroscience* **13,** 69–75 (Jan. 2010).

120. Werner, J., Arian, J., Bernhardt, I., Ryglewski, S. & Duch, C. Differential Localization of Voltage-Gated Potassium Channels during Drosophila Metamorphosis. *Journal of Neurogenetics* **34,** 133–150 (Jan. 2020).

121. Betts, M. J. & Russell, R. B. in *Bioinformatics for Geneticists* 289–316 (John Wiley & Sons, Ltd, 2003).

122. Liu, X. *et al.* Structural and Mutational Studies on an Aldo-Keto Reductase AKR5C3 from Gluconobacter Oxydans. *Protein Science : A Publication of the Protein Society* **23,** 1540–1549 (Nov. 2014).

123. Jenett, A. *et al.* A GAL4-driver Line Resource for Drosophila Neurobiology. *Cell Rep* **2,** 991–1001 (2012).

124. Colomb, J. & Brembs, B. Sub-Strains of Drosophila Canton-S Differ Markedly in Their Locomotor Behavior. *F1000Research* **3,** 176 (Apr. 2015).

125. Zimmerman, J. E., Chan, M. T., Jackson, N., Maislin, G. & Pack, A. I. Genetic Background Has a Major Impact on Differences in Sleep Resulting from Environmental Influences in Drosophila. *Sleep* **35,** 545–557 (Apr. 2012).

126. Tononi, G. & Cirelli, C. Sleep and Synaptic Homeostasis: A Hypothesis. *Brain Research Bulletin* **62,** 143–50 (2003).

127. Bushey, D., Tononi, G. & Cirelli, C. Sleep and Synaptic Homeostasis: Structural Evidence in Drosophila. *Science (New York, N.Y.)* **332,** 1576–1581 (June 2011).

128. Vyazovskiy, V. V., Cirelli, C., Pfister-Genskow, M., Faraguna, U. & Tononi, G. Molecular and Electrophysiological Evidence for Net Synaptic Potentiation in Wake and Depression in Sleep. *Nature Neuroscience* **11,** 200–208 (Feb. 2008).

129. Benington, J. H. & Heller, H. C. Restoration of Brain Energy Metabolism as the Function of Sleep. *Progress in Neurobiology* **45,** 347–60 (1995).

130. Scharf, M. T., Naidoo, N., Zimmerman, J. E. & Pack, A. I. The Energy Hypothesis of Sleep Revisited. *Progress in neurobiology* **86,** 264–280 (Nov. 2008).

131. Yanik, G., Glaum, S. & Radulovacki, M. The Dose-Response Effects of Caffeine on Sleep in Rats. *Brain Research* **403,** 177–180 (Feb. 1987).

132. Wu, M. N. *et al.* The Effects of Caffeine on Sleep in Drosophila Require PKA Activity, But Not the Adenosine Receptor. *Journal of Neuroscience* **29,** 11029–11037 (Sept. 2009).

133. Nall, A. H. *et al.* Caffeine Promotes Wakefulness via Dopamine Signaling in Drosophila. *Scientific Reports* **6,** 20938 (Feb. 2016).

134. Szymusiak, R. & McGinty, D. Hypothalamic Regulation of Sleep and Arousal. *Annals of the New York Academy of Sciences* **1129,** 275–286 (2008).

135. Alam, M. A., Kumar, S., McGinty, D., Alam, M. N. & Szymusiak, R. Neuronal Activity in the Preoptic Hypothalamus during Sleep Deprivation and Recovery Sleep. *Journal of Neurophysiology* **111,** 287–299 (Jan. 2014).

136. Lazarus, M., Oishi, Y., Bjorness, T. E. & Greene, R. W. Gating and the Need for Sleep: Dissociable Effects of Adenosine A1 and A2A Receptors. *Frontiers in Neuroscience* **13** (2019).

137. Holst, S. C. & Landolt, H.-P. Sleep Homeostasis, Metabolism, and Adenosine. *Current Sleep Medicine Reports* **1,** 27–37 (Mar. 2015).

138. Pascual, O. *et al.* Astrocytic Purinergic Signaling Coordinates Synaptic Networks. *Science (New York, N.Y.)* **310,** 113–116 (Oct. 2005).

139. Halassa, M. M. *et al.* Astrocytic Modulation of Sleep Homeostasis and Cognitive Consequences of Sleep Loss. *Neuron* **61,** 213–219 (Jan. 2009).

140. MacKinnon, R. Determination of the Subunit Stoichiometry of a Voltage-Activated Potassium Channel. *Nature* **350,** 232–235 (1991).

141. Douglas, C. L. *et al.* Sleep in Kcna2 Knockout Mice. *BMC Biology* **5,** 42 (Oct. 2007).

142. Vyazovskiy, V. V. *et al.* Sleep EEG in Mice That Are Deficient in the Potassium Channel Subunit K.v.3.2. *Brain Research* **947,** 204–211 (Aug. 2002).

143. Espinosa, F., Marks, G., Heintz, N. & Joho, R. H. Increased Motor Drive and Sleep Loss in Mice Lacking Kv3-type Potassium Channels. *Genes, Brain, and Behavior* **3,** 90–100 (Apr. 2004).

144. McCormack, K. *et al.* Genetic Analysis of the Mammalian K+ Channel Beta Subunit Kvbeta 2 (Kcnab2). *The Journal of Biological Chemistry* **277,** 13219–13228 (Apr. 2002).

145. Parvez, S. *et al.* T-REX on-Demand Redox Targeting in Live Cells. *Nature protocols* **11,** 2328–2356 (Dec. 2016).

146. Martin, H.-J. *et al.* The Drosophila Carbonyl Reductase Sniffer Is an Efficient 4-Oxonon-2-Enal (4ONE) Reductase. *Chemico-Biological Interactions. Enzymology and Molecular Biology of Carbonyl Metabolism* **191,** 48–54 (May 2011).

147. Botella, J. A. *et al.* The Drosophila Carbonyl Reductase Sniffer Prevents Oxidative Stress-Induced Neurodegeneration. *Current Biology* **14,** 782–786 (May 2004).

148. Lee, T. & Luo, L. Mosaic Analysis with a Repressible Cell Marker for Studies of Gene Function in Neuronal Morphogenesis. *Neuron* **22,** 451–61 (1999).

149. Cirelli, C. Searching for Sleep Mutants of Drosophila Melanogaster. *BioEssays* **25,** 940–949 (2003).

150. Wu, B. *et al.* Sexual Dimorphism of Sleep Regulated by Juvenile Hormone Signaling in Drosophila. *PLOS Genetics* **14** (ed Taghert, P. H.) e1007318 (Apr. 2018).

151. *Research Tools | Vecsey Lab*

152. Murthy, M. & Turner, G. Dissection of the Head Cuticle and Sheath of Living Flies for Whole-Cell Patch-Clamp Recordings in the Brain. *Cold Spring Harb Protoc* **2013,** 134–9 (2013).

153. Murthy, M. & Turner, G. Whole-Cell In Vivo Patch-Clamp Recordings in the Drosophila Brain. *Cold Spring Harbor Protocols* **2013,** pdb.prot071704 (Jan. 2013).

154. Rothman, J. S. & Silver, R. A. NeuroMatic: An Integrated Open-Source Software Toolkit for Acquisition, Analysis and Simulation of Electrophysiological Data. *Front Neuroinform* **12,** 14 (2018).